High Resolution FTIR and Diode Laser Spectroscopy of Supersonic Jets

M. Snels, V. Horká-Zelenková, H. Hollenstein, M. Quack

ETH Zürich, Laboratory of Physical Chemistry, Wolfgang-Pauli-Str. 10, CH-8093 Zürich, Switzerland, Email: Martin@Quack.ch

reprinted from

"Handbook of High-Resolution Spectroscopy"

Vol. 2, chapter 27, pages 1021–1067
M. Quack, and F. Merkt, Eds. Wiley Chichester, 2011,
ISBN-13: 978-0-470-06653-9,
Online ISBN: 9780470749593,
DOI: 10.1002/9780470749593.

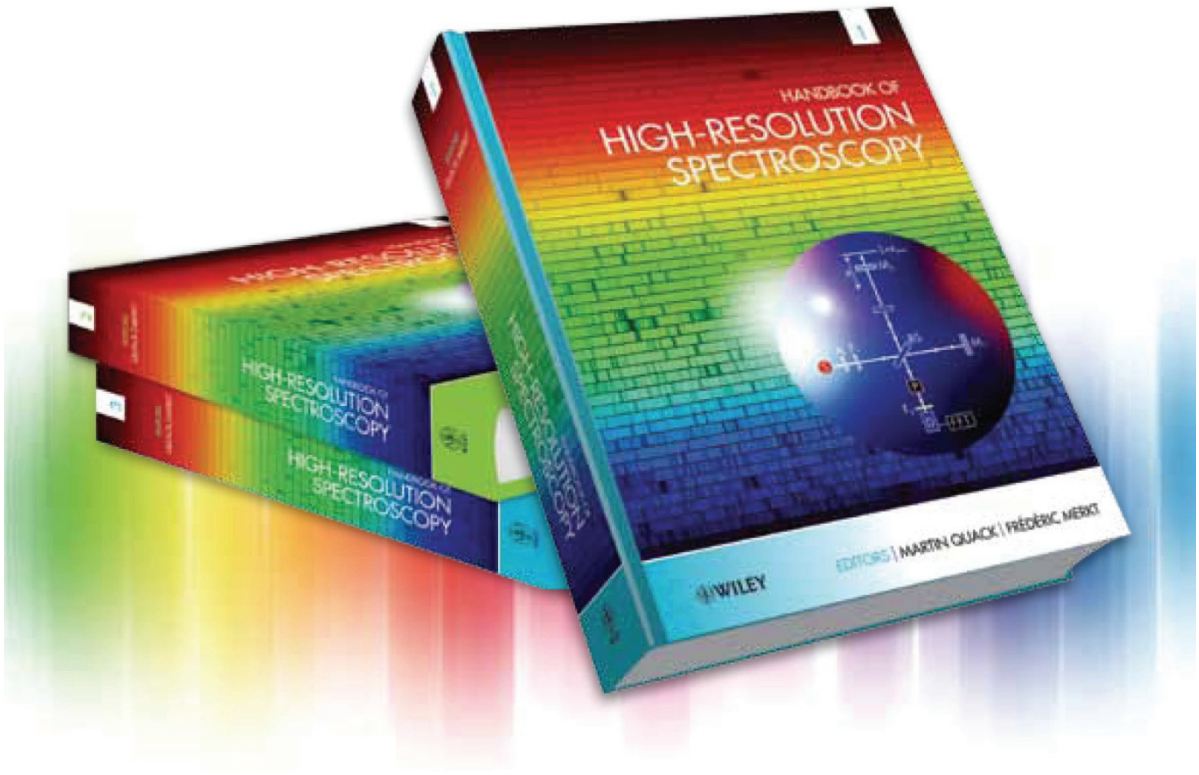

with compliments from Professor Martin Quack, ETH Zürich

Abstract

Fourier transform infrared (FTIR) spectrometers and tunable diode lasers in combination with a supersonic molecular beam expansion are a perfect tool for the investigation of molecules, ions, and radicals at low temperatures. The internal degrees of freedom of the molecules are adiabatically cooled to very low temperatures and thus only low-lying energy levels are populated. The reduction of the number of populated levels at low temperatures makes the assignment of the spectra much easier as compared to the congested room-temperature spectra. Under certain conditions, the Doppler linewidths are greatly reduced, corresponding to very low effective translational temperatures. Supersonic expansion also provides a suitable method for producing and investigating van der Waals clusters and hydrogen-bonded complexes. Unstable species such as radicals and ions can be efficiently produced and studied in a molecular beam. The low rotational temperature allows for the study of nuclear spin symmetry conservation or conversion between nuclear spin isomers. A molecular beam expansion can be obtained by expanding gas through a slit or a circular nozzle. Both expansion geometries can be used in combination with a multipass optical setup and with cavity ring down spectroscopy, which enhances the effective absorption path length. Cooling of the molecules can be promoted by seeding in noble gases. This article summarizes the general aspects of the experimental technique as well as current developments. To demonstrate how powerful the combination of a molecular beam expansion with tunable diode laser and FTIR spectroscopy can be, we report results on some important current examples.

Keywords: FTIR; supersonic jet; diode laser; molecular beam; clusters; van der Waals complexes; hydrogen bonds; nuclear spin symmetry conservation; infrared spectroscopy; isotopes

High-resolution FTIR and Diode Laser Spectroscopy of Supersonic Jets

Marcel Snels[1], Veronika Horká-Zelenková[2], Hans Hollenstein[2] and Martin Quack[2]

[1]*Institute of Atmospheric Sciences and Climate, Rome, Italy, m.snels@isac.cnr.it*
[2]*Laboratorium für Physikalische Chemie, ETH Zürich, Zürich, Switzerland, martin@quack.ch*

1 INTRODUCTION

1.1 Brief History

The combination of spectroscopy with atomic and molecular beams can be viewed as one of the most fruitful unions in science. Its history goes back both to the Stern–Gerlach experiment (Gerlach and Stern 1924, Gerlach 1925) and the subsequent development of nuclear magnetic resonance (NMR) experiments in atomic beams by Rabi (1937) in the first half of the twentieth century (see also Bennewitz and Paul (1954) and Goldenberg *et al*. (1960) for further development of the experimental technology). While this research was originally curiosity driven in order to get a better understanding of nuclear structure, today the results of modern NMR spectroscopy (Ernst *et al*. 1987) can be admired in every chemical and analytical laboratory as well as in terms of magnetic resonance imaging (MRI) in every major hospital. The somewhat related developments in molecular beam state selection and electric resonance (Dyke *et al*. 1972, Bennewitz *et al*. 1964, Trischka 1962, Novick *et al*. 1973, Meerts and Dymanus 1975, Meerts *et al*. 1979) and beam MASER spectroscopy (Gordon *et al*. 1955, Dymanus 1976) as well as later Fourier Transform Microwave (FT-MW) spectroscopy of beams (Bauder 2011: **Fundamentals of Rotational Spectroscopy**, this handbook) had already important applications in molecular spectroscopy. The early uses of molecular beams in optical spectroscopy are connected with sensitive detection techniques such as laser-induced fluorescence (Sinha *et al*. 1973, Smalley *et al*. 1974) and this early work has been reviewed by Smalley *et al*. (1977) and Levy (1980).

In the classic paper, largely related to the thesis work of the late Roger Miller, Gough *et al*. (1977) introduced mid-infrared diode laser absorption spectroscopy of supersonic jets (reviewed in part in Miller (1992)). This technique provided high, essentially Doppler-limited resolution, but has the serious drawback of very limited scanning abilities. Scanning of a typical laser diode can range between about 10 and 50 cm^{-1} at most, but scans are not continuous, often missing important parts of a spectrum. Continuous laser diode scans are frequently limited to about 2 cm^{-1}, which is far too small for an efficient rovibrational analysis of complex infrared bands.

Obvious infrared techniques with large scanning abilities covering the complete infrared spectral range are grating and FTIR spectrometers, which have both been used in the late 1970s and early 1980s in conjunction with supersonic jets (Kim *et al*. 1978, Snavely *et al*. 1981, 1983, 1984). These techniques reached only modest resolution of at most 0.06 cm^{-1}, which has the major drawback that the measured spectra are limited by the instrumental shape, resulting in only limited possibilities for rovibrational analysis and introducing artifacts concerning line strengths, which can be evaluated only if the instrumental bandwidth approaches the Doppler linewidth in the supersonic jet.

The Zürich group, therefore, in the 1980s developed high-resolution FTIR spectroscopy of supersonic jets under conditions that often satisfy the requirement

Handbook of High-resolution Spectroscopy. Edited by Martin Quack and Frédéric Merkt.
ISBN: 978-0-470-74959-3.

of Doppler-limited resolution (instrumental bandwidth $0.0024\,cm^{-1}$ or 72 MHz, unapodized) (Dübal *et al*. 1984, Amrein *et al*. 1987a,b,c, 1988a,b, 1989, Quack 1990). At the same time, it was recognized that an ideal combination would be to realize the advantages of high-resolution FTIR spectroscopy and diode laser spectroscopy in the same laboratory and such a combination was realized in the Zürich laboratory, leading among other things to the first analyses of the very complex infrared spectra of the important atmospheric window bands of the chlorofluoro(hydro)carbons $CHFCl_2$ (Snels and Quack 1991), CF_2Cl_2 (D'Amico *et al*. 2002), and $CFCl_3$ (Snels *et al*. 1995, 2001) and the complex spectra of CF_3I (Hollenstein *et al*. 1994, He *et al*. 2002); see also the work on $CHClF_2$ (Albert *et al*. 2010, 2004, Amrein *et al*. 1988a). It also led to the very first successful high-resolution rovibrational analyses of chiral molecules in the mid-1990s (Beil *et al*. 1994, Bauder *et al*. 1997), this work having significance well beyond ordinary rovibrational spectroscopy (Quack 2002, 2003, 2011, Quack *et al*. 2008). Until today, to our knowledge, only one other group has repeated a combination of these two spectroscopic techniques much more recently (Herman *et al*. 2007). Further important experimental developments concern the combination of pulsed supersonic jets with continuous scan FTIR spectroscopy (Luckhaus *et al*. 1995), a possibility, which was probably not anticipated by anyone, and the combination of pulsed supersonic jets with continuous laser cavity ring down spectroscopy, which provides very high sensitivity and very high resolution (1 MHz and potentially better), by Hippler and Quack (1999, 2002). The combination of pulsed IR-laser spectroscopy of pulsed supersonic jets with ionization and mass-selective detection resulted in mass- and isotope-selective spectroscopy reviewed by Hippler and Quack (2005) and Hippler *et al*. (2011): **Mass and Isotope-selective Infrared Spectroscopy**, this handbook. Such a mass-selective technique combined with supersonic-jet FTIR spectroscopy had been suggested already by Quack (1990) but has not been realized, so far, as it is technically very demanding.

1.2 Some Aspects of the Spectroscopy of Supersonic Jets and Related Developments

High-resolution spectroscopy in supersonic jets offers many advantages and opportunities as compared to experiments in static gas cells. One of the properties of a supersonic expansion is the adiabatic cooling of the internal degrees of freedom of a molecule. Whereas all degrees of freedom are in thermal equilibrium in a static gas sample, in a beam, the population of rotational and vibrational energy levels can be often approximately described by a Boltzmann distribution with different, very low rotational and vibrational temperatures. Most efficient cooling is obtained by diluting (seeding) the sample in an inert gas, typically a rare gas that promotes relaxation of rotational and vibrational levels of a polyatomic molecule. Typically rotational temperatures of 10–30 K can be routinely obtained, whereas the vibrational temperature is usually higher. In addition, because of the irregular spacing between vibrational energy levels, the population of vibration levels is not well described by a Boltzmann distribution. In some cases, bottlenecks might occur, trapping a substantial part of the population in an "isolated" vibrational level, i.e., with a high energy gap with respect to the next lower level. By varying the collision partner (He, Ne, Ar, or mixtures of noble gases), cooling can be made more efficient. At the same time, the large number of collisions in a supersonic expansion can also promote cluster formation, and thus the supersonic expansion has become an appropriate tool for generating van der Waals and hydrogen-bonded complexes. In a similar way, other unstable species, such as radicals and ions, can be generated in a supersonic expansion and successively cooled and studied. Yet another opportunity is the evaporation of solid material that can be entrained in a supersonic expansion of inert gases.

The Doppler broadening of spectral lines observed in supersonic jets can be substantial. In a supersonic expansion, the Doppler width of an absorption line is determined by the spread of the velocity component parallel to the laser beam, which is (usually) perpendicular to the direction of propagation of the jet expansion. When a gas mixture is expanded through a circular nozzle, the linewidth is determined by the average free flow velocity. In the case of a gas mixture with He as a major component, the resulting linewidth can be even larger than the Doppler width at room temperature. The linewidth can be much reduced by using planar jet expansions (slit-jet expansions).

Some disadvantages of molecular jets are the short absorption path (a few centimeters at most), the low local density (10^{18}–10^{19} molecules cm^{-3}), the strong variations in local density, the nonequilibrium conditions, the large gas consumption, and the necessity for large pumps. A way to obtain an appreciable local density without the need for large pumps is to use a pulsed jet expansion. This also reduces the gas consumption, which opens up possibilities for using costly isotopic species in a supersonic-pulsed jet experiment.

Hitherto, the spectroscopic study of molecules that are in the liquid or solid state at room temperature was limited either to matrix spectroscopy or to gas-phase spectroscopy by using Knudsen cells (Wagner 1984). The advent of molecular beams opened new possibilities, such as evaporating liquids and solids and allowing the vapors to be entrained in a supersonic expansion.

Pure carbon clusters can be produced in the laboratory by laser ablation of a graphite target (Scott *et al*. (2001) and references therein). Followed by an adiabatic supersonic expansion, clusters grow in size and appear in a variety of structures including linear chains, rings, and three-dimensional cage forms (Kroto *et al*. 1985, Kroto 1997). Unstable species such as radicals and molecular ions can be readily produced by combining a discharge with a pulsed supersonic (slit) jet. The transient species are successively cooled and transported in a collisionless environment. Concentrations of 10^{12} radicals cm^{-3} and 10^{10} ions cm^{-3} are obtainable with these techniques (Mazzotti *et al*. 2008, Guennoun and Maier 2011: **Electronic Spectroscopy of Transient Molecules**, this handbook).

A further important development concerns the formation of liquid He droplets in molecular beams, which are then used as an almost inert matrix for molecules at very low temperatures (Toennies and Vilesov 2004). This work is reviewed in the present handbook by Callegari and Ernst (2011): **Helium Droplets as Nanocryostats for Molecular Spectroscopy—from the Vacuum Ultraviolet to the Microwave Regime**, this handbook. It is also possible to use gaseous He as an inert "solvent", providing a cooling mechanism under both equilibrium and nonequilibrium conditions (Willey *et al*. 1989, Bauerecker *et al*. 2001, Albert *et al*. 2007). We have shown that with this more recent development FTIR spectra of gaseous molecular samples can be measured at high resolution and temperatures as low as 10 K and lower (Albert *et al*. 2007). This work is reviewed briefly in Albert *et al*. (2011): **High-resolution Fourier Transform Infrared Spectroscopy**, this handbook.

1.3 Organization of the Article

This article is organized as follows. In Section 2, we summarize the general aspects and experimental methods of the molecular spectroscopy of supersonic jets, including some of the basic equations for supersonic-jet expansions. We also review some of the basic experimental setups. In Section 3, we give a review of the FTIR-supersonic jet experiments. Section 4 reports the properties of a number of infrared laser sources used in supersonic-jet spectroscopy. In Section 5, we give a tabular literature overview of FTIR supersonic-jet spectroscopic investigations at high resolution. In Section 6, we discuss some selected examples in more detail. Section 7 presents the application of high-resolution infrared spectroscopy of supersonic jets to the study of nuclear spin symmetry conservation and violation. Section 8 reports a series of studies of van der Waals clusters and hydrogen-bonded molecular complexes. Section 9 is dedicated to radicals and ions. The field has developed to an extent that encyclopedic review is not really possible or desirable here. We have tried to concentrate on the most important aspects and applications, with presumably some weighting toward our own work, partly understandable from the historical development of the field, partly by the natural bias of specific knowledge, although we have made an effort to cover work from all groups. With apologies to those authors whose work is less than adequately covered, we mention here some relevant reviews, one that covers much of the early work (Quack 1990), and the other the general beam techniques in two volumes (Scoles 1988, 1992). The subsequent work of the group of Herman at the Université Libre de Bruxelles is well covered by the review of Herman *et al*. (2000). The work on $(H_2O)_n$ clusters can be found in reviews of Saykally and coworkers (Liu *et al*. 1994, 1996, 1997, Gregory *et al*. 1997, Paul *et al*. 1997, Keutsch *et al*. 2003). Some of the work of the Leutwyler group is covered in this handbook by Frey *et al*. (2011): **High-resolution Rotational Raman Coherence Spectroscopy with Femtosecond Pulses**, this handbook. The theoretical work related to experiment is far too exclusive to be covered here, but several articles in this handbook deal with the theoretical aspects. We draw attention to two reviews covering experimental and theoretical work on $(HF)_n$ clusters (Quack and Suhm 1997, 1998). For work on various types of clusters, we refer to Kappes and Leutwyler (1988). Work on molecular beam high-resolution laser spectroscopy with optothermal detection has been reviewed by Lehmann *et al*. (1994) (*see* also Scotoni *et al*. (1991) and the article by Demtröder (2011): **Doppler-free Laser Spectroscopy**, this handbook). The interesting applications of the results to short-time intramolecular dynamics are not covered here and we refer to Marquardt and Quack 2001, 2011: **Global Analytical Potential Energy Surfaces for High-resolution Molecular Spectroscopy and Reaction Dynamics**, Quack (2001, 2003) and Hippler *et al*. 2011: **Mass and Isotope-selective Infrared Spectroscopy**, this handbook and Albert *et al*. (2011). For sake of completeness, we draw explicit attention to all these reviews for further information.

2 GENERAL ASPECTS AND EXPERIMENTAL METHODS OF THE MOLECULAR SPECTROSCOPY OF SUPERSONIC JETS

2.1 Fundamentals of Supersonic Expansion

For the general background, we refer here to the two volumes of the handbook edited by Scoles (1988, 1992) and review here some fundamentals of supersonic expansion, as these are important for high-resolution spectroscopy (see

also, in particular, Miller (1988)) and the chapter "The molecular Beam" by Havenith (2002).

An expansion of a gas or liquid through an orifice into vacuum is supersonic if the velocity of the atoms or molecules in the expansion is larger than the local velocity of sound. The ratio of the velocity of the gas (v) with respect to the local velocity of sound v_{sound} is also called the *Mach number*.

$$M = \frac{v}{v_{\text{sound}}} \tag{1}$$

In the case of an ideal gas, the speed of sound becomes

$$v_{\text{sound}} = \sqrt{\frac{\gamma kT}{m}} \tag{2}$$

where γ is the ratio of heat capacities C_p/C_v, k is the Boltzmann constant, T is the temperature, and m is the molecular mass. For a monoatomic gas $\gamma = 5/3$ and for a diatomic gas $\gamma = 7/5$, in a simple limit.

Now we consider an isentropic flow of a perfect (ideal) gas, from a reservoir at pressure P_0, through a circular orifice with diameter d, into a vacuum chamber that is kept at a low background pressure P_b. The chamber is evacuated by a turbomolecular or a diffusion pump. The expanding gas while expanding will increase its speed and will cool down, and we can define a local temperature T, density n, and velocity v anywhere in the expansion. Roughly, we can distinguish several regimes or zones in the expansion (Figure 1); behind the orifice or nozzle, we have a zone where many collisions occur and where cooling and cluster formation is important. Once the gas density drops and collisions become rare, we have the so-called zone of silence, where the gas is expanding undisturbed, until it reaches a distance where the local density becomes similar to the density resulting from the background pressure: the Mach disk shock. The borders of the axisymmetric expansion consist of compression waves that are limited by a barrel shock, which has the shape of a paraboloid centered on the jet axis. Most spectroscopic measurements involve the regions close to the nozzle orifice or the zone of silence where we have free molecular flow.

Therefore, it is important to know where the Mach disk is located. In an ideal expansion of a gas, the final, or terminal velocity of the molecules is given by

$$v_t = \sqrt{2\frac{\gamma}{\gamma - 1}\frac{kT_0}{m}} \tag{3}$$

where T_0 is the temperature of the source.

Once the Mach number is known, other important parameters can be calculated, by using the equations (1)–(3) and the ideal gas law, such as the local density, pressure, and temperature n, P, and T from the equations

$$n = n_0 F^{-1/(\gamma-1)} \tag{4}$$

$$P = P_0 F^{-\gamma/(\gamma-1)} \tag{5}$$

$$T = T_0 F^{-1} \tag{6}$$

$$v = M\sqrt{\frac{\gamma kT_0}{m}} F^{-1/2} \tag{7}$$

where $F = 1 + (\gamma - 1)M^2/2$.

The Mach number in turn depends on the geometry of the expansion and can be generally expressed as a function of the distance from the nozzle x and of the orifice diameter d.

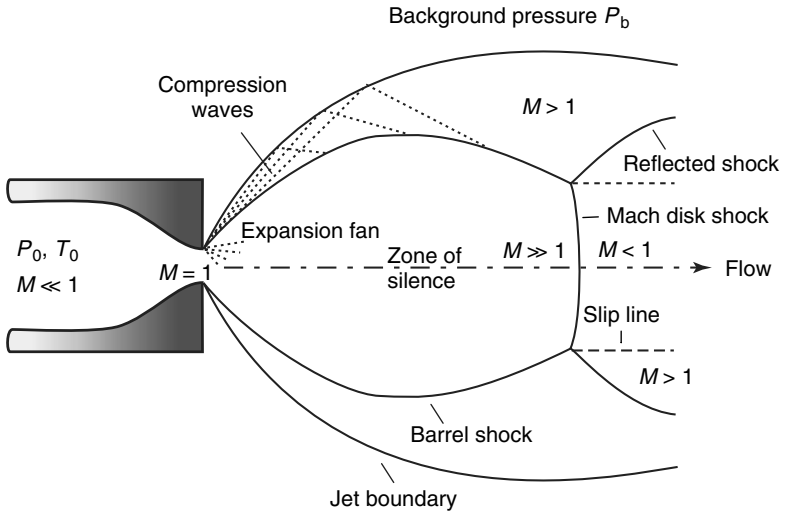

Figure 1 Schematic picture of a free jet expansion (After Miller 1988). P_0 and T_0 are source pressure and temperature. M is the Mach number, as defined in the text.

2.2 Axisymmetric and Planar Expansions

The most common expansion geometries are axisymmetric or planar. An axisymmetric expansion is produced when the gas expands through a circular orifice. In this case, the maximum density is found on the flow line and this decreases rapidly when the distance between source and the flow line increases. The corresponding Mach number can be described as

$$M = \left(\frac{x}{d}\right)^{(\gamma-1)} \left[A + A_1\left(\frac{d}{x}\right)^2 + A_2\left(\frac{d}{x}\right)^3 + A_3\left(\frac{d}{x}\right)^3\right] \tag{8}$$

where A, A_1, A_2, and A_3 are empirically determined numbers. It is easy to see that for $M \gg 1$ the density decreases with increasing distance from the source as x^{-2}.

The Mach disk location is given by

$$\frac{x_M}{d} = \frac{2}{3}\sqrt{\frac{P_0}{P_b}} \tag{9}$$

where x_M is the distance of the Mach disk from the nozzle, P_b is the background pressure, and d is the diameter of the nozzle.

A planar jet consists of a slit nozzle opening with a length L and a width d, where $L \gg d$ (Figure 2). Planar jets are usually operated in the pulsed mode although experiments with continuous slit jets have been reported as well (Amrein *et al*. 1988b). In the case of an ideal slit nozzle, the gas density approximately decreases as $n(x) \sim x^{-1}$.

The Mach number for planar jets, for $L \gg d$ and $x \ll$ L, and a adiabatic isentropic expansion is given by

$$M = A\left(\frac{x - x_0}{d}\right)^{(\gamma-1)/2} + b\left(\frac{x - x_0}{d}\right)^{-(\gamma-1)/2} \tag{10}$$

where A and b are empirical parameters.

The location of the Mach disk can be expressed as (Beylich 1979)

$$\frac{x_M}{d} = \frac{3}{2}\sqrt{\frac{P_0}{P_b}}\left(\frac{L}{d}\right)^{\epsilon} \tag{11}$$

where ϵ is a number between 0.47 and 0.735 and tends to smaller values for $L \gg d$, where L is the length of the slit.

The asymptotic expressions for T, n are ($d \ll x \ll L$)

$$\frac{T}{T_0} = C\left(\frac{x - x_0}{d}\right)^{-(\gamma-1)} \tag{12}$$

$$\frac{n}{n_0} = G\left(\frac{x - x_0}{d}\right)^{-1} \tag{13}$$

where C and G are empirical parameters. Detailed formulas for the axisymmetric and planar free jets can be found in Hagena (1981). An experimental investigation of supersonic slit jets is reported by Beylich (1979).

One of the major limitations of the supersonic-jet expansion through a nozzle is the short effective absorption path. One way to enhance the absorption path length is multipassing the laser beam through the expansion, but this is also troublesome because of the small dimensions of the nozzle. A planar (slit) expansion produces a longer absorption path with the same gas throughput, can be used in combination with multipass optical setups, and has the additional advantages of a narrower linewidth, a slower

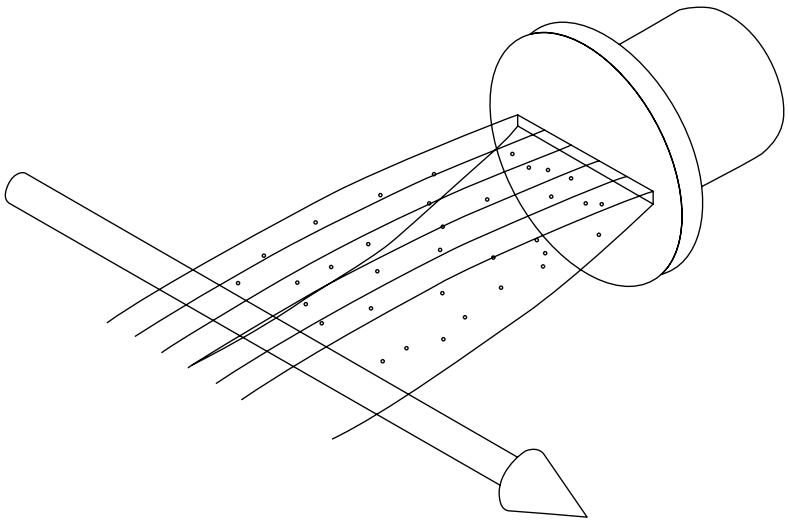

Figure 2 Slit-jet configuration. The laser beam is indicated by a cylindrical arrow.

cooling, and a more homogeneous density distribution along the laser path. The slit nozzle has also been successfully coupled to several discharge sources in order to produce molecular ions and radicals. With respect to an axisymmetric expansion, the molecular density n and the temperature decrease more slowly, providing larger two- and three-body collision rates, which enhance the cluster production. At the same time, it also guarantees a better cooling of the vibrational degrees of freedom. The Doppler width is substantially reduced because of the quenching of velocity components parallel to the slit.

2.3 Pulsed Jets and Continuous Jets

Both pulsed and continuous supersonic jets have been used to perform high-resolution spectroscopic measurements. Each method has its advantages and drawbacks. A continuous expansion requires large quantities of gas and elevated pumping speeds, whereas the gas consumption in pulsed experiments is limited and smaller pumping systems are sufficient to obtain a low background pressure between two gas pulses. As a consequence, pulsed experiments allow for higher reservoir pressure, which is important for cluster production and for slit nozzles with a larger surface. Generally, slit-jet expansions produce a higher molecular density behind the (slit) nozzle and eliminate most of the Doppler broadening of the absorption lines, owing to the velocity quenching parallel to the slit opening. Operating a continuous slit expansion would require very large pumps. Pulsed expansions are often combined with pulsed laser sources, for instance, in laser ablation or laser desorption experiments. In addition, the production of ions and radicals is often obtained by pulsed pyrolysis, ablation, or photolysis of precursors, which are obviously more efficiently combined with a pulsed expansion. However, when spectral scans and averaging processes require long recording times, the reduced duty cycle of a pulsed expansion with respect to a continuous jet can be a serious drawback.

2.4 Seeded Expansions

To obtain a more efficient cooling, a small amount of the heavier seed gas is often seeded in a lighter carrier gas. In the case of a binary mixture, one can easily obtain expressions for the average mass and velocities (n_s and n_c are the number densities of seed and carrier gas, respectively):

$$m_{av} = \left(\frac{n_c}{n_c + n_s}\right) m_c + \left(\frac{n_s}{n_c + n_s}\right) m_s \qquad (14)$$

which for $n_c \gg n_s$ becomes

$$m_{av} \approx m_c + \left(\frac{n_s}{n_c}\right) m_s \qquad (15)$$

whereas the most probable velocities become

$$v_c = \frac{1}{2}\left[u_c + \left(u_c^2 + \sqrt{\frac{8kT_c}{m_c}}\right)\right] \qquad (16)$$

$$v_s = \frac{1}{2}\left[u_s + \left(u_s^2 + \sqrt{\frac{8kT_s}{m_s}}\right)\right] \qquad (17)$$

At high source pressures, the seeded gas reaches the same velocity as the carrier, and for medium and low pressure, there is a velocity slip.

2.5 Pick-up Methods

While seeded expansions are used for expanding the seed gas diluted in a mixture with noble gas, a different solution has to be found to introduce in the expansion the molecules that cannot be mixed beforehand. This is the case of solids and liquids, which can be (laser) evaporated close to the nozzle exit and successively entrained in a supersonic expansion. The group of Giacinto Scoles developed the pick-up method to study the behavior of infrared chromophores in a solvent of noble gas clusters (Gu *et al*. 1990). The same authors crossed a molecular beam of CH_3F seeded in Ar with a second beam of HCl to study complex forming reactions in Ar clusters (Levandier *et al*. 1987). Refractory radicals, such as CaCl, can be entrained in a molecular expansion by crossing a noble gas expansion with a conventional effusive molecular beam (Steimle *et al*. 1991). In this way, the radicals can be cooled from 1200 down to 7.6 K, which simplifies their spectra enormously.

Thermally labile and nonvolatile species, such as biomolecules, can be brought in the gas phase by laser desorption and successively entrained in an expansion of He (Tembreull and Lubman 1987, Cable *et al*. 1987).

In the case of ions and radicals, a discharge source can be used to produce a large number of ions and radicals (Kim *et al*. 2005, Davis *et al*. 2001), which are picked up by the expansion and are cooled efficiently. To produce a variety of carbon clusters, a carbon rod is ablated by a pulsed laser and the products are introduced in the expansion. The field of the spectroscopy of molecules dissolved in cold He clusters has developed along independent lines (see the review by Toennies and Vilesov (2004) and Jäger and Xu 2011: **Fourier Transform Microwave Spectroscopy of Doped Helium Clusters**, this handbook).

2.6 Optical Setup

The molecular density in a molecular expansion is usually low and the absorption path very short, with respect to conventional cell measurements. One way of increasing the absorption in a jet is the so-called multipass setup, which consists of passing the laser beam several times through the supersonic expansion, possibly all at the same angle with respect to the flow velocity of the molecules and in the same (small) volume. Several schemes have been used, but we discuss only the most popular ones.

The most straightforward setup uses two flat parallel mirrors to pass the laser beam almost perpendicularly through the expanding jet (Figure 3a). This method is simple, but its main drawback is that the successive laser crossings are at increasing distances from the nozzle and hence probe different densities and populations at different temperatures.

A very interesting scheme has been proposed by Kaur *et al*. (1990), which consists of two concave mirrors at a distance that is slightly less than four times their focal length (Figure 3b). The laser beam is focused at the center of the cavity with a lens (or mirror) with a larger focal length than that of the two cavity mirrors and is refocused on every pass in a very small volume that intersects the molecular beam. The most advantageous configuration is the one where all successive passes are squeezed in a horizontal plane perpendicular to the flow

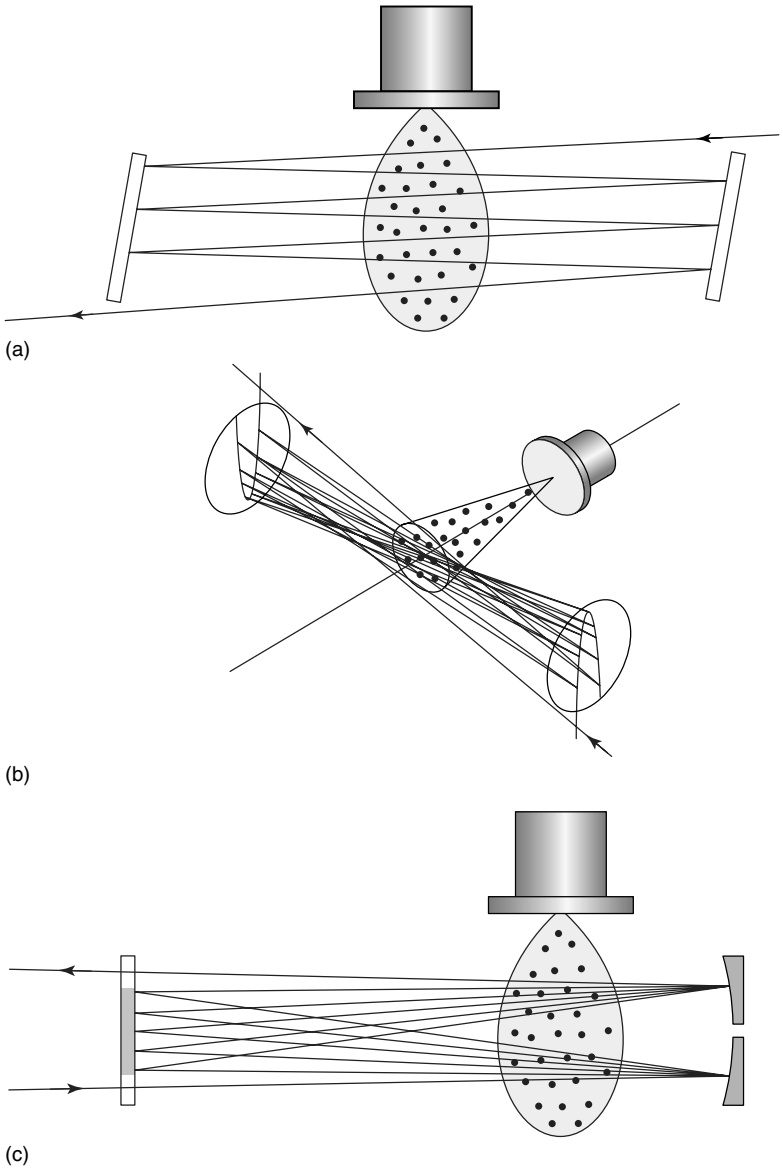

Figure 3 Three different optical multipass setups used in combination with molecular jets: (a) two plane parallel mirrors; (b) two concave mirrors; and (c) White-type optics.

velocity of the jet. The alignment of this configuration is rather troublesome and requires some expertise (and patience) because of the difficulty to refocus the out-coming beam on the detector. Nevertheless, this setup has been successfully used to measure the ν_6 fundamental of CF_2Cl_2 (Snels and Meerts 1988). The third scheme is based on compact White-type optics (White 1942). The incoming laser beam is only softly focused with a 1–2 m focal length mirror on the entrance of the White cell and is refocused several times on the field mirror by two concave mirrors at a distance of about 150 mm. Here, the familiar White cell pattern is formed and eventually a modestly diverging laser beam is focused onto a detector with an off-axis parabolic mirror. The interesting thing is that close to each of the two focusing mirrors, all odd (respectively even) passes cross in a very small volume (less than $2 \times 2 \times 20\,\text{mm}^3$). The nozzle is placed close to one of the focusing mirrors and a very good orthogonal crossing of the laser with the molecular jet can be obtained (Figure 3c). The number of crossings for each setup is typically 15–20, taking into account that in the flat-mirror setup, the successive crossings are less effective due to the decreasing density further from the nozzle. The main advantages of the White configuration with respect to the confocal mirror setup are the better optical stability and the possibility to vary the number of passes without changing the direction of the output beam (see also the details of the ETH Zürich setups described in Figures 7 and 8).

2.7 Cavity Ring Down (CRD) Spectroscopy in Supersonic Jets

As an alternative to multiple pass setups, which allow at most 20–50 passes through the expansion, cavity ring down and cavity-enhanced spectroscopy have been used to measure absorption spectra in supersonic jets. Both techniques rely on the use of resonant cavities, consisting of two highly reflective mirrors (typically $R > 99.95\%$), resulting in an increase of the effective absorption path length by a factor of several thousands. A key development was the combination of pulsed jets with continuous wave (cw) tunable near-infrared diode lasers for high-resolution CRD spectroscopy by Hippler and Quack (1999). The combination of high-resolution cw lasers (1 MHz bandwidth and better) with pulsed jets is nontrivial because for narrow bandwidths of the laser radiation the cavity has to be matched to the laser wavelength. When the gas pulse arrives, the resonance matching is lost because of the change of the index of refraction. This difficulty has been overcome by the Zürich group with a random wobble technique for one of the mirrors (He *et al*. 1998, Hippler and Quack 1999). These authors recorded very weak rovibrational lines of the $\nu_1 + \nu_3$ band of nitrous oxide near $7780\,\text{cm}^{-1}$, (HF) stretching overtones in $(HF)_2$ (Hippler *et al*. 2007), as well as an overtone level of the methane icosad (Hippler and Quack 2002). Tam *et al*. (2006) used a cw tunable lead-salt diode laser to measure the absorption of the CH-stretching band of methane in a supersonic jet. Other groups employed pulsed tunable lasers to investigate molecules and clusters in a supersonic-jet expansion. The group of Richard Saykally investigated a number of polycyclic aromatic hydrocarbons (PAHs) in the CH-stretching region (Schlemmer *et al*. 1994). They used a Nd : YAG-pumped dye laser to generate tunable pulsed visible radiation, which was then shifted by three Stokes shifts to produce infrared radiation with a bandwidth of $0.2\,\text{cm}^{-1}$, which could be reduced to $0.04\,\text{cm}^{-1}$, by using an intracavity etalon in the dye laser (Huneycutt *et al*. 2004). Bisson *et al*. (2007) generated pulsed tunable infrared laser radiation by difference frequency generation and recorded absorption spectra of the $\nu_1 + \nu_3$ and $2\nu_3$ bands of several SiH_4 isotopomers expanded in argon, helium, and hydrogen.

Ito and Nakanaga (2002) recorded CRD spectra of the formic acid dimer, including the OH stretching mode. The authors propose different mechanisms to explain the broad spectral features observed. *See also* Havenith and Birer 2011: **High-resolution IR-laser Jet Spectroscopy of Formic Acid Dimer**, this handbook.

CRD spectroscopy requires accurate mode matching and spatial filtering of the laser modes, in order to obtain single exponential decays. Other varieties of CRD-type spectroscopy exist with less strict requirements. One of these is the so-called cavity-enhanced absorption spectroscopy (CEAS). In the CEAS method, the optical cavity and laser wavelength are modulated in order to obtain many resonances, producing an almost continuous wavelength transmission with a long effective optical path length. Berden *et al*. (1999) used this CEAS technique to measure the absorption spectrum of ammonia in the 1.5 μm region in a supersonic seeded jet. The technique of Hippler and Quack (1999) has been successfully extended to the spectroscopy of ions by Birza *et al*. (2002).

2.8 Supersonic Jets Versus Alternative Techniques

The main advantages of doing absorption spectroscopy in a supersonic jet are the following. First, the efficient cooling of the internal degrees of freedom narrows the rotational distribution by populating only the lowest rotational energy levels and also removes population from most of the excited vibrational levels, transferring the population to the ground vibrational level. This leads to a significant reduction in the

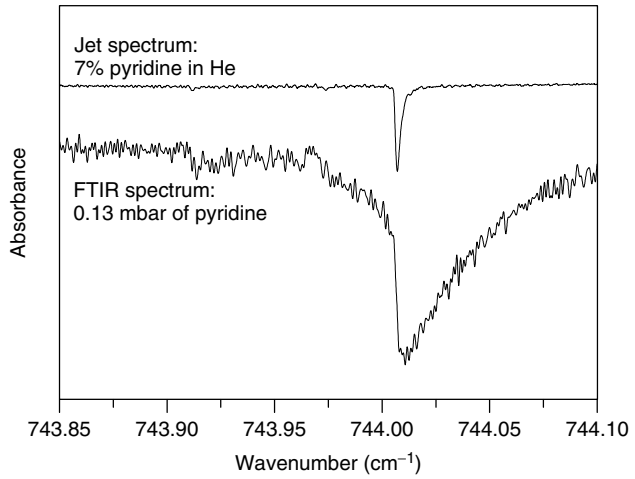

Figure 4 Pyridine, ν_4 band, Q-branch; upper trace: experimental diode laser slit-jet spectrum, expansion of 7% pyridine in He. Lower trace: FTIR spectrum, 0.13 mbar, $T = 298$ K, resolution 0.001 cm^{-1}, path length = 18 cm (jet spectrum measured at ETH Zürich by Horká-Zelenková, FTIR spectrum by Albert).

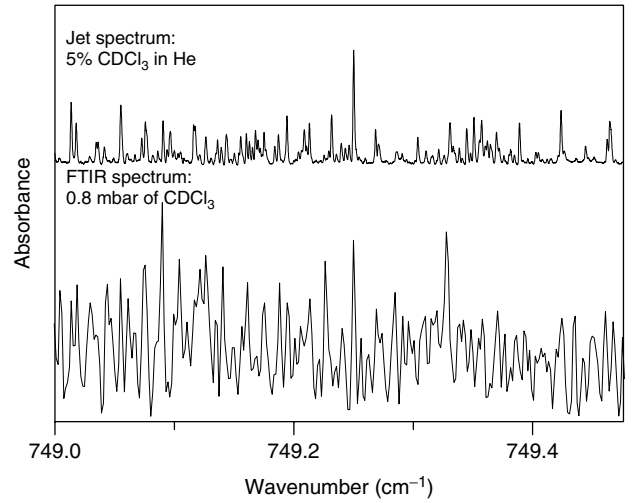

Figure 5 $CDCl_3$, ν_5 band; upper trace: experimental diode laser slit-jet spectrum, expansion of 5% $CDCl_3$ in He. Lower trace: FTIR spectrum, 0.8 mbar, $T = 298$ K, resolution 0.001 cm^{-1}, path length = 18 cm (spectra measured at ETH Zürich).

number of spectral lines of hot bands and makes assignment and spectral analysis much easier (Figures 4 and 5).

The same result is obtained, in principle, by cooling the gaseous sample in a conventional cold cell, down to the condensation limit. The problem of condensation is partly avoided by the collisional cooling technique, which uses a steady flow of cold gas (usually He or N_2) to cool down the absorbing molecules at low pressure (Bauerecker *et al*. 2001, Albert *et al*. 2007). Eventually, these molecules will condense on the cold cell walls, but as long as they are in the gas phase they will absorb radiation useful for spectroscopy.

The second advantage of the supersonic beam is the possibility to produce van der Waals clusters. This can also be done in a cold cell, but always within a limited temperature range, owing to the condensation limit. The collisional cooling technique is more difficult to apply for specific cluster production due to the low collision rates.

Radicals and ions can also be produced in drift tubes, using radio frequency techniques, but the temperature is usually very high (the rotational temperature is in the order of hundreds Kelvin), which renders the spectra complex and difficult to analyze (Gudeman and Saykally 1984, Sears 1987).

3 FTIR SPECTROSCOPY OF SUPERSONIC JETS: INSTRUMENTATION

The combination of high-resolution FTIR spectroscopy and cooling in supersonic expansions started in the 1980s. A survey of the basics of these two techniques and of the instrumentations developed in this field is given in the reviews by Quack (1990) and Herman *et al*. (2000), considering the main developments up to 2000. In a preliminary version of the Zürich group experiments, a jet setup was interfaced with a Bomem DA002 high-resolution spectrometer (Dübal *et al*. 1984). The jet assembly was placed outside of the spectrometer. The jet chamber was equipped with a circular nozzle of 100 μm diameter and was evacuated by means of a 3000 dm^3 s^{-1} oil diffusion pump backed by a 100 dm^3 s^{-1} roots pump and a 18 dm^3 s^{-1} rotary pump. By means of a transfer optical interface, the supersonic jet was crossed by the focused infrared beam in front of the nozzle. Spectra of CO_2 and CH_4, measured with apodized resolutions up to 0.006 cm^{-1}, revealed strong rotational cooling with effective rotational temperatures near 10 K in the supersonic expansions. These results encouraged further developments of this challenging technique.

In the second generation setup, the jet assembly was implemented into the sample compartment of the Bomem DA002 (Amrein *et al*. 1988b). A sketch of this arrangement is shown in Figure 6. The nozzle is positioned at a distance of a few millimeters in front of the focused infrared beam. An xyz translational stage allow for external adjustment of the nozzle position with respect to the infrared beam. In this version, there is no need for transfer optics to interface jet setup and spectrometer and therefore no light losses due to additional optical components and to their critical alignment. The pumping systems of the jet setup and of the spectrometer are completely separated. The latter consisted of a 14 m^3 s^{-1} oil diffusion pump and forepumps as in the

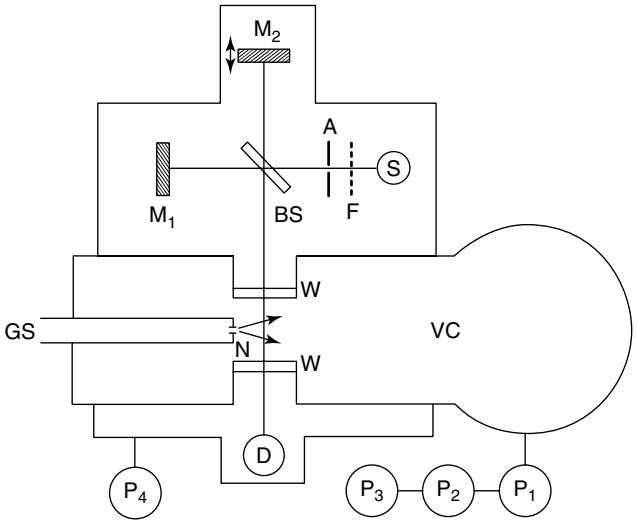

Figure 6 Sketch of FTIR-jet setup with jet equipment integrated in the spectrometer (After Amrein *et al*. 1988b). S, light source; F, optical filters; A, aperture; BS, beam splitter; M_1, fixed mirror; M_2, moving mirror; D, detector; GS, gas supply; N, nozzle; VC, vacuum chamber; W, window; P_1, oil diffusion pump; P_2, roots pump; P_3, rotary vane pump; and P_4, rotary vane pump.

first version. In typical experiments, stagnation pressures in the range 250–750 kPa were chosen, leading to residual (background) pressures in the jet chamber in the range 0.5–1.5 Pa when using circular nozzles of 100 or 150 μm diameter.

High-resolution rovibrational spectroscopy provides important information on the dynamics of coupled vibrational states and provides access to the modeling of short-time quantum dynamics in molecular systems. Supersonic-free jet expansions allow for the generation of molecules at low rotational and to a lesser extent vibrational temperatures. The combination of jet cooling with broad band FTIR spectroscopy provides a promising means to get access to a detailed analysis of complex rovibrational spectra. This was one of the main purposes in developing this challenging technique. A serious drawback of its application lies in the limited sensitivity due to the small absorption path length (in single path systems) and the low molecular densities in the detected region of the expansion. This limits the use of this technique to strong absorptions. Furthermore, because of less effective vibrational cooling, the simplification of the rovibrational structures in larger molecules is less effective due to the remaining contributions of hot-band spectra. A further limitation in the application of this technique lies in the need for large amounts of substance and in the requirements for large pumping power.

Sensitivity can be improved by using a multipass system, i.e., by increasing the absorption path length using optical tools. Several groups have reported such systems. Asselin *et al*. (1996) introduced a multireflection setup, which is similar to the White optics known from long-path gas cells. McNaughton *et al*. (1994) developed a multireflection setup based on a star-shaped arrangement of the light beams. A multipass system based on multiple reflections between two spherical mirrors was developed by Petry *et al*. (2002). A recently reported setup for investigating jet-cooled molecules, named *FANTASIO* (Herman *et al*. 2007), includes a multipass system closely analogous to the system by Petry *et al*. (2002).

We have developed a multipass accessory for our jet setup. Because of space limitations in the sample compartment of the spectrometer, we built a third-generation FTIR-jet setup with multipass optics and jet assembly located outside of the spectrometer. The main parts of this new version are sketched in Figure 7. We completely separated spectrometer and jet setup and therewith minimized mechanical couplings and distortions the very sensitive spectrometer may suffer from.

A casting containing the components of the optical interface is connected to the right port beam output of the Bomem DA002. This interface is based on $f/4$ optics similar to the optics of the spectrometer. It focuses the infrared beam into a newly designed jet assembly that contains a multipass system based on White optics. The design of this part is sketched in Figure 8. It consists of a plane mirror M_1 for the light input, three spherical mirrors M_2, M_3, and M_4 of the White system, and finally a plane mirror M_5 for the beam output. This design is strictly similar to the original multipass optics of White (1942). The radii of the spherical mirrors corresponding to the distance between the objective mirrors M_2, M_4, and the field mirror M_3 are chosen to be 5.1 cm. This short distance allowed for a compact construction of the multipass system and a straightforward combination with parts of the previous version as the casting containing gas inlet and nozzle positioning equipment. Furthermore, the short distance between the mirrors keeps the path of the light beam outside the jet region, and therewith the fraction of signals due to warm background molecules relatively small. The aperture images on the mirrors M_1, M_3, and M_5 form a row of equally spaced spots. The nozzle is positioned such that the jet passes a few millimeter above the spot row. The number of passes may be altered in steps of four by tilting of the mirror M_4. The maximum number of passes is limited by the diameter of the spots and by the length of mirror M_3 in the direction of the spot row. This length is chosen to be 1 cm. This choice proved to be a reasonable compromise in view of several drawbacks connected with a larger length, such as the d^{-2} drop of the molecular density in the expansion region, the larger fraction of warm spectra, the larger temperature span in the detected expansion region, and last but not the least, light

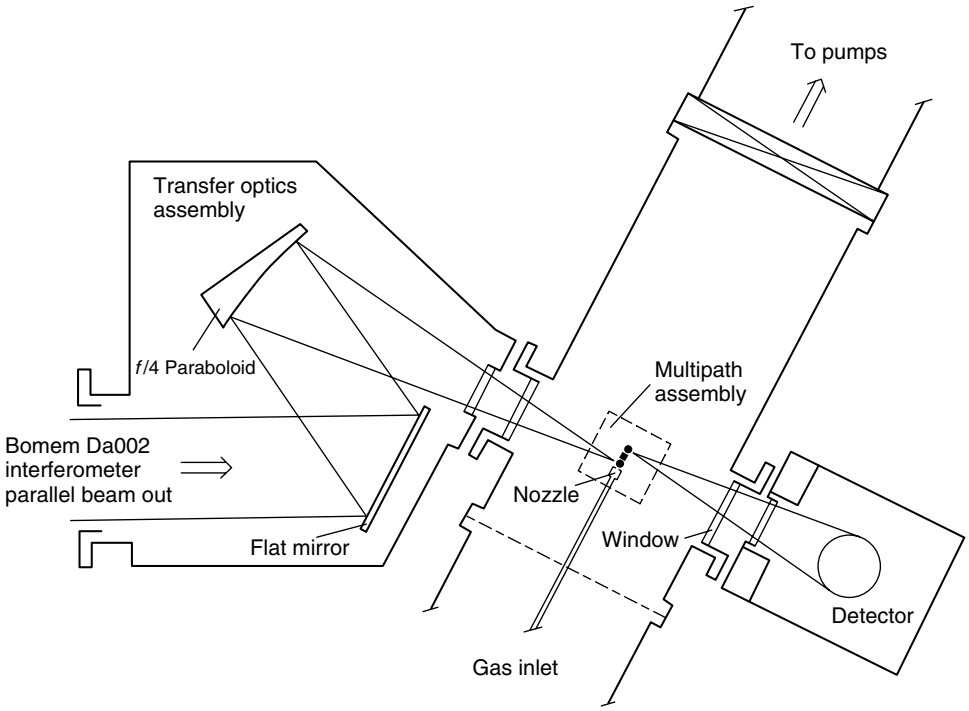

Figure 7 Sketch of FTIR-jet setup with jet equipment placed outside of the spectrometer and containing a multipass optics.

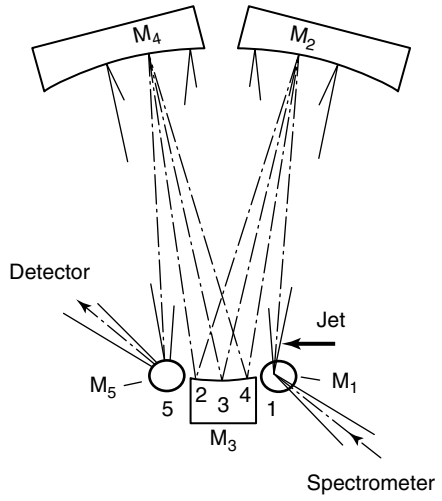

Figure 8 Jet multipass system. M_1, M_5, plane mirrors; M_2, M_3, M_4, spherical mirrors, radius 51 mm, diameter 25 mm.

losses due to critical alignment of the optical components. Good conditions were obtained with the number of passes set to 4 or 8.

The combination of supersonic jets with FTIR spectroscopy usually relies on continuous expansions, in contrast to laser spectroscopy, where mostly pulsed jets are used. Pulsed jets allow for a wider range of expansion conditions, which, for instance, is useful for the investigation of molecular clusters. The coupling of FTIR spectroscopy with pulsed nozzles requires complex techniques in order to properly synchronize jet pulsation with the data acquisition of the interferograms. Jet pulsation is operated typically with a repetition rate of 50 Hz and a pulse width of about 2 ms, whereas the data-acquisition rate for a measurement in the mid-infrared region typically amounts to 15 798 Hz (derived from He–Ne laser fringes, corresponding to a mirror speed of $0.5\,\mathrm{cm\,s^{-1}}$). A technique that uses an asynchronously pulsed supersonic jet in conjunction with an FTIR spectrometer was developed and applied in an investigation of HF-stretching spectra in HF clusters in our laboratory (Luckhaus *et al*. 1995). Preliminary measurements were made with NH_3, N_2O, and CH_4 in the mid-infrared region in order to test the applicability of this technique. Extended model calculations simulating the pulsed operation were performed for a synthetic interferogram corresponding to an artificial spectrum containing two lines on one hand and for a manipulated interferogram of the ν_2 band of NH_3 on the other. The results revealed that artifacts occurring in single scan experiments tend to cancel rapidly during the averaging process even for a small number of scans. In the case of the ν_2 band of NH_3, averaging over four scans leaves minor artifacts though the main features of the spectrum are clearly recognizable, and averaging over 64 scans reproduces the original (unmanipulated) spectrum almost perfectly. The possibilities of this technique merit further exploitation.

4 INFRARED LASERS FOR SUPERSONIC-JET SPECTROSCOPY

4.1 Mid-infrared Lasers

The mid-infrared spectral region (2–30 μm or about 300–5000 cm^{-1}) provides a broad field for various spectroscopic applications because it covers the fundamental vibrational modes of many polyatomic molecules except for very low frequency modes. For such spectroscopic measurements, an appropriate laser source has to be selected. The demands on such sources depend on the application. Usually broad tuning (emission), cw tuning, and sufficient optical power are required. The output power is usually in a range of microwatts to milliwatts except for CO and CO_2 lasers, which emit up to kilowatts of optical power in cw operation. A narrow linewidth is important for high measurement sensitivity and selectivity. The ideal laser also has single longitudinal mode behavior and small beam divergence. Moreover, compactness, robustness, and room temperature operation are important for in situ applications. Currently, various mid-infrared sources exist. They can be distinguished according to their active laser medium into gas, semiconductor, and solid-state lasers, which directly generate mid-infrared radiation or are based on nonlinear optical paramagnetic frequency conversion of near-infrared laser sources (Tittel *et al*. 2003). The most frequently applied lasers for supersonic-jet techniques are semiconductor lasers.

4.1.1 Semiconductor Lasers

Lead-salt diode lasers, quantum cascade lasers (QCLs), and antimonide lasers belong to this class, which are direct laser sources sharing some common features, for instance, laser cooling and similar collimation optics (Werle *et al*. 2002).

Lead-salt Diode Lasers

Lead-salt diode lasers consist of various nonstoichiometric binary alloys of the Pb compounds with IV–VI elements of the periodic table. These lasers can emit infrared light from 3 to 30 μm according to their composition and are commercially available for about 500–3300 cm^{-1}. Laser light is generated by electron–hole recombination in the p–n junction of n-doped and p-doped semiconductors. The optical resonator is formed by cleaved facets. Electron and holes drift toward the depletion region on the interface between n and p semiconductors where they recombine. Electrons occupy the bottom of the conduction band and are separated from the holes present in the valence band by the band-gap energy. The photon created by the electron–hole recombination has an energy that corresponds to the band-gap size. The band gap of the lead-salt lasers is narrow (i.e., the energy separation of the conduction and valence band is small), leading to a thermal population of the conduction band at room temperature. To prevent this effect, lead-salt lasers are typically cooled in a cryostat either by liquid nitrogen or by helium. The emission wavelength of the laser changes with its temperature. Fine tuning of the wavelength can be obtained by modulating the current applied to the diode laser. Depending on the tuning rate in terms of $cm^{-1}\,mA^{-1}$, an elevated stability of the injected current may be required. During the continuous wavelength tuning, mode hops may occur, which implies that the laser may emit more than one wavelength at the same time. In multimode operation of a laser, simultaneous oscillation on many modes can be observed. The transition from single mode to multimode operation can be discrete, but more continuous transitions can also be observed with the optical power being gradually redistributed. One may also obtain mode hops to higher order modes, or mode hops between modes with different polarization in lasers with polarization-independent gain. To select one wavelength during multimode operation of the laser, dispersive elements, such as a grating, can be used. Lead-salt diode lasers can be usually tuned around 100 cm^{-1} by varying the temperature and injected current. At a fixed temperature, a continuous tunability of about 0.5–2 cm^{-1} can be obtained by injection current modulation. Lead-salt diode lasers also exhibit quite strong beam divergence and astigmatism, which considerably complicate the alignment of the laser beam, in particular when multipass optics are used. This can be overcome partially by implementing special optical elements (e.g., parabolic mirrors for compensating for the beam divergence). For more information about lead-salt diode lasers, see the review from Brassington (1995) and the article by Sigrist (2011): **High-resolution Infrared Laser Spectroscopy and Gas Sensing Applications**, this handbook.

Antimonide Diode Lasers

Lasers based on III–V semiconductors emit in a region between 2 and 5 μm (2000–5000 cm^{-1}). The first successful mid infrared laser was based on InGaAsSb double heterostructure (DH)-active region grown by liquid epitaxy, operating at room temperature and emitting at 2.2 μm (Caneau *et al*. 1985). Lately, the material quality and, hence, the performance of the lasers have been improved by using molecular beam epitaxy (MBE). Because the DH-active region limits the device's performance, such as high threshold current, low output power, and low maximum operating temperature, quantum well (QW) structures were used in the active region of the laser, which improve these properties. A QW acting as a potential well is a very

thin middle layer where the vertical variation of the electron's wavefunction, and thus a component of its energy is quantized. Lasers containing more than one QW layer are known as *multiple QW lasers*. Multiple QWs improve the overlap of the gain region with the optical waveguide mode. These lasers dispose of relatively high-optical output power up to 20 mW in comparison with lead-salt diode lasers. Antimonide QW diode lasers emitting light at 2–3 μm usually can operate at room temperature and in cw regime. Sources operating at 3–5 μm usually require operation at reduced temperature. For more details, see reviews from Joullié *et al*. (2003) and Yin and Tang (2007).

Quantum Cascade Laser (QCL)

The QCL operates between 3 and 15 μm (about 700–3300 cm^{-1}), which includes the so-called atmospheric window absorption as well as the "fingerprint" range of the infrared and thus can be a powerful tool for applications in this spectral range. After 15 years of development, QCLs are now available for cw operation at room temperature and have high optical output power. They demonstrate a large tuning range of up to 400 cm^{-1} (Hugi *et al*. 2009). On the other hand, they, like all semiconductor lasers, have quite large beam divergence and astigmatism. The main difference between QCLs and standard interband lasers is the cascading principle. The QCL is formed by 20–40 identical periods. An electron injected from one side passes through the first period, emits a photon, and is injected into the following period. Thus, one electron can emit more photons before leaving the structure. Moreover, no holes are involved in either electron transport or photon emission. However, the internal quantum efficiency is lowered due to the presence of nonradiative scattering mechanisms. One period is a nonperiodic alternating sequence of thin layers of two different semiconductors, several nanometers thick. Different values of the band gap of the two semiconductors provide the conduction band profile that forms multi-QWs in the direction perpendicular to the layers (growth direction). The quantum confinement gives rise to the intersubbands whose energy can be tailored by changing the QW/barrier thicknesses. The laser emission wavelength is determined by the subband spacing and, therefore, can be directly changed by changing the layer thicknesses. The electrons are injected into the upper state (subband) of the laser transition by resonant tunneling through the thick (injection) potential barrier. It undergoes radiative transitions from the upper subband to the lower subband, emitting the excessive energy in the form of photons. The electrons tunnel away through another potential (extraction) barrier and are injected into the upper state of the next period. The population inversion necessary for the lasing action is ensured by long upper and short lower lasing state lifetimes. The electron lifetimes can be tailored by the proper design of the active region. The main drawback of this approach is the fast carrier's nonradiative relaxation from the higher states (subbands) due to longitudinal optical (LO) phonon-assisted scattering, which decreases the radiative efficiency due to the depletion of the upper lasing state, thus lowering the electron inversion. For a more detailed description of the QCLs and their operation characteristics, design, and their application, see Hofstetter and Faist (2003), Capasso *et al*. (2000) and Faist *et al*. (1994a,b). An application of QCLs for infrared spectroscopy of jet-cooled molecules and complexes is reported by Xu *et al*. (2009).

4.1.2 Difference Frequency Generation (DFG) and Optical Parametric Oscillator (OPO)

DFG is based on parametric frequency conversion of near-infrared sources. The nonresonant optical setup includes two laser beams (pump and signal). The emission of the pump laser at higher frequency is combined with a second laser emission (signal) with a lower frequency, in order to generate a different frequency (idler) in a nonlinear optical material such as $LiNbO_3$ and periodically poled lithium niobate (PPLN). Since the idler wave is build up when the beams pass through a nonlinear material, all three waves must stay in phase. Tuning of the idler wave is performed by tuning the pump, signal beam, or both together. The optical parametric oscillator (OPO) uses nonlinear optical material in a resonant cavity to generate two laser beams (idler and signal) from one pump laser beam. The cavity can be resonant for either idler or signal beam, or for both. Optical parametric generation is a second-order nonlinear process and is less efficient than DFG. An OPO can operate in the pulsed regime from picosecond to femtosecond timescales or in cw mode. As mentioned above, DFG and OPO laser sources are based on nonlinear optical parametric frequency conversion of near-infrared laser sources and can operate in a spectral range up to 2 μm. Their operation depends on spectral and spatial properties of the lasers used for generation and also on properties of the nonlinear material. Frequently used lasers for these techniques are Nd : Yag, Ti : sapphire, external cavity diode laser (ECDL), and, for DFG, OPOs can also be used as pump or signal lasers. Mid-infrared nonlinear materials and some of their optical characteristics for DFG and OPO applications are summarized in reviews by Ebrahimzadeh (2003) and Fischer and Sigrist (2003) (*see* Sigrist 2011: **High-resolution Infrared Laser Spectroscopy and Gas Sensing Applications**, this handbook). Very recent developments of high-power cw OPOs allow for very high resolution Doppler

free double resonance spectroscopy in the infrared (Dietiker *et al.* 2010).

4.1.3 CO_2 and CO gas laser

The CO_2 laser operates in the 9.2–10.8 μm range and is characterized by high output power. The laser can be tuned on discrete levels of the emission spectrum of CO_2. The gas mixture in a CO_2 laser consists of CO_2, N_2, and He. The N_2 molecule is excited by an electrical discharge to a metastable long-lived state and transfers its energy by collisions to an excited vibrational state of CO_2, thus creating the population inversion necessary for the stimulated emission of photons. The lower vibrational states of CO_2 are successively depopulated through collisions with He atoms. For more details, see Patel (1965), Witteman (1967), and Repond and Sigrist (1996). By substituting the $^{12}CO_2$ by $^{13}CO_2$ or by other CO_2 isotopomers, a dense manifold of laser emissions on discrete wavelengths can be generated in the 9–12 μm range (Freed *et al.* 1980). In addition, N_2O (Herlemont *et al.* 1979) can be used to produce laser emissions in the 10.4–11 μm range. Although the CO_2 laser is essentially a line tunable laser, several possibilities exist for using it as a continuously tunable laser. In the high-pressure pulsed (TEA) CO_2 laser, the gain profile is pressure broadened, allowing for an almost continuous tuning in the range 900–1100 cm^{-1}, although with a linewidth of about 2 GHz, which can be reduced by using an intracavity prism to about 250 MHz (Duarte 1985 and Repond and Sigrist 1996). A higher resolution can be obtained by using a CO_2 waveguide laser, which can be tuned over typically 1 GHz, with a linewidth better than 1 MHz (Olafsson and Henningsen 1995). A third option is to use a GaAs waveguide modulator to create side bands on the CO_2 laser line emissions up to a few gigahertz from the line center (Cheo 1994). The CO laser emits in the spectral range 5–6.5 μm. By using the overtone emission of CO, the 2.5 μm range can also be covered (Utkin *et al.* 2006). This laser works similarly to the CO_2 laser. With respect to the CO_2 laser, the CO laser offers only discrete line tunability, but has higher efficiency. This efficiency increases with decreasing gas temperature. Because of this, this laser requires more sophisticated cooling.

4.2 Near-infrared Lasers

The near-infrared region (0.8–2 μm or 5000–12 000 cm^{-1}) is almost completely covered by tunable diode lasers. Compared to the lead-salt diode lasers used in the mid-infrared, the NIR diode lasers do not require cooling, and being operated at ambient temperature, they have found many applications in medicine and telecommunications. The most commonly used diode lasers (Fabry Perot lasers) are DH lasers.

In these devices, a layer of low band-gap material is sandwiched between two high band-gap layers. One commonly used pair of materials is gallium arsenide (GaAs) with aluminum gallium arsenide ($Al_xGa_{(1-x)}As$). Each of the junctions between different band-gap materials is called a *heterostructure* and, hence, the name *double heterostructure laser* or *DH laser*.

The advantage of a DH laser is that the region where free electrons and holes exist simultaneously, the active region, is confined to the thin middle layer. This means that many more of the electron–hole pairs can contribute to amplification. Relatively few are located in the poorly amplifying periphery. In addition, light is reflected from the heterojunction; hence, the light is confined to the region where the amplification takes place. Typical dimensions of these emitting regions are 2 μm × 500 μm. The DH lasers are multimode lasers and emit several modes simultaneously. The tuning can be performed by temperature and current variations and can be as much as 100 nm. Lately, vertical cavity surface emitting diode lasers (VCSELs) have been developed, which have a short cavity, thus limiting the multimode character and a very small emitting surface (5 × 5 μm typically). Single mode tunable lasers can be obtained by introducing wavelength-selecting devices inside or outside the diode laser structure. In a distributed feedback (DFB) laser, a diffraction grating is etched close to the p–n junction of the diode. This grating acts like an optical filter, causing a single wavelength to be fed back to the gain region and lase. Since the grating provides the feedback that is required for lasing, reflection from the facets is not required. In the distributed Bragg reflection (DBR) lasers, the selective regions are combined with gain regions. Both DFB and DBR lasers are single mode lasers and can be temperature tuned, typically over few (3–10) nm. They have output powers of 10–100 mW and a linewidth of 3–10 MHz typically (Buus *et al.* 2005).

The ECDL uses an external grating to construct a selective cavity around a Fabry–Perot laser, which has an antireflection coating applied to one surface. Several configurations (Littrow, Littman/Metcalf) are commercially available and produce a single mode output of typically 10 mW, with a linewidth better than 1 MHz and a tunability up to 150 nm (see, for example, http://www.santec.com).

The gain medium determines the wavelength of the emitted radiation; 750–1000 nm for AlGaAs, 1.2–2.0 μm for InGaAsP. The most popular wavelengths are those used for medical applications (850–980 nm) and in telecommunication (1.31 and 1.55 μm). The Zürich group had built a homemade temperature-controlled laser of this kind in

the 1980s when these lasers were not yet available commercially, but later this laser was replaced by the more powerful laser from Radians-Innova (Ha *et al*. 1995, He *et al*. 1995). The International Telecommunication Union has defined the so-called ITU grid, which covers the O, E, S, C, and L bands (1260–1625 nm), with a spacing of 100 GHz (about 0.8 nm). Recently, a second series with a spacing of 50 GHz has been introduced. Single mode DFB lasers covering the ITU grid are commercially available and are often used for high-resolution spectroscopy in the NIR. Commercial external cavity lasers cover the range from 760 to 1050 nm and from 1260 to 1680 nm. Often the linewidth of these lasers is far below the Doppler width of a molecule at room temperature. This implies that the Doppler line shape and width of an absorption line can be measured with high accuracy, allowing one to determine the temperature with a high precision from the linewidth, as can be seen in Figure 9. Thus, high-resolution laser spectroscopy of isolated spectral lines can be used as an in situ "thermometer" both for bulk samples and for supersonic jets (He *et al*. 2007).

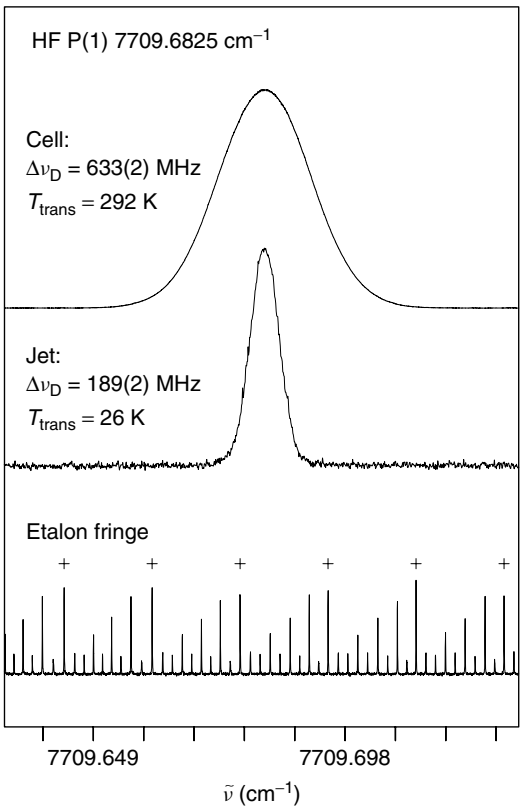

Figure 9 Spectral line of the first HF-stretching overtone transition of HF monomer measured in an absorption cell at room temperature (upper trace) and in a supersonic-jet expansion (middle trace); the bottom trace shows the etalon signal. [Reproduced from He *et al*. 2007 by permission.]

5 AN OVERVIEW OF FTIR SPECTROSCOPIC SUPERSONIC-JET INVESTIGATIONS

An early review of the work of the Zürich group has been given by Quack (1990). A literature review dedicated to FTIR absorption spectroscopy of jet-cooled species covering also the period subsequent to the early developments up to the year 2000 was included in the review article of Herman *et al*. (2000). In Table 1, we present an updated review, which we have restricted to high-resolution investigations. We mention the following research groups active in this field with particular topics: the Université Libre de Bruxelles (hydrocarbons (Lee *et al*. 2007, Hurtmans *et al*. 2001, Lafferty *et al*. 2006, Flaud *et al*. 2001)); Université de Rennes (small clusters (Thiévin *et al*. 2006)), Monash University (fluorohydrocarbons (Thompson *et al*. 2003)); Université Pierre et Marie Curie, Paris (XY_4 and XY_6 spherical tops (Asselin *et al*. 2008, Rey *et al*. 2001), clusters (Asselin *et al*. 2006, 2007)); and our group at ETH Zürich (simple molecules and spherical tops, methane (Dübal *et al*. 1984, Amrein *et al*. 1988a,b), ammonia (Snels *et al*. 2006a), substituted methanes (D'Amico *et al*. 2002), XY_6 spherical tops and Jahn–Teller molecules (Boudon *et al*. 2002), fluoro(hydro, chloro)carbons, hydrogenfluoride clusters, and other applications (Snels *et al*. 1995, Luckhaus *et al*. 1995, He *et al*. 2007, Hippler *et al*. 2007)) and chiral molecules (Beil *et al*. 1994, Bauder *et al*. 1997) see also Albert and Quack (2007), Albert *et al*. (2011), and Quack (2011).

The large spectral coverage combined with strong rotational cooling makes the FTIR-jet technique an ideal means to investigate complex rovibrational band systems of stable species. The analysis of such spectra provides access to accurate spectroscopic parameters of the states involved and, in particular, to vibrational and rovibrational coupling parameters that are of great importance for the understanding and modeling of time-dependent quantum dynamics and processes such as intramolecular vibrational and rotational vibrational redistribution (Marquardt and Quack 2001, Quack and Kutzelnigg 1995). In Table 2 we give a survey of the investigations performed in our laboratory using the FTIR-jet technique, including also the further recent work not reviewed in Quack (1990), Herman *et al*. (2000). The listing in Table 2 contains information about the species investigated, relevant spectrometer settings, and jet parameters, the main focus of the study, and the band systems analyzed. Instructive examples demonstrating the high value of this method are the anharmonically coupled $\nu_1, 2\nu_5$ band system of CF_3I, the ν_3, ν_8 Coriolis resonance band system of $CHClF_2$, and the tunneling doublets of the bending fundamentals of the ammonia isotopomers NH_2D and ND_2H. We discuss

Table 1 High-resolution FTIR investigations of molecular species in supersonic jet expansions. Literature review from the year 2000 up to the present.

Species	Spectral range (cm^{-1})	Resolution (cm^{-1})	T_{rot} (K)	Band(s) investigated band center(s) (cm^{-1})	References
NH_2D	1150–1750	0.01	70–100	$\nu_{4a}(s)$, 1605.6404 $\nu_{4a}(a)$, 1591.0019 $\nu_{4b}(s)$, 1389.9063 $\nu_{4b}(a)$, 1390.4953	Snels *et al.* (2006a)
ND_2H				$\nu_{4a}(s)$, 1233.3740 $\nu_{4a}(a)$, 1235.8904 $\nu_{4b}(s)$, 1461.7941 $\nu_{4b}(a)$, 1461.9918	
N_2O	Near 2200	0.0043	22 3	$R(0)$ line of ν_3, line profile analysis vib-vib energy transfer between v_2 states of N_2O and OCS	Didriche *et al.* (2007) Herman *et al.* (2005)
CF_2Cl_2	450–1450	0.004	60	$\nu_3 + \nu_7(^{35}Cl_2)$, 888.49689 $\nu_3 + \nu_7(^{35}Cl,^{37}Cl)$, 883.20389	D'Amico *et al.* (2002)
C_2H_2	700–1400	0.0043	6–7	ν_5, 729.163 $\nu_4 + \nu_5$, 1328.081	Lee *et al.* (2007)
	3270–3310			ν_3, 3281.899 $\nu_2 + \nu_4 + \nu_5$, 3294.839	
C_2H_4	700–2400	0.005	50	ν_{12}, 1442.44270 $\nu_7 + \nu_8$, 1888.97823 $\nu_6 + \nu_{10}$, 2047.775832	Hurtmans *et al.* (2001)
CF_3CH_2F	Near 1000	0.0035	65	ν_6, 1104.532116	Thompson *et al.* (2003)
$(CH_3)_2O$	Near 1000	0.005	70	ν_6, 933.9066 ν_{21}, 1103.951	Coudert *et al.* (2002)
	Near 2800			ν_{17}, 2817.385	
CH_3CHCH_2	Near 950	0.005	80	ν_{18}, 990.77605 ν_{19}, 912.66776	Lafferty *et al.* (2006)
$CH_3CH_2CH_3$	1300–1500	0.005	80	ν_{19}, 1338.965 ν_{18}, 1376.850 ν_{24}, 1471.874 ν_4, 1476.710	Flaud *et al.* (2001)
C_6H_6, CH_3OH	Near 3000	0.015	20–25	CH stretch region, tests of experimental setup	Georges *et al.* (2002)
$Ni(CO)_4$	1950–2100	0.006	25	ν_5, 2061.30937	Asselin *et al.* (2008)
$V(CO)_6$	1960–2020	0.01	13	ν_6, 1994.48, band profile analysis	Rey *et al.* (2001)
WF_6	Near 720	0.0024	50	$\nu_3(^{182}W)$, 714.53819 $\nu_3(^{183}W)$, 714.21406 $\nu_3(^{184}W)$, 713.89544 $\nu_3(^{186}W)$, 713.26621	Boudon *et al.* (2002)
ReF_6	Near 700	0.1, 0.5		ν_3; very complex spectrum (combined with diode laser study)	Boudon *et al.* (2002)
H_2S-HF D_2S-DF	Near 3700 Near 2700	0.05, 0.02	20	ν_s(HF stretch), 3724.29 ν_s(DF stretch), 2734.46	Asselin *et al.* (2006)
H_2S-HCl	Near 2750	0.02, 0.05	12	$\nu_s(H^{35}Cl$ stretch), 2755.23 $\nu_s(H^{37}Cl$ stretch), 2753.15	Asselin *et al.* (2007)
D_2S-DCl	Near 2000			$\nu_s(D^{35}Cl$ stretch), 1993.88 $\nu_s(D^{37}Cl$ stretch), 1991.05	
Ar-CO_2 CO_2-CO_2	2250–2400	0.01, 0.05	6, 9	$\nu_{as}(CO_2)$, 2348.6738 $\nu_{as}(CO_2)$, 2350.7716	Thiévin *et al.* (2006)
$CFCl_3$	800–1100			Combined with diode laser spectra	Snels *et al.* (1995, 2001)

Table 2 High-resolution FTIR investigations of species in supersonic jet expansions. Investigations performed at ETH Zürich including, in part, combinations with diode laser spectroscopy.

Species	Spectral range (cm^{-1})	Resolution[a] (cm^{-1})	p_o[b] (10^5Pa)	p_r[c] (Pa)	T_{rot} (K)	Subject	References
CO_2	Near 2350	0.006	1.6	0.5	11	ν_2, rot. cooling	Dübal *et al.* (1984)
CH_4	Near 3030	0.006	2.0	0.5	12	ν_3, nuclear spin relaxation	
CF_3Cl	1050–1250	0.004	4.2–4.5	0.8	35	ν_1, $\nu_1 + \nu_6 - \nu_6$ and ν_4, bands rot. analysis and vibr. cooling	Amrein *et al.* (1987a)
CO	2050–2230	0.004	6.75	0.9	6–13	Fundamental band, rot. cooling	Amrein *et al.* (1988b)
NO	Near 1880	0.004	6.50	0.6	17	Transitions in $^1\Pi_{\frac{1}{2}}$ and $^2\Pi_{\frac{3}{2}}$ el. states relaxation of electronic degree	
CH_4	2960–3140	0.004	7.50; 2.75	0.7; 0.9	11; 36	ν_3 band, nuclear spin relaxation	
C_2H_2	3180–3365	0.01	2.40	1	31	Fermi doublet ν_3, $\nu_2 + \nu_4 + \nu_5$, rot. cooling, evidence for dimers and nuclear spin conservation	
CH_3CCH	3230–3435	0.015	2.50	1.5	50	ν_1 fundamental and hot bands, rot. and vibr. cooling	
CF_3H	Near 1100	0.004	2.75	1	40	ν_2, ν_5, $\nu_3 + \nu_6$ Coriolis–Fermi–Triad	
	2960–3140	0.008	3	1	<100	band system in ν_1 region Simplification of complex spectra	
$CHClF_2$	1030–1380	0.004	2.3	0.8	50	ν_3 and ν_8 bands, rot. analysis	Amrein *et al.* (1988a)
	2870–3175	0.018	2.37	0.75	50	ν_1 band, Q-branch features	
N_2O	Near 1300	0.004	4.2	7.5	26	ν_1, $\nu_1 + \nu_2 - \nu_2$, rot. and vibr. cooling	Amrein *et al.* (1989)
CF_3Br	1020–1280	0.004	2.46	7.0	45	ν_1, rot. analysis, $\nu_1 + \nu_6 - \nu_6$, rot. analysis and vibr. cooling	
CF_3I	920–1280	0.004	2.4		50	ν_4, rot. analysis	

(*continued overleaf*)

Table 2 (*Continued*).

Species	Spectral range (cm^{-1})	Resolution[a] (cm^{-1})	p_o[b] (10^5Pa)	p_r[c] (Pa)	T_{rot} (K)	Subject	References
CF_3I	Near 1100	0.005	2.4		45	ν_1 band system, vib. rot. analysis including $\nu_1, 2\nu_5^0$ and $\nu_3 + 3\nu_6^{-3}$	Bürger *et al.* (1989)
					60	ν_1 band system, vib. rot. analysis including $\nu_1, 2\nu_5^0$, $\nu_3 + 3\nu_6^{\pm1}$ and $\nu_3 + 3\nu_6^{\pm3}$	Hollenstein *et al.* (1994)
						ν_1 band system, vib. rot. analysis including in addition $2\nu_5^{\pm2}$	He *et al.* (2002)
$CHCl_2F$	700–1300	0.004	1.10	0.8	70	ν_3, ν_7 and ν_8, rot. analysis	Snels and Quack (1991)
NO_2, N_2O_4	700–1800	0.0024	4–7[d]	0.15–1[d]	20[d], 100[e]	rot. analysis of ν_9, ν_{11} and Q-branches of resonance doublet ν_{12}, $\nu_6 + \nu_{12}$ of N_2O_4	Luckhaus and Quack (1992)
CCl_3F	1050–1120	0.0024	1.1	0.8	80	ν_1, rot. analysis	Snels *et al.* (1995)
SPF_3	Near 1000	0.0024	2.2	0.6	80	ν_1, rot. analysis	Bürger *et al.* (1996)
CHBrClF	Near 1100	0.0024	0.5	1.0–1.3	100	ν_4, rot. analysis	Bauder *et al.* (1997), Beil *et al.* (1994)
WF_6, ReF_6	650–780	0.0024	2	4	50	ν_3 of WF_6, rot. analysis ν_3 Q-branch of ReF_6, profile at lower resolution	Boudon *et al.* (2002)
CF_2Cl_2	450–1450	0.004	4.0	10	100	$\nu_3 + \nu_7$, rot. analysis	D'Amico *et al.* (2002)
NH_2D, ND_2H	1150–1750	0.01	4.0	10	70–100	Bending fundamentals ν_{4a} and ν_{4b} both *s*- and *a* tunneling components	Snels *et al.* (2006a)

[a] Values of 0.004 and 0.0024 cm^{-1} corresponding to maximum apodized and unapodized resolution, respectively, of the Bomem DA002.
[b] Stagnation pressure.
[c] Residual pressure in jet chamber.
[d] Seeded in Ar.
[e] Neat substance.

these three examples in the following sections. In the first two cases, FTIR-jet spectra were used in the initial step of the analysis, yielding a first set of assignments and parameters, which later on formed the basis for the analysis of spectra at higher temperatures. For a summary of results specially directed at chiral molecules, we refer to Quack (2011) in this handbook.

6 DISCUSSIONS OF SPECIFIC MOLECULAR EXAMPLES

6.1 Ammonia Isotopomer Spectra

High-resolution spectroscopy of ammonia is of fundamental interest in relation to vibration–rotation tunneling dynamics. Recent interest has been concentrated on full-dimensional potential and electric dipole hypersurfaces as well as quantum wave packet dynamics (*see* Marquardt and Quack 2011: **Global Analytical Potential Energy Surfaces for High-resolution Molecular Spectroscopy and Reaction Dynamics**, this handbook). Furthermore, ammonia is an important pollutant in the Earth's atmosphere and has been detected in planetary atmospheres and interstellar clouds. In this context, the partially deuterated species NH_2D and ND_2H are particularly noteworthy (see Snels *et al*. (2006a) and references cited therein for the above-mentioned applications).

The investigation of the bending vibrations of NH_2D and ND_2H (Snels *et al*. 2006a) was part of a systematic high-resolution analysis of the infrared spectra of deuterated ammonia isotopomers in the range of the fundamental vibrations (Snels *et al*. 2000, 2003, 2006b). Figure 10 shows a graphical survey of the fundamentals of the various NH_nD_m species and the correlation between them. While for the symmetric isotopomers NH_3 and ND_3, the proper symmetry group for the vibration–inversion–rotation problem is a group isomorphous to D_{3h}, the symmetry is reduced for the partially deuterated species NH_2D and ND_2H to a group isomorphous to C_{2v}. The bending fundamentals, which are degenerate in the case of the symmetric isotopomers, are split into two components. Considering the large values of the rotational constants giving rise to largely extended rotational structures, furthermore the tunneling effects due to the inversion barrier, and the fact that in the case of the mixed H/D isotopomers, we have to deal with isotopic mixtures rather than pure isotopic species, the region of the bending fundamentals (1100–1800 cm^{-1}) of the mixed species appears extremely crowded in spectra taken at room temperature. Rotational cooling in supersonic expansions combined with FTIR spectroscopy was, therefore, chosen as the ideal technique in order to unravel and

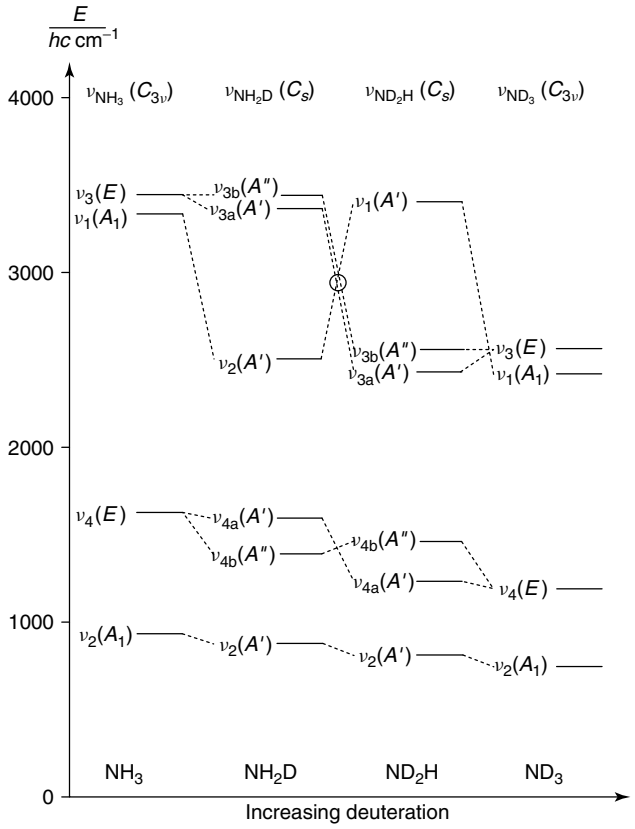

Figure 10 Survey and correlation of vibrational fundamentals for H/D ammonia isotopomer. [Reproduced from Snels *et al*. 2006a, by permission.]

analyze this complex region. Because of the large amount of substance needed in continuous jet experiments, we did not scan the spectra with the maximal available spectral resolution of our FTIR spectrometer (Bomem DA002, 0.004 cm^{-1} FWHM, apodized), but reduced it to 0.01 cm^{-1}. Furthermore, we used our multipass jet setup described in Section 3. The measurement of different isotopic mixtures obtained by mixing NH_3 and ND_3 in ratios 1 : 2 and 2 : 1 then allowed us to identify and assign line structures to the distinct tunneling components of the bending fundamentals of NH_2D and ND_2H. Peaks due to these isotopomers were sorted out and were used to establish corrected ("cleaned-up") line spectra from the peak files where only those peaks were retained that could be definitely associated with NH_2D and ND_2H, respectively. Absorptions due to residual H_2O and isotopic species being particularly strong in this spectral region were also eliminated by this procedure. Figure 11 shows a measured and a cleaned-up spectrum in the 1310–1470 cm^{-1} region in comparison with a calculated spectrum obtained with best-fit parameters for a rotational temperature of 100 K.

The calculations were based on Watson-type Hamiltonians for the vibration–inversion states up to sextic terms,

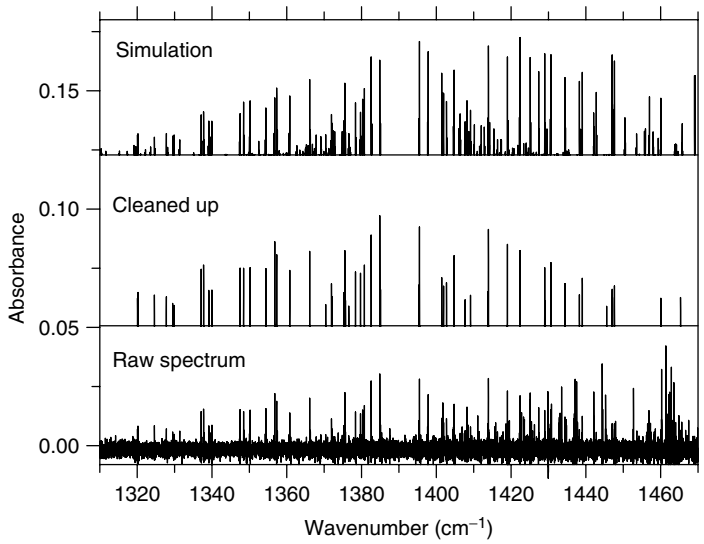

Figure 11 Survey jet spectrum of NH_2D in the 1310–1470 cm^{-1} range; upper trace: simulation of the ν_{4b} fundamental band of NH_2D, using best-fit parameters and an effective rotational temperature $T_{rot} = 100$ K; middle trace: cleaned up spectrum, see text for details; lower trace: raw spectrum as measured by FTIR spectroscopy of the supersonic-jet expansion. [Reproduced from Snels *et al*. 2006a. © American Institute of Physics, 2006.]

and an inversion–rotation interaction Hamiltonian given by

$$\hat{H}_{01} = F(\hat{J}_x\hat{J}_z + \hat{J}_z\hat{J}_x) + F_J\hat{J}^2\left(\hat{J}_x\hat{J}_z + \hat{J}_z\hat{J}_x\right) + F_K\left[\hat{J}_z^2\left(\hat{J}_x\hat{J}_z + \hat{J}_z\hat{J}_x\right) + \left(\hat{J}_x\hat{J}_z + \hat{J}_z\hat{J}_x\right)\hat{J}_z^2\right] \quad (18)$$

The fitting procedure yielded reliable values for about 20 spectroscopic parameters for each fundamental. The term values obtained are listed in Table 3. Increased inversion splittings in the case of ν_{4a} of ND_2H and a strongly increased splitting and an inverted order of the two inversion levels in the case of ν_{4a} of NH_2D were traced to Fermi resonance interactions involving the overtone $2\nu_2$ of the inversion vibration.

The term values of the vibrational-tunneling levels allow us to draw conclusions on the mode-selective interplay of fundamental vibrational excitations with the inversion-tunneling dynamics. In Table 4, we give for all fundamentals of the mixed isotopomers a listing of the tunneling times for stereomutation defined by

$$\tau_{L\to R} = \frac{1}{2\,c\Delta\tilde{\nu}} \quad (19)$$

The results obtained from the rotational analysis of the bending fundamentals of NH_2D and ND_2H completes the data set for the fundamental absorptions in all H/D isotopic species, providing a benchmark for comparisons with calculations using full-dimensional electric dipole and potential energy hypersurfaces for ammonia (Marquardt and Quack 2011: **Global Analytical Potential Energy Surfaces for High-resolution Molecular Spectroscopy and Reaction Dynamics**, this handbook, Lin *et al*. 2002, Marquardt *et al*. 2005). Furthermore, the completed spectroscopic data base is of importance for spectroscopic observations of

Table 3 Tunneling term values of the bending fundamentals of NH_2D and ND_2H.

		T_s (cm^{-1})	T_a (cm^{-1})
NH_2D	ν_{4a}	1605.6404	1591.0019
	ν_{4b}	1389.9063	1390.4953
ND_2H	ν_{4a}	1233.3740	1235.8904
	ν_{4b}	1461.7941	1461.9918

(from Snels *et al*. (2006a)

Table 4 Summary of tunneling times $\tau_{L\to R}$ (in picoseconds) for NH_2D and ND_2H ground states and fundamentals.

	NH_2D		ND_2H	
	$\tilde{\nu}$(cm^{-1})	$\tau_{L\to R}$ (ps)	$\tilde{\nu}$(cm^{-1})	$\tau_{L\to R}$ (ps)
ν_0	0	41	0	98
ν_1	2506	27	3404	214
ν_2	886	0.83	815	1.8
ν_{3a}	3366	7.1	2433	4.4
ν_{3b}	3439	99	2560	107
ν_{4a}	1598	1.1	1235	6.6
ν_{4b}	1390	28.1	1462	84

(After Snels *et al*. (2006a))

ammonia isotopomers in planetary atmospheres and interstellar clouds.

6.2 $CHClF_2$

Chlorodifluoromethane (CFC22) attracted our attention as an important system for the investigation of intramolecular redistribution dynamics and related topics (Albert *et al.* 2004, Quack 1990, Marquardt and Quack 2001, 2011: **Global Analytical Potential Energy Surfaces for High-resolution Molecular Spectroscopy and Reaction Dynamics**, this handbook, and references cited therein). Rovibrational spectroscopy provides important information for the understanding and modeling of such processes. This molecule represents a particularly interesting system for the investigation of the effects of vibrational and rovibrational interactions since most of its fundamentals are involved in anharmonic and/or rovibrational (Coriolis) resonances. This is illustrated in Figure 12, which shows a diagram of the vibrational levels in the region below 1450 cm^{-1} grouped according to coupling polyads. The diagram reveals that the only isolated levels in this range are the fundamental ν_5 and to some extent its overtone $2\nu_5$.

The CF-stretching fundamentals ν_3 and ν_8 are very close in energy and are involved in a strong Coriolis resonance. This band system was considered to be an appropriate case for the investigation of the effects of Coriolis coupling in low-symmetry asymmetric tops (point group C_s). Furthermore, this band system lies in the atmospheric window for infrared radiation and since $CHClF_2$ is known to be a relevant atmospheric trace gas, the analysis of this band system is also of interest in this context.

The rovibrational analysis of this Coriolis resonance band has been subject of a number of investigations. The first analysis was based on FTIR-jet spectra obtained in our laboratory using the Bomem DA002 high-resolution spectrometer operated at the maximum apodized resolution of 0.004 cm^{-1} and using expansion conditions resulting in a rotational cooling down to about 50 K (Amrein *et al.* 1988a). Figure 13 shows a part of the ν_3 fundamental, illustrating the effect of rotational cooling and the good agreement between FTIR-jet spectrum and model calculation.

This first high-resolution study formed a valuable basis for the analysis of spectra measured at room temperature under Doppler-limited conditions at ETH-Zürich using the Bruker 125HR Zürich prototype interferometer (maximum unapodized resolution 0.0007 cm^{-1}) (Albert *et al.* 2004). To unravel and fit the largely increased data set, additional interactions affecting particular regions of the spectrum turned out to be important. The additional perturbers were found to be the combination levels $\nu_6 + 2\nu_9$ and $3\nu_9$.

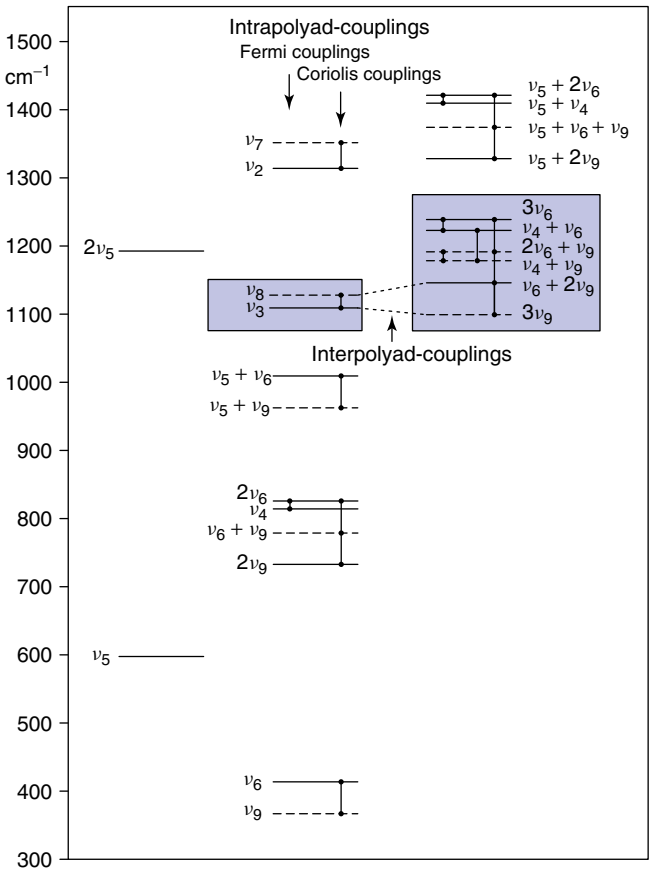

Figure 12 Vibrational levels of $CH^{35}ClF_2$ below 1450 cm^{-1} grouped according to polyads. [After Albert *et al.* 2010.]

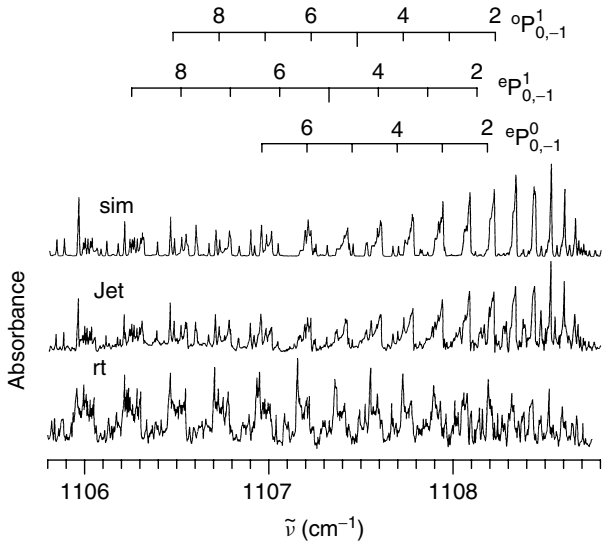

Figure 13 Part of the ν_3 fundamental of $CHClF_2$. Simulated spectrum in comparison with supersonic-jet FTIR spectrum and room temperature FTIR spectrum. [Reproduced from Amrein *et al.* 1988a. © Elsevier, 1988.]

A closer inspection of the levels in the neighborhood of the ν_3, ν_8 dyad revealed that these perturbers belong to a Coriolis–Fermi polyad, including the six levels $3\nu_6$, $2\nu_6 + \nu_9$, $\nu_6 + 2\nu_9$, $3\nu_9$, $\nu_4 + \nu_6$, and $\nu_4 + \nu_9$. A related Coriolis–Fermi polyad including the levels $2\nu_6$, ν_4, $\nu_6 + \nu_9$, and $2\nu_9$ was applied in a recent rovibrational analysis of the region of the ν_4 fundamental (Albert *et al.* 2006). Couplings within the polyads (intrapolyad couplings) are defined to arise from the first-order terms of the usual expansion of the vibration–rotation Hamiltonian, which are (Papoušek and Aliev 1982)

$$\hat{H}_{30} = \frac{1}{6} \sum_{l,m,n} k_{lmn} q_l q_m q_n \tag{20}$$

giving rise to Fermi resonances, and

$$\hat{H}_{21} = -2 \sum_{k,l} \left(\frac{\omega_l}{\omega_k} \right)^{1/2} q_k \hat{p}_l \sum_{\alpha} B_\alpha \zeta_{kl}^{\alpha} \hat{J}_\alpha \tag{21}$$

giving rise to Coriolis resonances. Interactions between polyads (interpolyad couplings) are due to higher order terms of the expansion. The polyad structure in the low-energy region of this molecule is illustrated in Figure 12.

A revised analysis of the ν_3, ν_8 band system (Albert *et al.* 2010) was based on this extended polyad model and on a combination of our previous data set (Albert *et al.* 2004) and of the set of a closely analogous investigation performed at the Monash University, Australia (Thompson *et al.* 2004). The effective rotational Hamiltonians used in this treatment are diagonal operators of the Watson-type according to the A-reduction scheme and off-diagonal operators for the couplings between the levels v' and v given by

$$\hat{H}_{\text{interaction}}^{v',v} = \langle v' | \hat{H}_{\text{interaction}} | v \rangle \tag{22}$$

where $\hat{H}_{\text{interaction}}$ are coupling operators $\hat{H}_{30}$ and $\hat{H}_{21}$. Figure 14 illustrates the structure (J-blocks) of the Hamiltonian matrix for the eight interacting levels.

In the final calculation, the data sets used comprised 10 402 transition wavenumbers for the isotopomer $CH^{35}ClF_2$ and 6522 for $CH^{37}ClF_2$. The fitting procedure yielded well-determined and physically reliable parameters of the polyad model, the root mean square deviations being $0.334 \times 10^{-3}\,\text{cm}^{-1}$ for the $CH^{35}ClF_2$ and $0.373 \times 10^{-3}\,\text{cm}^{-1}$ for the $CH^{37}ClF_2$ species (Albert *et al.* 2010).

6.3 $CHCl_2F$

The analysis of rovibrational fine structures of chlorofluorocarbons in the range 700–1400 cm^{-1} is of importance for the understanding of atmospheric infrared absorption. Fluorodichloromethane ($CHCl_2F$, CFC-21) reveals three fundamentals in this range: ν_3 near 1079 cm^{-1} (CF-stretching), ν_7 near 1239 cm^{-1} (CH-bending), and ν_8 near 807 cm^{-1} (Cl-stretching). Although $CHCl_2F$ is a molecule of modest complexity, spectra taken at room temperature appear extremely complex due to the presence of three isotopic species $CH^{35}Cl_2F$, $CH^{35}Cl^{37}ClF$, and $CH^{37}Cl_2F$, hot bands, and rotational congestion. The combination of supersonic-jet expansion with FTIR spectroscopy proved to be a particularly effective technique to investigate these bands. The simplification of the spectra due to rotational and vibrational cooling was of central importance in order to get access to a detailed rovibrational analysis. The measurements were performed using the continuous-flow supersonic-jet system as described in Amrein *et al.* (1988b) in combination with a Bomem DA002 high-resolution Fourier transform spectrometer, operated at the maximum available apodized resolution of 0.004 cm^{-1}. For the rotational analysis of all three fundamental bands, an effective S-reduced Watson-type Hamiltonian including terms up to quartic proved adequate. The explicit consideration of anharmonic and rovibrational interaction was not required for an adequate fitting, which yielded well- determined spectroscopic constants for all three fundamentals of the isotopomers: $CH^{35}Cl_2F$ and $CH^{35}Cl^{37}ClF$ (Snels and Quack 1991).

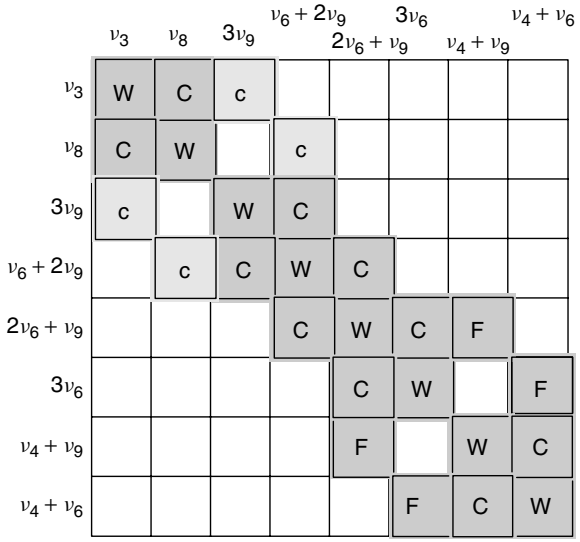

Figure 14 Analysis of the ν_3, ν_8 band system of $CHClF_2$. Block structure of Hamiltonian matrix (J-blocks) for the eight interacting levels. W: Watson blocks, F: Fermi resonance blocks, C: Coriolis resonance blocks, and c: blocks due to higher order Coriolis interactions (local interactions). [After Albert *et al.* 2010.]

6.4 CCl_3F

The CCl_3F molecule is important for the monitoring of the freon concentrations in the upper atmosphere, in relation to their ozone destruction and global-warming potentials. At room temperature, many vibrational levels are populated and give rise to hot-band absorptions. Heavy molecules also have small rotational constants, implying a dense manifold of rotational levels for each vibrational level. Hot bands and small rotational constants produce congested spectra with many overlapping absorption lines. In some cases, the presence of different isotopomers complicates the analysis of room temperature spectra even more. In traditional infrared spectroscopy, the spectrum of a molecule, such as CCl_3F, was considered "nonanalyzable" and its spectra resisted attempts of analysis in spite of its importance as one of the major atmospheric global pollutants. By using supersonic-jet-diode laser spectroscopy, rotational and vibrational temperatures can be reduced significantly, leading to a strong reduction of the number of the absorption lines observed. Furthermore, CCl_3F, because of the presence of three chlorine atoms, has four isotopomers of which the two major ones are evident in the spectrum ($C^{35}Cl_3F$, $C^{35}Cl_2^{37}ClF$). Analysis of room temperature and cold cell spectra was prohibitive, until diode laser slit-jet spectra were recorded with a resolution of about $0.0006\,cm^{-1}$. In the case of the parallel band ν_1, the analysis of three isotopomers was done ($C^{35}Cl_3F$, $C^{35}Cl_2{}^{37}ClF$ and $C^{35}Cl^{37}Cl_2F$), while the ν_4 perpendicular band was analyzed only for the symmetric top molecule $C^{35}Cl_3F$.

6.4.1 *Analysis of the ν_1 Band of CCl_3F*

Although cold cell spectra of CCl_3F were available in natural abundance and enriched in ^{35}Cl, analysis was prohibitive until supersonic-jet spectra were recorded (Snels *et al.* 1995, 2001). By using a pulsed slit expansion of 5% CCl_3F in He, a rotational temperature of about 20 K was achieved, and hot bands were efficiently cooled. The low temperature together with the sub-Doppler resolution (about $0.0006\,cm^{-1}$) produced well-resolved transitions of the three most abundant isotopomers ($C^{35}Cl_3F$, 43.1%; $C^{35}Cl_2^{37}ClF$, 41.3%; $C^{35}Cl^{37}Cl_2F$, 13.2%) (Figure 15). The first isotopomer is a symmetric top, and the other two are asymmetric tops. The assignment of the supersonic-jet spectra was straightforward and the analysis yielded accurate effective rotational constants. The unusual trend of the excited state rotational constants C in the three isotopomers indicates that the ν_1 band is perturbed by a nearby overtone or combination band ($\nu_4 + \nu_6$). This perturber might also be responsible for the absorption around $1085\,cm^{-1}$.

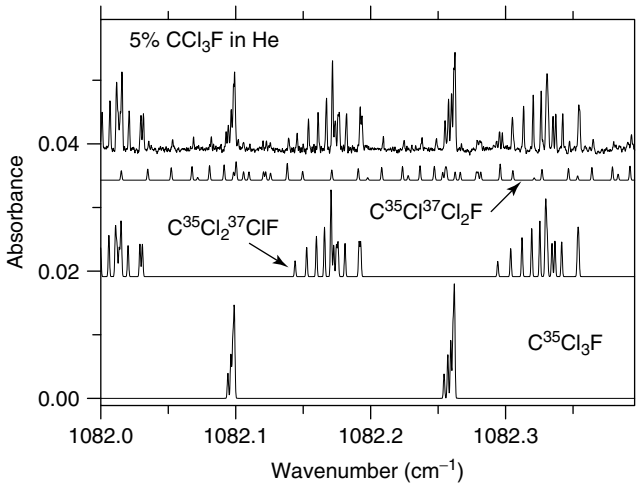

Figure 15 CCl_3F, ν_1 band; upper trace: experimental diode laser slit-jet spectrum, expansion of 5% CCl_3F in He; lower traces: Simulations of the contributions of the three most abundant isotopomers, using the molecular constants reported by Snels *et al.* (1995).

6.4.2 *Analysis of the ν_4 band of CCl_3F*

While the ν_1 band appeared as a very congested parallel band, with regular P-, Q-, and R-branches, the room temperature spectrum of the perpendicular band ν_4 has a peculiar structure, with very sharp peaks on the higher wavenumber side of the band origin and a unstructured low wavenumber side (Figure 16).

No plausible explanation was proposed to understand this unusual appearance, until the supersonic-jet spectra were measured and analyzed (Snels *et al.* 2001). The energy levels for a twofold degenerate vibrational mode of an

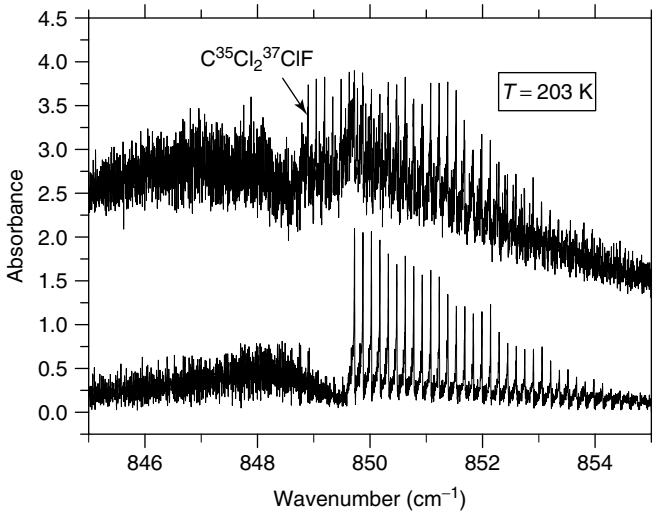

Figure 16 CCl_3F, ν_4 band, survey; upper trace: FTIR spectrum recorded for $T = 203$ K; lower trace: Simulation of $C^{35}Cl_3F$ using the molecular constants reported by Snels *et al.* (2001).

oblate symmetric top molecule are, up to quartic terms

$$\begin{aligned} E_v/hc = {} & \tilde{\nu}_0 + B_v J(J+1) + (C_v - B_v)k^2 \\ & - 2(C\zeta)_v kl + \eta_J^v J(J+1)kl + \eta_K^v k^3 l \\ & - D_J^v J^2(J+1)^2 - D_{JK}^v J(J+1)k^2 \\ & - D_K^v k^4 \end{aligned} \tag{23}$$

The expressions for $\Delta J = +1$ and $\Delta K = +1$ transitions, neglecting quartic terms, are

$$\begin{aligned} {}^{\mathrm{R}}R_K(J) = {} & \tilde{\nu}_0 + (C_0 + B_0) - 2(C\zeta)_v + 2B_0 J \\ & + 2[C_0 - (C\zeta)_v - B_0]K \\ & + \Delta B(J+1)(J+2) \\ & + (\Delta C - \Delta B)(K+1)^2 \end{aligned} \tag{24}$$

For $\Delta J = -1$ and $\Delta K = -1$ transitions, we have

$$\begin{aligned} {}^{\mathrm{P}}P_K(J) = {} & \tilde{\nu}_0 + (C_0 - B_0) - 2(C\zeta)_v - 2B_0 J \\ & - 2[C_0 - (C\zeta)_v - B_0]K \\ & + \Delta B J(J-1) \\ & + (\Delta C - \Delta B)(K-1)^2 \end{aligned} \tag{25}$$

If we assume that the Coriolis constant ζ in the Hamiltonian is close to 1, we can show that ${}^{\mathrm{R}}R$ and ${}^{\mathrm{P}}P$ transitions form regular clusters for $K = J - \Delta$, where $\Delta = 0, 1, 2, 3, \ldots$

$$\begin{aligned} {}^{\mathrm{R}}R_{K=J-\Delta}(J) = {} & \tilde{\nu}_0 + (C_0 + B_0) - 2(C\zeta)_v \\ & - 2\Delta[C_0 - (C\zeta)_v - B_0] \\ & + \Delta C(\Delta - 1)^2 \\ & + \Delta B[2 - (\Delta - 1)^2] \\ & + 2[C_0 - (C\zeta)_v]J + \Delta C J^2 \\ & + \text{higher order terms} \end{aligned} \tag{26}$$

$$\begin{aligned} {}^{\mathrm{P}}P_{K=J-\Delta}(J) = {} & \tilde{\nu}_0 + (C_0 - B_0) - 2(C\zeta)_v \\ & + 2\Delta[C_0 - (C\zeta)_v - B_0] \\ & + \Delta C(\Delta + 1)^2 \\ & + \Delta B[2 - (\Delta + 1)^2] \\ & - 2[C_0 - (C\zeta)_v]J + \Delta C J^2 \\ & + \text{higher order terms} \end{aligned} \tag{27}$$

Thus, we find clusters of ${}^{\mathrm{R}}R_{K=J-\Delta}(J)$ transitions with a regular spacing of $2[C_0 - (C\zeta)_4 - B_0]$ between successive values of Δ and a progression of $(J, J - \Delta)$ lines within each cluster given by $2[C_0 - (C\zeta)_v]J + \Delta C J^2$. The ${}^{\mathrm{P}}P_{K=J-\Delta}(J)$ clusters behave in a similar way, but here the progression goes as follows $-2[C_0 - (C\zeta)_v] + \Delta C J^2$. For a negative value of $\Delta C = C_4 - C_0$, this implies that we have J-progressions to higher wavenumbers for ${}^{\mathrm{R}}R$ clusters with decreasing intervals between two adjacent transitions, eventually leading to a bandhead (Figure 17), and to lower wavenumbers for the ${}^{\mathrm{P}}P$ clusters, with increasing spacings for higher J.

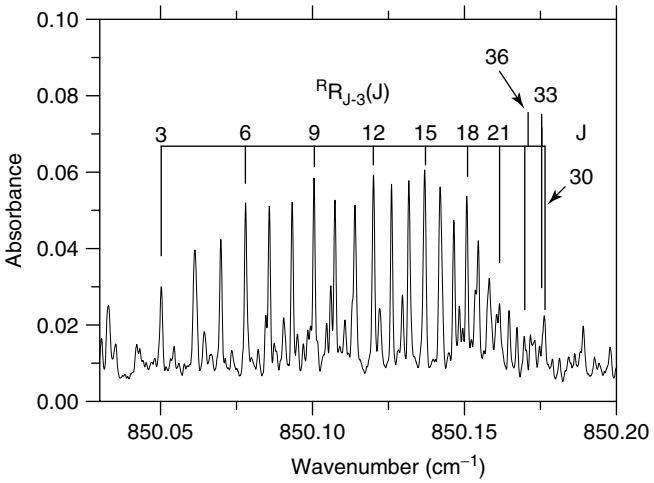

Figure 17 CCl_3F, ν_4 band, detail showing the band head occurring for the ${}^{\mathrm{R}}R_{J-3}(\mathrm{J})$ manifold; Diode laser spectrum reported by Snels *et al*. (2001).

In the room temperature spectra, the ${}^{\mathrm{R}}R$ clusters are observed as sharp peaks and the ${}^{\mathrm{P}}P$ clusters appear as broad structureless features.

A computer simulation at a tropospheric temperature (200 K) is in very good agreement with a cold cell (203 K) FTIR spectrum as can be seen in Figure 16. In the same figure, a second series of peaks can be observed, which is assigned to the $C^{35}Cl_2{}^{37}ClF$ isotopomer. Although the room temperature and cold cell FTIR spectrum show very similar structures for the two most abundant isotopomers, we should be aware that in one case ($C^{35}Cl_3F$) we have a symmetric top species, with one degenerate vibrational band and in the other case ($C^{35}Cl_2{}^{37}ClF$) an asymmetric top with two almost degenerate fundamental modes. The splitting between the two modes is estimated to be of the order of $1\,\mathrm{cm}^{-1}$ from ab initio calculations. The asymmetry splitting in the rotational structure becomes negligible for higher K quantum numbers, which explains the observation of sharp band heads in the FTIR spectra. In the diode laser jet spectra, we expect that the asymmetry splitting plays an important role (as can be observed in the ν_1 fundamental) and tends to smear out the spectral structures.

6.5 CF_3I

An understanding of the detailed rovibrational structure of the ν_1 band system in the range 1060–1090 cm^{-1} (symmetric CF-stretching fundamental) is of interest for a variety of applications (see, for instance, He *et al.* (2002) and references cited therein). We emphasize its role as a prototype system for the investigation of infrared multiphoton excitation and laser chemistry for isotope separation using excitation by CO_2 laser radiation (Lupo and Quack 1987, He *et al.* 1995). The rovibrational structure of this band system reveals highly complex features due to couplings with neighboring levels, and in spite of many attempts, a complete understanding of this band complex is still not available. In the first high-resolution study based on room temperature static cell spectra, Fermi resonance interaction with the overtone $2\nu_5^0$ was taken into consideration (Bürger *et al.* 1985). A partial analysis was based on J-clusters rather than on line-resolved data. A decisive progress in the understanding of this band system was achieved by means of FTIR-jet spectra obtained in our laboratory (Bürger *et al.* 1989). The strong rotational cooling in the supersonic expansion ($T_{rot} = 45 \pm 15$ K) allowed for a more detailed analysis and evidenced anharmonic interaction with the combination level $\nu_3 + 3\nu_6^{-3}$, in addition to the Fermi resonance with $2\nu_5^0$, to be important in order to achieve a better modeling of the perturbed rovibrational features. However, distinct regions of the ν_1 band system still remained unexplained.

A further step forward was possible by the measurement of slit-jet diode laser spectra using a spectrometer setup built in our laboratory (Hollenstein *et al.* 1994), yielding well-resolved spectra in distinct spectral windows in the region between 1073 and 1083 cm^{-1}. Furthermore, we measured new FTIR-jet spectra corresponding to an effective rotational temperature of 60 K. With the help of the new data, the consideration of further levels and interactions turned out to be important for an adequate description. The additional levels are $\nu_3 + 3\nu_6^{+3}$ (anharmonically coupled to ν_1) and $\nu_3 + 3\nu_6^{\pm 1}$ (Coriolis interaction with ν_1, local perturbation at level crossings). Figure 18 shows the supersonic-jet FTIR spectrum in comparison with the calculated spectrum in the central regions of the ν_1 and $2\nu_5^0$ systems, and Figure 19 gives an illustrative detail of the slit-jet diode laser spectrum and calculated spectrum.

In the next step undertaken in order to get further insight into this complex system, we obtained new slit-jet diode laser spectra of CF_3I (neat and seeded in He) at rotational temperatures of 7, 30, and 70 K (He *et al.* 2002). In an extended description, anharmonic coupling between the levels $\nu_3 + 3\nu_6^{-3}$ and $\nu_3 + 3\nu_6^{+3}$ proved relevant and perturbations arising from $2\nu_5^{\pm 2}$ turned out to be important. The model for the description of the complex ν_1 band system now includes a polyad with eight excited levels, which are ν_1, $2\nu_5^0$, $2\nu_5^{\pm 2}$, $\nu_3 + 3\nu_6^{\pm 1}$, and $\nu_3 + 3\nu_6^{\pm 3}$. Figure 20 gives a survey of the vibrational and rovibrational interactions and couplings considered in the modeling. Furthermore, Figure 21 shows a diagram of reduced energies in the critical region defined by

$$E_{red}(J, K', v, l) = E(J, K', v, l) - hc \left[B_0 J(J+1) + (A_0 - B_0) K^2 \right] \tag{28}$$

The quantum number K' is equal to K for ν_1 and the anharmonically coupled levels, but different from K for the rovibrationally coupled levels, fulfilling the selection rule

$$K' - K - \sum_i \Delta l_i = 0 \mod 3 \tag{29}$$

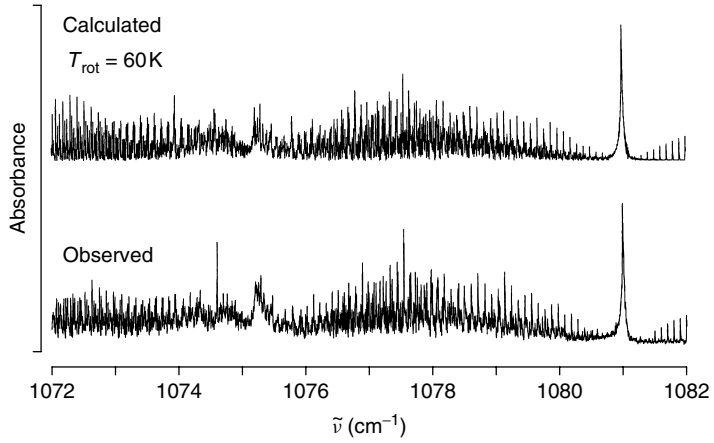

Figure 18 Supersonic-jet FTIR spectrum and calculated spectrum showing the central region of the ν_1 and $2\nu_5^0$ systems of CF_3I. [Reproduced from Hollenstein *et al.* 1994 by permission.]

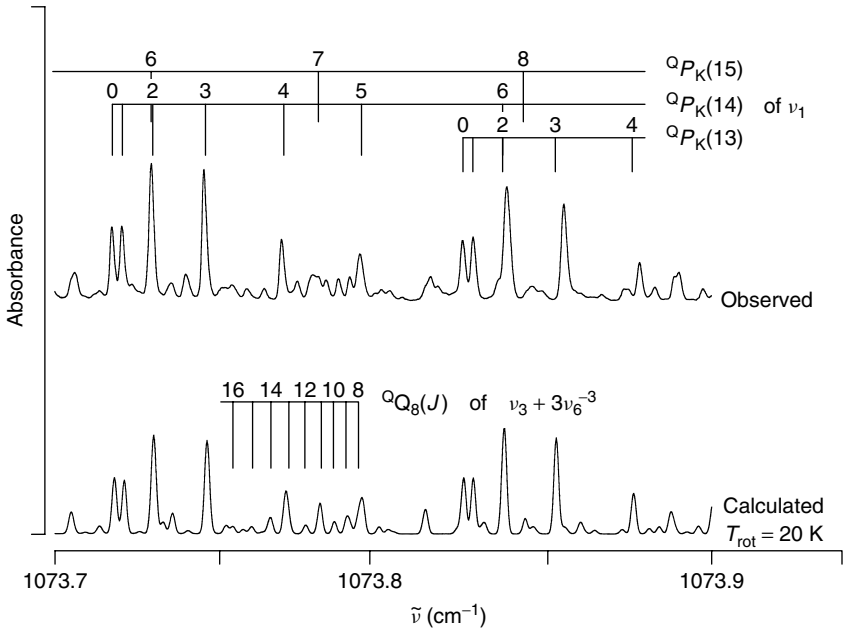

Figure 19 Slit-jet diode laser spectrum of CF_3I showing the region of the $^{Q}P(14)$ subbranch of ν_1. [Reproduced from Hollenstein *et al*. 1994. © Elsevier, 1994.]

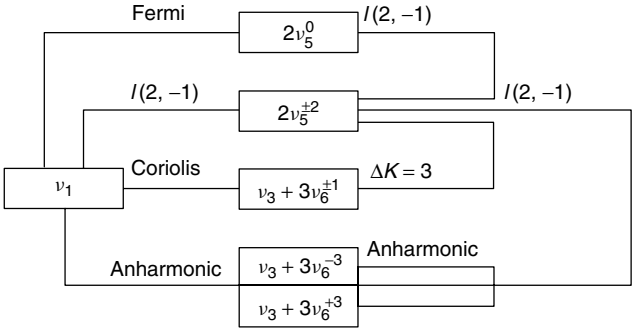

Figure 20 Coupling scheme applied in the analysis of the ν_1 band system of CF_3I.

For a given value of K, the diagram shows the relative positions of the levels, which may interact by virtue of this selection rule. The diagram includes further levels not belonging to the polyad considered, such as $\nu_3 + \nu_5^{-1} + \nu_6^{+1}$, which might influence the system by anharmonic interaction and might be included in the final step of the analysis, if additional spectral information and information from high-level ab initio calculations might become available in the future.

In distinct regions of the diode laser spectra, effects arising from nuclear quadrupole interaction due to the iodine nucleus ($I = \frac{5}{2}$) are clearly visible and turned out to be important for correctly assigning the spectra. We included quadrupole hyperfine interaction in our model taking into account the first-order terms (diagonal contributions):

$$E_Q = eQq \left(\frac{3K^2}{J(J+1)} - 1 \right) Y(J, I, F) \qquad (30)$$

where

$$Y(J, I, F) = \frac{\frac{3}{4}C(C+1) - I(I+1)J(J+1)}{2(2J-1)(2J+3)I(2I-1)} \qquad (31)$$

and

$$C = F(F+1) - I(I+1) - J(J+1) \qquad (32)$$

with $|J - I| \leq F \leq J + I$ in integer steps, and the usual quantum numbers J, K for rotational angular momentum, I for nuclear spin, and F for total angular momentum. We considered all allowed transitions according to the selection rule $\Delta F = 0, \pm 1$ in the simulation of the spectra. Figure 22 shows the P-subbranch region for low J quantum numbers of ν_1, revealing rather strong effects arising from nuclear quadrupole interaction. In the case of $^{Q}P(1)$, we could identify all three expected transitions. Figure 23 shows the FTIR-jet spectrum of the ν_1 band system for an effective rotational temperature of 60 K in comparison with a calculated trace using the eight-level polyad model.

6.6 $PFCl_2$

All the fundamentals of the $PFCl_2$ molecules lie below 1000 cm^{-1}. The two most abundant isotopomers $PF^{35}Cl_2$

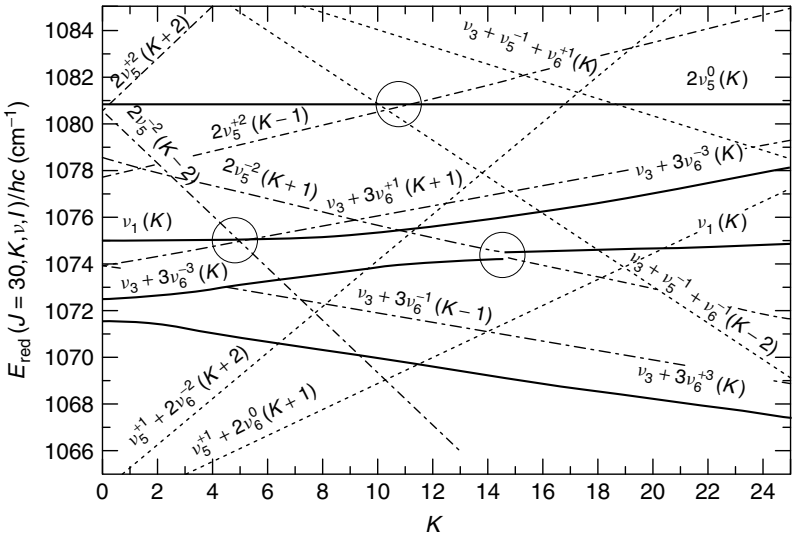

Figure 21 Diagram of reduced energies in the neighborhood of the ν_1 level of CF_3I, calculated for $J = 30$. The circles indicate observed crossings. [Reproduced from He *et al*. 2002 by permission.]

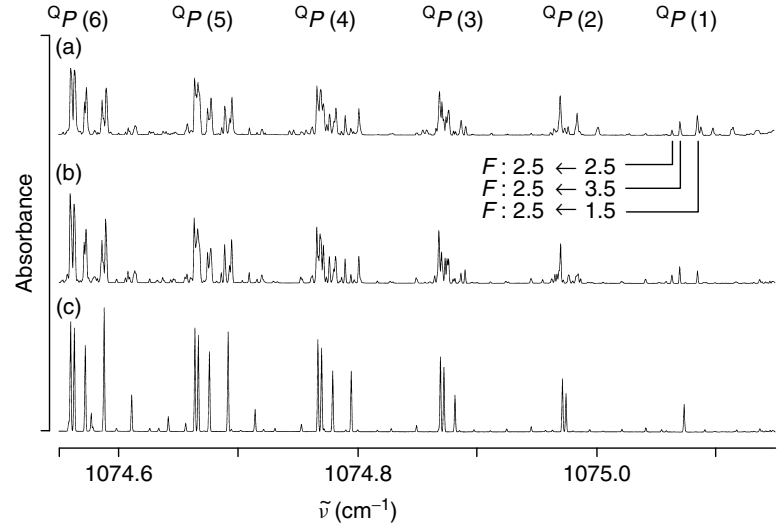

Figure 22 *P* subbranches for low *J* quantum numbers showing strong effects arising from nuclear quadrupole interaction. (a) Slit-jet diode laser spectrum, $T_{rot} \approx 7$ K. (b) Calculated spectrum including quadrupole interaction. (c) Calculated spectrum without quadrupole interaction. [Reproduced from He *et al*. 2002 by permission.]

(58%) and $PF^{35}Cl^{37}Cl$ (36%) dominate the spectra. The PF-stretching mode ν_1 has the band center at about $\tilde{\nu}_0 = 836.6\,cm^{-1}$ for $PF^{35}Cl_2$ and at about $\tilde{\nu}_0 = 835.5\,cm^{-1}$ for $PF^{35}Cl^{37}Cl$ (Horká *et al*. 2008). The absorption spectra of $PFCl_2$ have been measured with a diode laser spectrometer in a supersonic jet in the temperature range between 15 and 20 K and with a Bruker ZP 2001 prototype spectrometer (Albert and Quack 2007) with a resolution of $0.001\,cm^{-1}$ at room temperature.

Both isotopomers appear as asymmetric rotors. A Watson A-reduced effective Hamilton operator (Watson 1977) has been used for the analysis:

$$\begin{aligned}\hat{H}^v_{rot} = {} & A\hat{J}_a^2 + B\hat{J}_b^2 + C\hat{J}_c^2 - \Delta_J\hat{J}^4 - \Delta_{JK}\hat{J}^2\hat{J}_z^2 \\ & - \Delta_K\hat{J}_z^4 - \frac{1}{2}[\delta_J\hat{J}^2 + \delta_K\hat{J}_z^2, \hat{J}_+^2 + \hat{J}_-^2]_+ \\ & + \phi_J\hat{J}^6 + \phi_{JK}\hat{J}^4\hat{J}_z^2 + \phi_{KJ}\hat{J}^2\hat{J}_z^4 + \phi_K\hat{J}_z^6 \\ & + \frac{1}{2}[\varphi_J\hat{J}^4 + \varphi_{JK}\hat{J}^2\hat{J}_z^2 + \varphi_K\hat{J}_z^4, \hat{J}_+^2 + \hat{J}_-^2]_+ \end{aligned} \quad (33)$$

where $\hat{J}$ is the angular momentum operator with $\hat{J}^2 = \hat{J}_a^2 + \hat{J}_b^2 + \hat{J}_c^2$. $\hat{J}_\pm = \hat{J}_x \pm i\hat{J}_y$ and $[X,Y]_+$ represents the

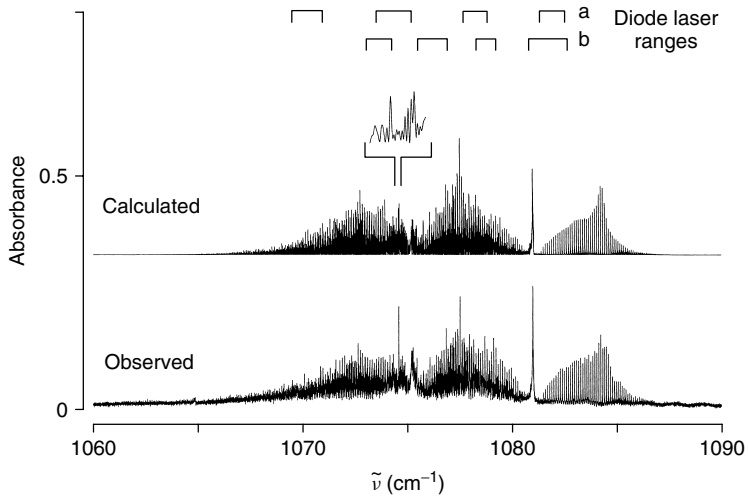

Figure 23 Supersonic-jet FTIR spectrum of the ν_1 band system of CF_3I and simulated spectrum calculated for a temperature of $T_{\text{rot}} = 60\,\text{K}$. [Reproduced from He *et al*. 2002 by permission.]

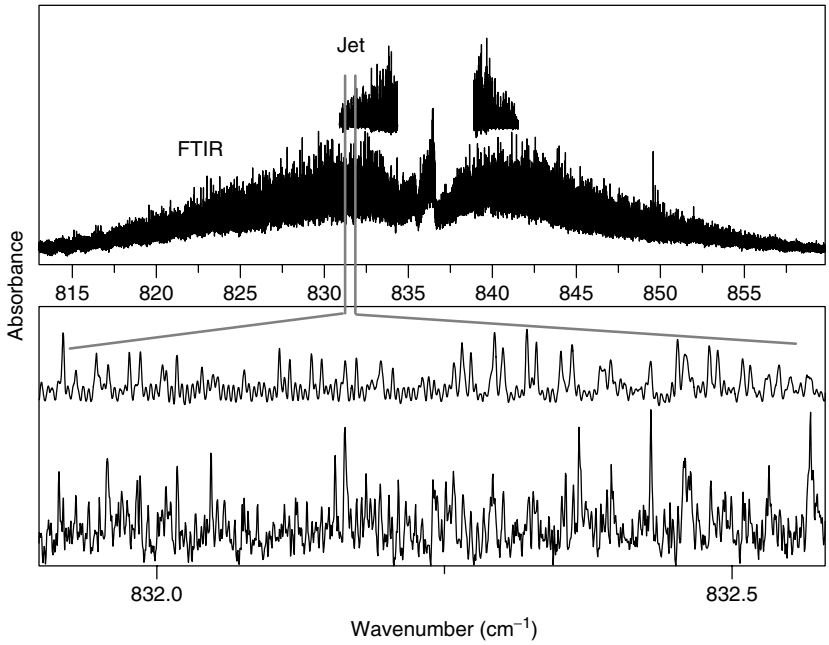

Figure 24 $PFCl_2$, ν_1 band; upper trace: experimental diode laser slit-jet spectrum, expansion of 5% $PFCl_2$ in He and FTIR spectrum, 4 mbar, $T = 298\,\text{K}$, resolution $0.0007\,\text{cm}^{-1}$, path length = 18 cm; lower trace: this is an extension of the upper part. [Reproduced from Horká *et al*. 2008 by permission.]

anticommutator XY+YX. A, B, C are the rotational constants, Δ_J, Δ_K, Δ_{JK}, δ_J, and δ_K are quartic and ϕ_J, $\varphi_K\phi_{JK}, \phi_{KJ}, \varphi_J, \varphi_{JK}$ and φ_K are sextic centrifugal constants.

The hybrid *c/b*-type band structure of the PF-stretching mode of $PF^{35}Cl_2$ has been successfully analyzed. However, this band is strongly perturbed in both isotopomers by a Coriolis-type resonance through the $\nu_3 + \nu_5$ band. Similar Coriolis resonances were identified in PH_2F and PH_2Cl (Beckers *et al*. 1994). The cold diode laser spectra at 15 K simplified the spectra considerably (Figure 24) and permitted the observation and assignment of many absorption lines of the ν_1 band of the isotopic chiral molecule $PF^{35}Cl^{37}Cl$. The analysis of the FTIR spectrum (room temperature spectra) resulted in a fit of 603 lines of $PF^{35}Cl_2$ with an RMS of $0.581 \times 10^{-3}\,\text{cm}^{-1}$, whereas the fit of 65 lines assigned in the jet spectra (20 K) of $PF^{35}Cl^{37}Cl$ resulted in an RMS of $0.439 \times 10^{-3}\,\text{cm}^{-1}$ (Horká *et al*. 2008). Figure 25 shows very good agreement between measured and simulated spectrum.

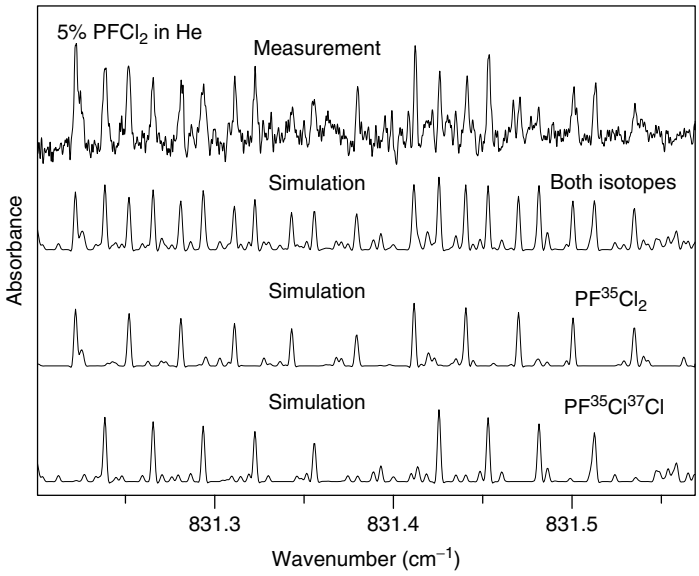

Figure 25 $PFCl_2$, ν_1 band; upper trace: experimental diode laser slit-jet spectrum, expansion of 5% $PFCl_2$ in He; lower traces: simulated spectrum of $PF^{35}Cl_2$, $PF^{35}Cl^{37}Cl$, and the sum of both spectra. [Reproduced from Horká *et al*. 2008 by permission.]

The isotopomer $PF^{35}Cl^{37}Cl$ is of interest as the first example of an isotopically chiral molecule, where quantitative predictions concerning a fundamentally new isotope effect due to the electroweak interactions have been made (Berger *et al*. 2005, Quack 2011). The high-resolution spectroscopic analysis provides the starting point for future experimental studies of this effect.

6.7 Larger Molecules

With the advent of increasingly sophisticated supersonic-jet techniques, spectroscopic investigation of larger molecules, with a resolution of rotational lines, permitting to obtain structural information has become possible. The group of Richard Saykally reported the first observation of a rotationally resolved spectrum of a nucleotide base, uracil (Viant *et al*. 1995). They used a tunable diode laser in combination with a heated pulsed slit nozzle to record the absorption spectrum of uracil around $1703\,cm^{-1}$ and analyzed the rotational structure of the fundamental ν_6 mode, which is a predominant out-of-phase mixed carbonyl stretching vibration. In the same laboratory, infrared absorption spectra have been measured by using the cavity ring down technique, of jet-cooled PAHs, such as naphthalene, anthracene, phenantracene, pyrene, and perylene with a resolution of $0.04\,cm^{-1}$ (Huneycutt *et al*. 2004, Schlemmer *et al*. 1994).

Supersonic rotationally resolved jet spectra ($0.001\,cm^{-1}$) of large chlorofluorocarbons have been measured in a supersonic jet by Snels *et al*. (1995, 2001, 2003), D'Amico and Snels (2002, 2003). They recorded spectra of CFC142b (1,1,1-difluorochloroethane) and analyzed the ν_7, ν_6, and ν_{14} bands of both isotopomers. The same authors reported the analysis of the ν_{14} band of HFC 134a (1,1,1,2-tetrafluoroethane) (Snels and D'Amico 2003). The ν_6 band of the CFC142b exhibits a remarkable splitting of all rotation–vibrational transitions due to a torsional Coriolis interaction with a highly excited torsional overtone band (Di Lauro *et al*. 2009). Duan and Luckhaus (2004) investigated malonaldehyde and observed the two tunnel components of the ν_6 band. For heavy transition metal hexafluorides such as WF_6 and ReF_6, the room temperature spectra are heavily congested by hot bands, owing to the presence of hot bands originating from low-energy vibrational modes. By cooling WF_6 in a WF_6/He expansion, the vibrational ground-state population could be increased from 1.3% at room temperature up to about 95% at 50 K vibrational temperature. A full rotational analysis of the ν_3 band has been performed for the four most abundant isotopic species. ReF_6 is an open-shell molecule and a most interesting Jahn–Teller system with a highly degenerate electronic ground state. It is the first time that line-resolved supersonic-jet spectra for a system of such a complexity were obtained (Boudon *et al*. 2002). The splitting increases the complexity of the infrared spectrum enormously and distributes the absorption strength over many transitions. For this reason, FTIR-jet spectra could not be recorded at the highest instrumental resolution. A tunable diode laser, however, combined with a supersonic slit jet and a multiple pass optical setup, permitted the recording of well-resolved ReF_6 spectra. The analysis of these spectra is still not complete.

7 STUDIES OF NUCLEAR SPIN SYMMETRY CONSERVATION IN JET EXPANSIONS

The principles of nuclear spin symmetry and parity conservation are among the most fundamental aspects of spectroscopy and reaction dynamics (Quack 1977, 1983, 1985) (*see also* Oka (2011): **Orders of Magnitude and Symmetry in Molecular Spectroscopy** and Quack (2011): **Fundamental Symmetries and Symmetry Violations from High-resolution Spectroscopy**, this handbook). Polyatomic molecules possessing identical nuclei with nonzero spin in symmetrically equivalent positions exist in several forms of nuclear spin isomers. This led to the separation of *para*- and *ortho*-H_2 already in 1929 through cooling in the presence of a magnetic catalyst (Bonhoeffer and Harteck 1929). Nuclear spin isomers play an important role in fundamental research and the theory can be used in different fields such as astronomy and astrophysics to study the abundance ratio of nuclear spin isotopomers in the interstellar space, kinetics of the chemical reactions in the gas phase, NMR spectroscopy, etc. At the present time, several techniques exist for the separation of spin isomers reviewed by Chapovsky and Hermans (1999), *see also* Oka (2011): **Orders of Magnitude and Symmetry in Molecular Spectroscopy** and Quack (2011): **Fundamental Symmetries and Symmetry Violations from High-resolution Spectroscopy**, this handbook. One method to study nuclear spin isomers is the utilization of supersonic-jet expansion with high-resolution spectroscopy. To study this phenomenon, exact line intensities and rotational temperatures have to be derived. To obtain information about the spin symmetry conservation or spin symmetry interconversion, the line intensities have to be calculated under different hypotheses and compared with those from measurement. The intensity of the rotational lines of a spherical top molecules is given by

$$G(J, \Gamma, i) = (\text{const})\, p(J, \Gamma, i) A(J) \tag{34}$$

with the rotational factor

$$A(J) = \frac{2J' + 1}{2J + 1} \tag{35}$$

where J is the angular momentum quantum number for the ground state and J' for the excited state. Γ denotes the nuclear spin isomer. The population of the states $p(J,\Gamma,i)$ can be considered under two extreme situations with complete equilibration among all states (relaxed distribution) or complete nuclear spin symmetry conservation (conserved) (see Amrein *et al*. 1988b). The relaxed distribution is given by

$$p_{\mathrm{r}}(J, \Gamma, i) = g_{\mathrm{I}}(\Gamma)(2J + 1)\exp[-E_i(J)/kT_{\mathrm{rot}}]/Q_{\mathrm{r}}^{\mathrm{rot}} \tag{36}$$

where $g_{\mathrm{I}}(\Gamma)$ is the nuclear spin statistical weight and $Q_{\mathrm{r}}^{\mathrm{rot}}$ is the relaxed rotational partition function including nuclear spin at a rotational temperature T_{rot}

$$Q_{\mathrm{r}}^{\mathrm{rot}} = \sum_{\Gamma} g_{\mathrm{I}}(\Gamma) Q_{\mathrm{rot}}(\Gamma)\exp[-E_0(\Gamma)/kT_{\mathrm{rot}}] \tag{37}$$

with

$$Q_{\mathrm{rot}}(\Gamma) = \sum_{J} N(J, \Gamma)(2J + 1) \times \exp(-[E(J) - E_0(\Gamma)]/kT_{\mathrm{rot}}) \tag{38}$$

where $E_0(\Gamma)$ is the lowest level of nuclear spin isomer Γ and $E(J)$ is the energy for a given J in the vibrational ground state. $N(J,\Gamma)$ is the number of levels of isomer Γ for J.

For a complete nuclear spin symmetry conservation, one gets

$$p_{\mathrm{c}}(J, \Gamma, i) = x(\Gamma)(2J + 1) \times \exp(-[E(J) - E_0(\Gamma)]/kT_{\mathrm{rot}})/Q_{\mathrm{rot}}(\Gamma) \tag{39}$$

where $x(\Gamma)$ is the mole fraction of the nuclear spin isomer Γ at the temperature T before the expansion, at which the isotopomers are assumed to be equilibrated. The relative line strength of a single rovibrational line is given by

$$G(J) = \frac{1}{cL} \int_{\mathrm{line}} \ln(I_0/I)\tilde{\nu}^{-1} \mathrm{d}\tilde{\nu} \tag{40}$$

where c is the concentration and L is the absorption pathlength. The interconversion of nuclear spin isomers for CH_4 has been investigated already in supersonic-jet expansions with FTIR spectroscopy by the Zürich group (Dübal *et al*. 1984, Amrein *et al*. 1988b). The measurements showed that the nuclear spin is conserved during the expansion (Figures 26 and 27). We have extended these investigations to partially deuterated methane isotopomers (Horká-Zelenková *et al*. 2010). To investigate the dynamical processes during the expansion, the intensities of the measured absorption lines have to be determined with high accuracy. This accuracy can only be achieved if the considered rotational lines are measured in a single scan, ensuring identical experimental conditions for all the lines. As the scanning range of the diode laser is $1–2\,\mathrm{cm}^{-1}$ at most and as for molecules of the type CX_3Y, the intensities of rotational lines with different K quantum numbers have to be compared, the experiments are preferentially done on the P-

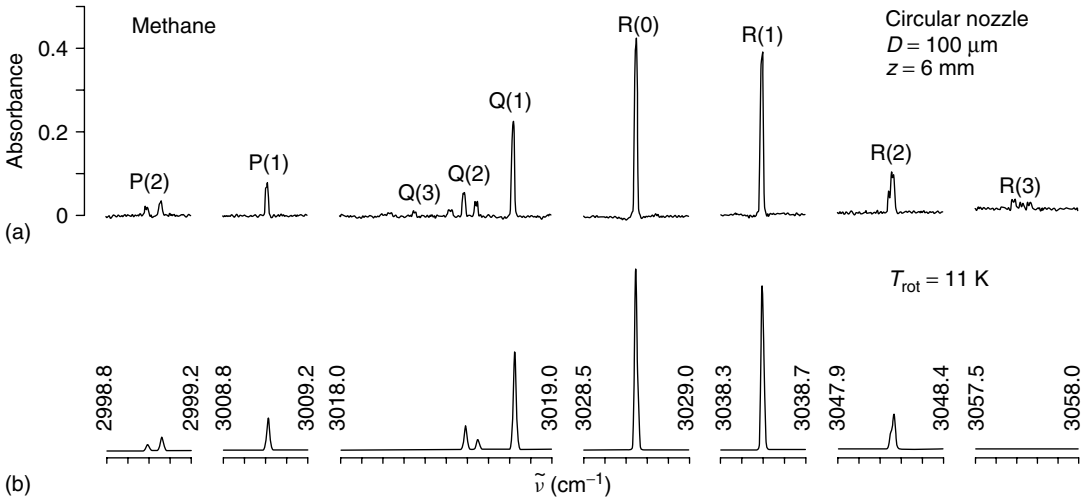

Figure 26 (a) High-resolution jet-FTIR spectrum of methane. (b) Computed spectrum for a rotational temperature of 11 K. [After Amrein *et al*. 1988b by permission.]

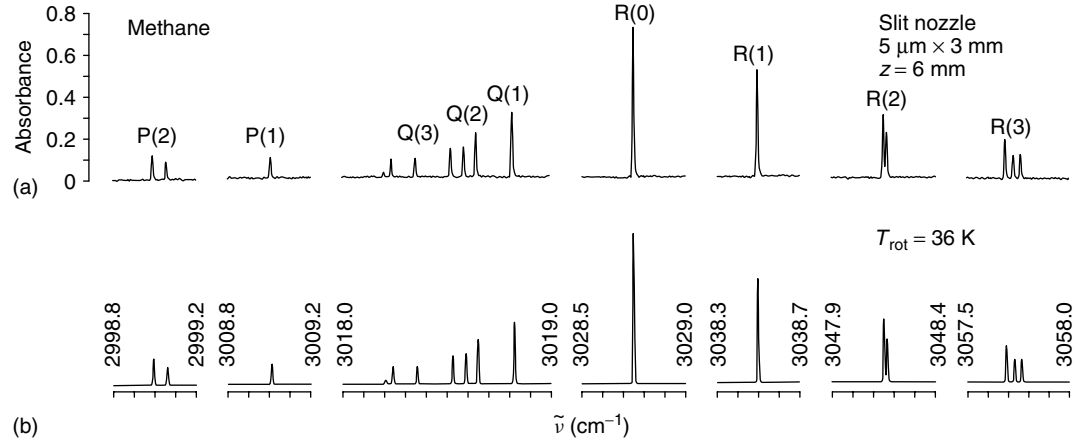

Figure 27 (a) High-resolution jet-FTIR spectrum of methane. (b) Computed spectrum for a rotational temperature of 36 K. [Reproduced from Amrein *et al*. 1988b by permission.]

or R-branch of a parallel band ($A_1 \rightarrow A_1$ transition) with $\Delta K = 0$, because for a given quantum number J, the lines for the different K quantum numbers are close enough to be covered in a single scan. Additional complications may arise from the fact that the complete spectral range is not reachable with a single laser diode.

Different criteria have to be considered for a proper choice of the measured rotational lines. Both nuclear spin isomers must have an absorption line in the considered spectral range and at least one of the nuclear spin isomers must have more than one single line to allow for the determination of a rotational temperature. All lines with $J = 2$ or larger fulfill these criteria. On the other hand, to decide whether the nuclear spin is conserved during the expansion phase of the molecular beam or not, very low rotational temperatures have to be reached (below 15 K for CHD_3 (Horká-Zelenková *et al*. 2010)). For these temperatures, the rotational lines with $J = 3$ or larger are only weakly populated and the accuracy for the determined line intensities is poor. These two restrictions make the $P(3)$- or $R(2)$-lines of the CH-stretching vibration (ν_1) an ideal choice to study spin symmetry relaxation of CHD_3 in the expansion zone of a molecular beam (Horká-Zelenková *et al*. 2010).

8 STUDIES OF CLUSTERS

By using the cooling in a supersonic-jet expansion, clusters can be produced in a more or less controlled way, by varying source pressure, nozzle temperature, mixing ratio, and carrier gas.

The spectroscopic investigation of molecular clusters is important for the study of intramolecular dynamics

and tunneling phenomena, and it provides fundamental information on the nature and strength of the weak van der Waals forces and the much stronger hydrogen bonds in clusters, and allows to determine the structure of the complexes in vibrationally excited states.

An incomplete list of scientific publications regarding spectra of clusters resolving rotational levels is made available by Novick (2008).

It is intriguing to build clusters from isolated molecules and atoms. The structure of stable isomers sometimes can be calculated from current ab initio theory with a good precision (Marquardt and Quack 2011: **Global Analytical Potential Energy Surfaces for High-resolution Molecular Spectroscopy and Reaction Dynamics**, this handbook, Quack and Suhm 1997, 1998, Klopper *et al*. 1996, 1998 and Maerker *et al*. 1997), depending on the cluster size. Infrared and Raman bands can also be calculated theoretically and these provide a starting point for exploring infrared spectra, mostly recorded for molecular beam expansions, which contain different clusters. Sometimes several isomers are found experimentally, also depending on the production method.

8.1 Van der Waals Clusters

Some van der Waals complexes studied consist of diatomic and triatomic molecules bound to noble gas atoms, such as CO–Rg (Brookes and McKellar 1998, McKellar *et al*. 1999), N_2O–Rg (Herrebout *et al*. 1998), CO_2–Rg (McKellar 2006), and OCS–Rg (Hayman *et al*. 1989), where Rg stands for He, Ne, Ar, Kr, and Xe. All these clusters are weakly bound van der Waals complexes, with a binding energy of a few hundreds of cm^{-1} at most. OCS–Rg and N_2O–Rg were shown to be T-shape complexes, with the rare gas atom displaced versus the oxygen atom. The long-range attractive forces (inductive and dispersive) scale with the polarizability of the rare gas atoms and the potential well depth increases with the polarizability of the rare gas atoms (Ne < Ar < Kr < Xe). In addition, the CO_2–Rg and CO–Rg complexes behave in a similar way. Molecular complexes involving CO might occur in interstellar space due to the fact that CO is the most abundant polar molecule in outer space.

Several complexes of tetrahedral molecules with rare gases were studied, such as CH_4–Rg and SiH_4–Rg. The interesting point in studying these light spherical-top rare-gas complexes is the existence of internal rotation effects. CH_4–He, CH_4–Ar, and CH_4–Kr were subject of several studies by Pak *et al*. (1998) and Wangler *et al*. (2001). Infrared spectra of SiH_4–Ne and SiH_4–Ar were explored in detail by Howard and coworkers (Randall *et al*. 1994a,b, Brookes *et al*. 1996, 1997). They also developed a model for the energy levels of rare gas spherical top complexes, which was successful in describing the hindered rotational structure of SiH_4–Ar (Randall *et al*. 1994a). Analysis of SiH_4–Ar is simpler since it is a much more strongly anisotropic system than CH_4–Ar, and shows a behavior between free rotor and rigid molecule limit. SiH_4–Ne has a smaller anisotropy than SiH_4–Ar, resulting in a new angular momentum coupling scheme and from the derived rotational constant, it appears that the silane monomer is closer to the free internal rotational limit. The Coriolis model developed by Brookes *et al*. (1996) was also applied to CH_4–Rg complexes, which are also relatively close to free internal rotation behavior.

In addition, high-resolution spectra of complexes involving heavy spherical top molecules such as SiF_4 and SF_6 were reported. From the analysis of the infrared spectra recorded for SF_6–Rg complexes (Rg = Ne, Ar, Kr, Xe) in liquid helium droplets (Hartmann *et al*. 1996), it appears that the SF_6–Rg complex is embedded in a layer of 10–12 He atoms, which contribute to the very small rotational constants of this embedded cluster. Urban *et al*. (1995) measured fully resolved rovibrational spectra of SiF_4–Rg. Spectroscopic constants for the complexes SiF_4–Ar and SiF_4–Kr were obtained.

All complexes mentioned so far involved small molecules and rare gas atoms. The pioneering work on clusters of small molecules with noble gas atoms was gradually extended to dimers and trimers of larger molecules. Clusters involving molecules with tetrahedral and spherical symmetry, such as SF_6, CH_4, SiF_4, have been studied by Urban and Takami (1995a, b). In these complexes, the attractive forces are due to induced dipole moments in each of the molecules. For instance in the free jet infrared spectra of SF_6, SiF_4, and CH_4 dimers, two absorption bands have been observed and explained in terms of a resonant dipole–dipole interaction between the two monomers. In the SF_6 dimer, when the ν_3 threefold degenerate vibration (in the monomer) is excited, two distinct bands appear in the dimer spectrum, one is a parallel band and the other a perpendicular band, as predicted by the dipole–dipole model (Snels and Fantoni 1986).

In the SiF_4 dimer spectrum, two different bands could be observed, one parallel transition and one perpendicular band, which had been observed many years before by Snels and Fantoni (1986) in low-resolution infrared predissociation measurements. Urban and Takami (1995a,b) propose three different structures for both dimers, with C_{3v}, D_{2d}, and C_{2h} symmetry. They argue that the dimer with C_{3v} symmetry should exhibit a first-order Coriolis interaction in the perpendicular band and they expect a strong–weak–weak intensity alternation in the same band, due to the threefold symmetry along the a-axis. In addition, the D_{2d} symmetry should give rise to

a first-order Coriolis interaction, but would show intensity alternation for even and odd K, due to C_2 symmetry along the a-axis. The dimer with C_{2h} symmetry would have a degenerate perpendicular band without a first-order Coriolis interaction. The dimer spectrum of SiF_4 shows neither a Coriolis interaction nor any intensity alternation, which indicates a structure with C_{2h} symmetry. The case of the SF_6 dimer is more complicated; the perpendicular band exhibits a clear first-order Coriolis interaction, which excludes the C_{2h} symmetry. They further make the hypothesis of internal rotation in the SF_6 dimer.

From these relatively simple molecular clusters, the interest moved toward larger clusters, involving more noble gas atoms, up to nano droplets, which form a particular environment where superfluidity was observed. Very interesting studies of van der Waals clusters in liquid helium droplets have been performed by Scheele *et al.* (2005), Hartmann *et al.* (1996), Xu *et al.* (2003), McKellar (2004, 2008), Tang and McKellar (2004), Lehnig and Jäger (2006). Their results demonstrate that liquid He droplets (usually consisting of several thousands of He atoms) provide a very cold environment where molecules can rotate almost freely and that the rotational structure of the molecules trapped in the droplets produces information about the interaction between molecules and the droplet.

The CO_2 dimer was measured by the group of Brian Howard, by using a pulsed jet diode laser spectrometer (Walsh *et al.* 1987). The structure was found to be a parallel staggered configuration. Two distinct isomers of the CO_2 trimer have been identified by means of infrared spectroscopy. The first, which is a symmetric top with a cyclic planar structure and C_{3h} symmetry, was originally observed in the CO_2 monomer $\nu_3 + \nu_2$ combination band region by Fraser *et al.* (1987) and later in the monomer ν_3 fundamental region by Weida *et al.* (1995). The second isomer, which is an asymmetric top with a C_2 symmetry and a barrel-shaped structure, was observed in the monomer ν_3 fundamental region also by Weida and Nesbitt (1996). McKellar and coworkers (Dehghany *et al.* 2008) observed two combination bands $\nu_3 + \nu_{\text{torsion}}$ for the cyclic trimer. Possible larger CO_2 cluster spectra are under study in the McKellar group.

The structure of the N_2O dimer, determined from jet absorption spectra in the ν_1 (Ohshima *et al.* 1988), ν_3 (Qian *et al.* 1997), and $\nu_1 + \nu_3$ (Huang and Miller 1988) regions, proved to be a nonpolar slipped parallel structure. Later, Miller and Pedersen also found a polar isomer in the ν_1 band region, as well as the first trimer of N_2O (Miller and Pedersen 1998). This trimer can be thought of as a slightly distorted nonpolar dimer with a third N_2O molecule above the dimer plane, similar to the noncyclic CO_2 trimer. The same authors also measured the N_2O tetramer (Miller and Pedersen 1997) in the ν_1 and $\nu_1 + \nu_3$ region. This tetramer can be considered as two dimer units stacked one on top of the other. Surprisingly, a second tetramer band has been observed in the ν_1 region, this time a perpendicular band. Other N_2O cluster bands have also been observed but not assigned to a specific cluster up to now.

In all the clusters mentioned above, the van der Waals bonds are rather weak and can be explained in terms of dipole and quadrupole moments of the molecules involved.

8.2 Hydrogen Bonds

The hydrogen bond plays an important role as a significant intermolecular interaction, ranging from small molecules such as water and hydrogen fluoride to the complex biological systems as nucleic acids and proteins. The hydrogen bond results in part from a dipole–dipole force between a hydrogen atom and an electronegative atom, such as nitrogen, oxygen, or fluorine. The dynamics of hydrogen bond formation and breaking is important for the understanding of biological processes and for evaporation and condensation phenomena in hydrogen bond liquids such as water and hydrogen fluoride. The binding energies for neutral hydrogen bonds are in a range of up to a few thousand cm^{-1} and thus are one order of magnitude stronger than the bonds in van der Waals clusters. One of the simplest hydrogen bond systems can be found in the HF dimer. The vibrational spectrum shows some interesting features, such as tunneling splitting, rotational saturation, and rovibrational perturbations, of this molecule due to its nonrigidity and near linearity. The rearrangement of its hydrogen bond is governed by the coupled low-frequency modes and rotation about the F–F axis. The HF dimer has been studied by various spectroscopic methods and an accurate full-dimensional potential has been derived by ab initio theory (Quack and Suhm 1990b, 1991, Klopper *et al.* 1996, 1998). Our group at ETH Zürich used FTIR and supersonic-jet techniques for the measurement of the spectra, resulting in the analysis of the fundamental out-of-plane F–H–F bending vibration ν_6, $K = 1$ (von Puttkamer and Quack 1987), $K = 2$ (von Puttkamer *et al.* 1989) up to $K = 4$ (von Puttkamer *et al.* 1988) and in-plane bending ν_5 (Quack and Suhm 1990a). We also studied HF-stretching overtones in $(HF)_2$ and HFDF around 7500–7800 cm^{-1} using both diode laser direct absorption and cavity ring down spectroscopy (He *et al.* 2007, Hippler *et al.* 2007). From the analysis of these rotationally resolved spectra, hydrogen predissociation lifetimes and tunneling switching times were obtained. Figure 28(a) and (b) shows as an example the very different appearance of the $N_j = 2_2$ overtone band of $(HF)_2$, which has a very small vibrational predissociation rate and line broadening and the 2_1 polyad band where the very considerable line broadening is easily visible. The predissociation

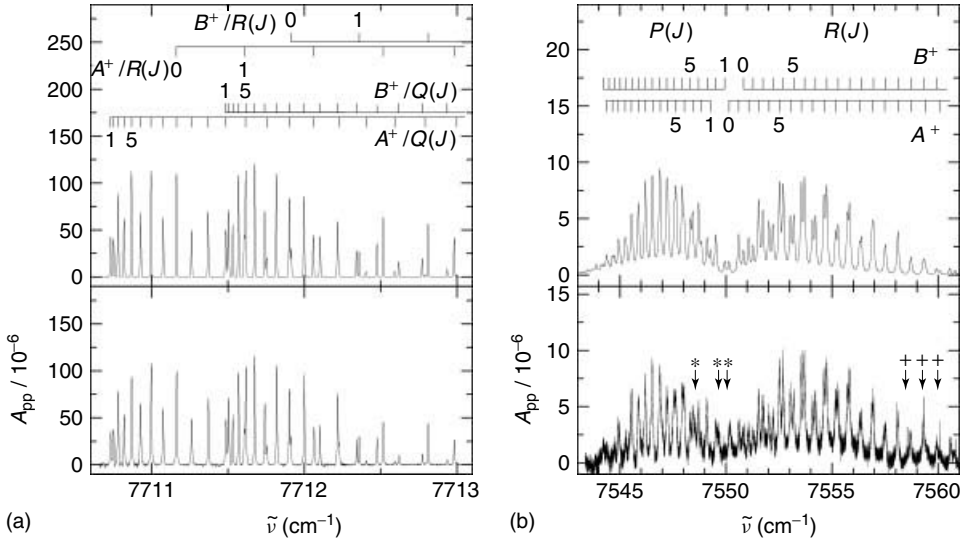

Figure 28 (a) The N_j=2_2 band of $(HF)_2$: experimental CRD spectrum in the slit-jet expansion (lower part) and simulation for a rotational temperature of 25.9 K (upper part). (b) The N_j=2_1 band of $(HF)_2$: experimental CRD spectrum in the slit-jet expansion (lower part) and simulation for a rotational temperature of 26.0 K (upper part) showing also a much larger predissociation broadening. [Adapted from Hippler *et al*. 2007 by permission.]

rates have been analyzed quantitatively and one finds that full quantum dynamics describes the process essentially correctly, whereas classical dynamics is quite unable to provide a quantitatively satisfactory description (Manca *et al*. 2008). From theoretical studies, $(HF)_3$ is calculated to be cyclic and the F–F distance is shorter than in $(HF)_2$ (Suhm *et al*. 1993, Quack *et al*. 1993b, 2001). The other hydrogen halides and their isotopomers, such as $(HCl)_3$ (Fárník and Nesbitt 2004), $(DCl)_2$ (Schuder *et al*. 1993), $(HBr)_2$ (Castillo-Chara *et al*. 2004), and $(HI)_2$ (McIntosh *et al*. 2000), have also been studied in jet expansion with diode lasers.

Numerous studies were also done on hydrogen halides bounded via hydrogen bonds to other functional groups such as HCN–HF (Bender *et al*. 1987) and OC–HCl, OC–HBr, N_2–HBr dimer (Wang *et al*. 2004), etc. One can point out that the dimer $(HF)_2$ has been the prototype for high-resolution spectroscopic studies of hydrogen-bonded complexes, starting with the work of Dyke *et al*. (1972). We have mentioned some highlights of the spectroscopy of these complexes above and draw attention to the reviews of Quack and Suhm (1997, 1998). Detailed spectroscopic identification of large clusters of HF have been possible up to $(HF)_5$ and perhaps $(HF)_6$ (Quack *et al*. 1993a, Luckhaus *et al*. 1995). $(HF)_n$ and $(DF)_n$ as well as mixed isotopomer clusters have also been at the origin of the very first infrared spectroscopic identification of hydrogen-bonded nanoclusters in supersonic jets (Quack *et al*. 1997). In the mean time, this general field has had enormous development of obvious importance for atmospheric physics and astrophysics (Firanescu *et al*. 2006).

H_2O is another important molecule forming hydrogen-bonded clusters. The hydrogen bond in water involves electron pairs on the oxygen atom interacting with the hydrogen atom of other molecules. Thus, the water molecule can create hydrogen bonds with up to four other molecules. This bonding is responsible for the high boiling point, melting point, and viscosity of water in liquid phase in comparison with other similar substances. Water clusters and water-containing complexes play an important role in atmospheric processes and acid rain formation (Kolb *et al*. 1994) and, of course, atmospheric water vapor contributes to the greenhouse effect, in particular, due to absorption in the mid- and near-infrared range (Cess *et al*. 1995, Li *et al*. 1995, Vaida *et al*. 2001).

Water-containing complexes frequently display a tunneling splitting arising from proton exchange. Some of these complexes have also been studied via jet-diode laser spectroscopy as N_2O–H_2O (Gimmler and Havenith 2002), Ar–H_2O (Weida and Nesbitt 1997), CO–H_2O (Brookes and McKellar 1998), H_2O–CO_2, and H_2O–HCCH (Block *et al*. 1992).

Double hydrogen bonds play an important role in DNA base pairs; moreover, multiple proton transfer in hydrogen-bonded systems is one of the most fundamental processes in chemistry and biology. The formic acid dimer is one of the smallest organic complexes serving as a prototype for multiple proton transfer. The antisymmetric C–O vibrational band of this complex was studied by Ortlieb and Havenith (2007). It shows slow tunneling motion in comparison with the overall rotation and thus confirms the existence of deep local minima in the C_{2h} structure. This and more recent

work are reviewed by Havenith and Birer in this handbook (Havenith and Birer 2011: **High-resolution IR-laser Jet Spectroscopy of Formic Acid Dimer**, this handbook).

8.3 Carbon Clusters

Laboratory spectroscopy of atomic and molecular carbon in its various forms has always been of great interest and importance for a number of reasons. The discovery of the presence of carbon-chain molecules in interstellar space intensified laboratory studies concerning the production and spectroscopic observation of pure carbon clusters.

Carbon atoms form stable covalent carbon–carbon bonds. The single, double, and triple carbon–carbon bonds permit the formation of a large variety of pure carbon molecules, ranging from linear chains to branched chains, cyclic molecules, as well as three-dimensional structures such as C_{60}. The spectroscopic investigations have been supported by high-level ab initio calculations, which predict stable linear, cyclic, and three-dimensional structures. The linear chains appear to be the most stable form for a relatively small number of carbon atoms (up to 10), larger clusters are supposed to form rings (up to 30 atoms), and still larger carbon molecules closed three-dimensional cages.

Matsumura *et al*. (1988) observed the rotationally resolved infrared spectrum of C_3. In rapid succession, other small carbon chains were produced and spectroscopically studied in the laboratory, such as C_4 (Heath and Saykally 1991b), C_5 (Heath *et al*. 1989), C_6 (Hwang *et al*. 1993), C_7 (Heath *et al*. 1990, Heath and Saykally 1991a), and C_9 (Heath and Saykally 1990) using a laser ablation carbon cluster source in combination with a sensitive infrared tunable diode laser spectrometer. During the same period, C_3 and linear C_5 were detected in the envelope of the carbon star IRC+10216 by Hinkle *et al*. (1988), Bernath *et al*. (1989). The largest carbon chain observed in laboratory experiments at high resolution was reported by Giesen *et al*. (1994). They have attributed the rotationally resolved spectrum at 1809 cm^{-1} to an asymmetric stretching mode of a 13-atom counting linear carbon chain. *See also* Guennoun and Maier 2011: **Electronic Spectroscopy of Transient Molecules**, this handbook.

Kroto *et al*. (1985) discovered an icosahedral carbon cluster, consisting of 60 carbon atoms, which they called *Buckminsterfullerene*. In 1996 Curl, Kroto, and Smalley were awarded with the Nobel price in Chemistry for their discovery (Kroto 1997). C_{60} has 174 vibrational degrees of freedom, but only four F_{1u} IR-active modes (1432, 1183, 577, 528 cm^{-1}). A gas-phase IR spectrum has been observed at a temperature of 1065 K, but no rotational structure was resolved (Frum *et al*. 1991). Other stable carbon cage clusters (fullerenes) were discovered (C_n, $n =$ 24, 28, 32, 50, 60, and 70, (Kroto 1987)). Continuing their work during 1985–1990, Curl, Kroto, and Smalley obtained further evidence for the proposed C_{60} structure. Among other things, they succeeded in producing and identifying carbon clusters that enclosed one or more metal atoms. In 1990, the group led by W. Krätschmer and D.R. Huffman (Ajie *et al*. 1990) produced large quantities of C_{60} using an arc discharge between two graphite rods in a helium atmosphere and extracting the carbon condensate so formed using an organic solvent. They obtained a mixture of C_{60} and C_{70}, and they also determined their structures. This confirmed the correctness of the C_{60} hypothesis. The way was thus open for studying the chemical properties of C_{60} and other carbon clusters such as C_{70},C_{76},C_{78}, and C_{84}. New substances were produced from these compounds, with new and unexpected properties. A new branch of "fullerene" chemistry developed, with diverse areas of interest such as astrochemistry, superconductivity, and material chemistry and physics.

9 RADICALS AND IONS

Free radicals, molecular ions, and ionic complexes are important reactive intermediates in many chemical environments, ranging from combustion processes and plasmas to atmospheric chemistry and interstellar space (Linnartz *et al*. 2000).

Pioneering spectroscopic work on some important molecular ions was started in the early 1980s, by using hollow cathode discharge tubes. The first infrared spectrum of the H_3^+ ion was reported by Oka (1980). The analysis of the ν_2 band was accomplished by J.K.G. Watson (Oka 1980). The ν_3 band of the hydronium ion, H_3O^+, was analyzed by Saykally's group (Begemann *et al*. 1983). Saykally also proposed the velocity modulation technique, which allows an efficient discrimination of spectral features due to ions with respect to neutrals (Gudeman and Saykally 1984). The ν_2 bending-inversion vibration of H_3O^+ was measured and analyzed by Liu and Oka (1985), who also determined the inversion splitting in the ground state and the $v_2 = 1$ state. In rapid succession, several other molecular ions were studied in discharge flow tubes, such as OH^- (Liu and Oka 1986), HNN^+, DNN^+ (Owrutsky *et al*. 1986), H_2D^+ (Amano and Watson 1984), and many others. We draw attention to a review paper on the early days of infrared absorption spectroscopy of molecular ions by Sears (1987).

Although discharge flow tubes have produced a wealth of spectroscopic data of molecular ions (Sears 1987), the discharge environment inevitably produces high translational, vibrational, and rotational temperatures. This can

be troublesome in the case of heavier and weakly bound instable species, because spectral congestion and population of many hot bands render the observed spectra extremely complex. In addition, the linewidths of single transitions are highly Doppler broadened due to the high translational temperatures. Both effects reduce the overall detection efficiency of the species.

The often complicated spectra of large free radicals and ions can be significantly simplified by cooling them in a supersonic expansion. A supersonic expansion provides an almost collision-free environment, enhancing the lifetime of free radicals and making their spectroscopic investigation easier. It also allows the production of weakly bound molecular ionic complexes.

Several methods for generating a sufficiently high number density of radicals and ions in a supersonic jet, allowing for infrared absorption spectroscopy have been developed. The most popular ones use an electrical discharge at the beginning of the expansion, in a way that a relatively high density of radicals and ions can be created in the high-pressure region, and successively cooled in the supersonic expansion. As an alternative to electric discharges, the methods of pulsed pyrolysis, laser ablation, and photolysis of suitable precursors have been applied. Photolysis with an ultraviolet laser produces radicals efficiently, but has a low-duty cycle with respect to pulsed supersonic jets and cw diode lasers (Tanaka *et al*. 1997, Sumiyoshi *et al*. 1994). To overcome the low absorption path length by crossing the radiation of a tunable laser with a supersonic pinhole expansion, pulsed planar (slit) expansions have been developed. The slit-jet configuration reduces the Doppler width and has a longer effective absorption path length. Typical concentrations of 10^{14} radicals cm^{-3} have been reported (Davis *et al*. 1997) while using electrical discharges combined with a supersonic slit-jet expansion.

The slit supersonic discharge source has been used in several laboratories to produce radicals and molecular ions (Hilpert *et al*. 1994, Fukushima *et al*. 1994). An alternative method to produce low-energy cooled plasmas uses electron impact ionization in a slit expansion. This technique allowed to measure the infrared spectra of weakly bound ionic complexes (Verdes *et al*. 1999, Linnartz *et al*. 1998, 2000).

Another method uses pulse pyrolysis to obtain free radicals and uses a Thermocoax wire to resistively heat the nozzle exit (Liu *et al*. 1998, Tanaka *et al*. 1999). Ions and radicals can be also prepared via laser vaporization (Heath and Saykally 1990, 1991a).

John Maier and his coworkers developed a molecular beam apparatus to study the vibrational infrared photodissociation of mass-selected ionic complexes. The cluster ions were generated in a pulsed supersonic expansion crossed by two electron beams. After mass selection of the species of interest in a quadrupole mass spectrometer, the selected ions are injected in an octupole ion guide, where they interact with a counterpropagating infrared laser pulse generated by an OPO. Several ionic clusters have been investigated by using this method, ranging from open-shell complexes such as $He–HNH^+$ (Dopfer *et al*. 1999a) and $Ne–HNH^+$ (Roth *et al*. 2000) to larger clusters such as $Ne_nHN_2^+$ ($N = 1–5$) (Nizkorodov *et al*. 1998), $C_6H_6^+$, $C_6H_6^+–N_2$, and $C_6H_6^+–(CH_4)_{1-4}$ (Dopfer *et al*. 1999b), $C_3H_3^+ – N_2$ (Dopfer *et al*. 2002). They have also adapted the cw-CRD scheme of Hippler and Quack (1999, 2002) to the study of molecular ions (*see also* Birza *et al*. (2002), Guennoun and Maier 2011: **Electronic Spectroscopy of Transient Molecules**, this handbook for review). Spectroscopic studies of individual conformations of peptides with more than a dozen amino acids in a gas phase was investigated by the group of Rizzo *et al*. (2009). They combine electrospray

Table 5 Spectroscopic tools developed and used in the Zürich molecular kinetics and spectroscopy group (After Quack 2003).

Powerful spectroscopic tools to apply to atmospheric analysis and quantum chemical kinetics

Measures of Power
1. Effective absorption length L
2. Resolving power $R_P = \frac{\nu}{\delta\nu}$
3. Effective resolution (Instr. Bandwidth) $\delta\nu$
4. Scanning power $S_P = \frac{\Delta\nu}{\delta\nu}$
5. Effective scanning range $\Delta\tilde{\nu}$

	R_P	S_P	$\delta\nu$ (MHz)	$\Delta\tilde{\nu}$ (cm^{-1})	L (m)
FTIR	$\leq 2 \times 10^6$	$\sim 10^7$	20–70	20 000	100
Diode direct Abs.	$\gtrsim 2 \times 10^6$	$< 5 \times 10^4$	20–30	20 (2500)	100
NIR-Diode CW-CRD	$\gtrsim 2 \times 10^8$	$< 10^7$	~ 1	500	1000–10 000
ISOS/IRSIMS	$\gtrsim 6 \times 10^5$	$\geq 30\,000$ ($\geq 10^6$)	~ 500	500 (20 000)	(10^{-3}) Ion-detector

ionization producing large biological molecules in a gas phase with collisional cooling in and ion trap and IR–UV double resonance techniques to simplify the spectra. Recently, the discovery of the first negative ion C_6H^- (McCarthy *et al*. 2006) in interstellar clouds has brought about a revival of interest in laboratory studies of anions.

A spectroscopic data base (Vibrational and Electronic Energy Levels (VEEL) of Small Polyatomic Transient Molecules Database) including 1796 short-lived molecules is available from the Commerce Department's National Institute of Standards and Technology.

10 CONCLUSION AND OUTLOOK

High-resolution spectroscopy of isolated molecules and clusters in supersonic-jet expansions has developed into one of the most powerful tools for the analysis of complex molecular spectra. While the use of every one of the FTIR and laser spectroscopic techniques with molecular beams has great merit, it is, in particular, the unique combination of diode laser and FTIR spectroscopy together with supersonic jets that greatly enhances the spectroscopic power. Table 5 summarizes this combination originally developed at the Zürich laboratory in the 1980s and 1990s in terms of various "measures of power", the effective absorption length as a measure of sensitivity, the resolving power, the effective resolution, the scanning power, and the effective scanning range. As more experimental groups join these efforts, one can anticipate many important applications, ranging from atmospheric chemistry to fundamental quantum physics, and thus quite a bright outlook into the future.

ACKNOWLEDGMENTS

We are greatly indebted to S. Albert, K. Keppler Albert, C. Manca Tanner, E. Miloglyadov, and G. Seyfang for help and discussions as well as to Ruth Schüpbach, in particular, for secretarial help in the preparation of this article. Our research has profited from numerous collaborations cited in the references and from financial support from ETH Zürich and Schweizerischer Nationalfonds.

ABBREVIATIONS AND ACRONYMS

CEAS	cavity-enhanced absorption spectroscopy
cw	continuous wave
DBR	distributed Bragg reflection
DFB	distributed feedback
DH	double heterostructure
ECDL	external cavity diode laser
LO	longitudinal optical
MBE	molecular beam epitaxy
MRI	magnetic resonance imaging
NMR	nuclear magnetic resonance
OPO	optical parametric oscillator
PAH	polycyclic aromatic hydrocarbons
PPLN	periodically poled lithium niobate
QCL	quantum cascade lasers
QW	quantum well
VCSEL	vertical cavity surface emitting laser

REFERENCES

Ajie, H., Alvarez, M.M., Anz, S.J., Beck, R.D., Diederich, F., Fostiropoulos, K., Huffman, D.R., Krätschmer, W., Rubin, Y., Schriver, K.E. *et al*. (1990) Characterization of the soluble all-carbon molecules C_{60} and C_{70}. *Journal of Physical Chemistry*, **94**(24), 8630–8633.

Albert, S. and Quack, M. (2007) High resolution rovibrational spectroscopy of chiral and aromatic compounds. *ChemPhys Chem*, **8**(9), 1271–1281.

Albert, S., Bauerecker, S., Quack, M., and Steinlin, A. (2007) Rovibrational analysis of the $2\nu_3$, $3\nu_3$ and ν_1 bands of $CHCl_2F$ measured at 170 and 298 K by high-resolution FTIR spectroscopy. *Molecular Physics*, **105**, 541–558.

Albert, S., Hollenstein, H., Quack, M., and Willeke, M. (2004) Doppler-limited FTIR spectrum of the $\nu_3(a')/\nu_8(a'')$ Coriolis resonance dyad of $CHClF_2$: analysis and comparison with ab initio calculations. *Molecular Physics*, **102**, 1671–1686.

Albert, S., Hollenstein, H., Quack, M., and Willeke, M. (2006) Rovibrational analysis of the $\nu_4, 2\nu_6$ Fermi resonance band of $CH^{35}ClF_2$ by means of a polyad Hamiltonian involving the vibrational levels ν_4, $2\nu_6$, $\nu_6 + \nu_9$ and $2\nu_9$, and comparison with ab initio calculations. *Molecular Physics*, **104**(16–17), 2719–2735.

Albert, S., Hollenstein, H., Quack, M., Willeke, M., Puskar, L., McNaughton, D., Robertson, E.G. (2010) in preparation.

Albert, S., Albert, K.K., Hollenstein, H., Tanner, C.M., and Quack, M. (2011) Fundamentals of rotation–vibration spectra, in *Handbook of High-resolution Spectroscopy*, Quack, M. and Merkt, F. (eds), John Wiley & Sons, Ltd., Chichester, UK.

Albert, S., Albert, K.K., and Quack, M. (2011) High-resolution Fourier transform infrared spectroscopy, in *Handbook of High-resolution Spectroscopy*, Quack, M. and Merkt, F. (eds), John Wiley & Sons, Ltd., Chichester, UK.

Amano, T. and Watson, J.K.G. (1984) Observation of the ν_1 fundamental band of H_2D^+. *Journal of Chemical Physics*, **81**(7), 2869–2871.

Amrein, A., Hollenstein, H., Locher, P., Quack, M., Schmitt, U., and Bürger, H. (1987a) Analysis of the ν_4 and ν_1 bands of CF_3Cl measured by supersonic free-jet FTIR spectroscopy. *Chemical Physics Letters*, **139**(1), 82–88.

Amrein, A., Quack, M., and Schmitt, U. (1987b) High resolution interferometric Fourier transform infrared absorption spectroscopy in a supersonic free jet expansion: the interacting states ν_2, ν_5 and $\nu_3 + \nu_6$ of trifluoromethane. *Molecular Physics*, **60**(1), 237–248.

Amrein, A., Quack, M., and Schmitt, U. (1987c) High resolution interferometric Fourier transform infrared absorption spectroscopy in supersonic free jet expansions-A new technique for ultracold gaseous samples. *Zeitschrift für Physikalische Chemie*, **154**, 59–72.

Amrein, A., Luckhaus, D., Merkt, F., and Quack, M. (1988a) High-resolution FTIR spectroscopy of $CHClF_2$ in a supersonic free jet expansion. *Chemical Physics Letters*, **152**(4–5), 275–280.

Amrein, A., Quack, M., and Schmitt, U. (1988b) High-resolution interferometric Fourier transform infrared absorption spectroscopy in supersonic free jet expansions: carbon monoxide, nitric oxide, methane, ethyne, propyne, and trifluoromethane. *Journal of Physical Chemistry*, **92**(19), 5455–5466.

Amrein, A., Hollenstein, H., Quack, M., and Schmitt, U. (1989) High resolution interferometric Fourier transform infrared spectroscopy in supersonic free jet expansions: N_2O, $CBrF_3$ and CF_3I. *Infrared Physics*, **29**(2–4), 561–574.

Asselin, P., Soulard, P., and Boudon, V. (2008) Jet-cooled FTIR spectroscopy and analysis of the ν_5 C-O stretch fundamental of $Ni(CO)_4$. *Molecular Physics*, **106**, 1135–1141.

Asselin, P., Soulard, P., Madabène, B., Alikhani, M.E., and Lewerenz, M. (2006) Vibrational dynamics of the hydrogen bond in H_2S-HF: Fourier-transform-infrared spectra and ab initio theory. *Physical Chemistry Chemical Physics*, **8**, 1785–1793.

Asselin, P., Soulard, P., Madabène, B., and Lewerenz, M. (2007) Fourier transform infrared spectroscopy and ab initio theory of acid-hydrogen sulfide clusters: H_2S-HCl, D_2S-DCl and H_2S-$(HCl)_2$. *Physical Chemistry Chemical Physics*, **9**, 2868–2876.

Asselin, P., Soulard, P., Tarrago, G., Lacome, N., and Manceron, L. (1996) High resolution Fourier transform infrared spectroscopy of the ν_6 and ν_{10} bands of jet-cooled $Fe(CO)_5$. *Journal of Chemical Physics*, **104**(12), 4427–4433.

Bauder, A. (2011) Fundamentals of rotational spectroscopy, in *Handbook of High-resolution Spectroscopy*, Quack, M. and Merkt, F. (eds), John Wiley & Sons, Ltd., Chichester, UK.

Bauder, A., Beil, A., Luckhaus, D., Müller, F., and Quack, M. (1997) Combined high resolution infrared and microwave study of bromochlorofluoromethane. *Journal of Chemical Physics*, **106**(18), 7558–7570.

Bauerecker, S., Taraschewski, M., Weitkamp, C., and Cammenga, H.K. (2001) Liquid-helium temperature long-path infrared spectroscopy of molecular clusters and supercooled molecules. *Review of Scientific Instruments*, **72**(10), 3946–3955.

Beckers, H., Bürger, H., Kuna, R., Paplewski, M., and Thiel, W. (1994) Ab-initio calculations on monohalogenophosphanes PH_2X (X=F,Cl,Br,I), and experimental detection and characterization of PH_2F and PH_2Cl by high-resolution infrared-spectroscopy. *Journal of Chemical Physics*, **101**(7), 5585–5595.

Begemann, M.H., Gudeman, C.S., Pfaff, J., and Saykally, R.J. (1983) Detection of the hydronium Ion (H_3O^+) by high-resolution infrared spectroscopy. *Physical Review Letters*, **51**(7), 554–557.

Beil, A., Luckhaus, D., Marquardt, R., Quack, M. (1994) Intramolcular energy transfer and vibrational redistribution in chiral molecules: experiment and theory. *Faraday Discussions*, **99**, 49–76.

Bender, D., Eliades, M., Danzeiser, D.A., Jackson, M., and Bevan, J.W. (1987) The gas-phase infrared-spectrum of ν_1 and $\nu_1 - \nu_4$ HCN–HF. *Journal of Chemical Physics*, **86**(3), 1225–1234.

Bennewitz, H.G. and Paul, W. (1954) Eine Methode zur Bestimmung von Kernmomenten mit fokussiertem Atomstrahl. *Zeitschrift für Physik*, **139**(5), 489–497.

Bennewitz, H.G., Kramer, K.H., Toennies, J.P., and Paul, W. (1964) Messung der Anisotropie des van Der Waals-potentials durch Streuung von Molekülen in definiertem Quantenzustand. *Zeitschrift für Physik*, **177**(1), 84.

Berden, G., Peeters, R., and Meijer, G. (1999) Cavity-enhanced absorption spectroscopy of the 1.5 μm band system of jet-cooled ammonia. *Chemical Physics Letters*, **307**(3–4), 131–138.

Berger, R., Laubender, G., Quack, M., Sieben, A., Stohner, J., and Willeke, M. (2005) Isotopic chirality and molecular parity violation. *Angewandte Chemie (International ed. in English)*, **44**(23), 3623–3626. 10.1002/anie.200462088.

Bernath, P.F., Hinkle, K.H., and Keady, J.J. (1989) Detection of C_5 in the circumstellar shell of IRC+10216. *Science*, **244**(4904), 562–564.

Beylich, A.E. (1979) Structure of supersonic free-jets produced by slit orifices. *Zeitschrift fur Flugwissenschaften und Weltraumforschung*, **3**, 48–58.

Birza, P., Motylewski, T., Khoroshev, D., Chirokolava, A., Linnartz, H., and Maier, J. (2002) CW cavity ring down spectroscopy in a pulsed planar plasma expansion. *Chemical Physics*, **283**(1–2, Sp. ISS. SI), 119–124.

Bisson, R., Dang, T.T., Sacchi, M., and Beck, R.D. (2007) Cavity ring-down spectroscopy of jet-cooled silane isotopomers in the Si-H stretch overtone region. *Journal of Chemical Physics*, **127**(24), 244–301.

Block, P.A., Marshall, M.D., Pedersen, L.G., and Miller, R.E. (1992) Wide amplitude motion in the water carbon-dioxide and water-acetylene complexes. *Journal of Chemical Physics*, **96**(10), 7321–7332.

Bonhoeffer, K.F. and Harteck, P. (1929) Experiments on para-hydrogen and ortho-hydrogen. *Naturwissenschaften*, **17**, 182.

Boudon, V., Rotger, M., He, Y., Hollenstein, H., Quack, M., and Schmitt, U. (2002) High-resolution spectroscopy of the ν_3 band of WF_6 and ReF_6 in a supersonic jet. *Journal of Chemical Physics*, **117**(7), 3196–3207.

Boudon, V., Champion, J.-P., Gabard, T., Loëte, M., Rotger, M., and Wenger, C. (2011) Spherical top theory and molecular spectra, in *Handbook of High-resolution Spectroscopy*, Quack, M. and Merkt, F. (eds), John Wiley & Sons, Ltd., Chichester, UK.

Brassington, D.J. (1995) Tunable diode laser absorption spectroscopy for the measurement of atmospheric species, in Advances in spectroscopy, in *Spectroscopy in Environmental Science*, Hester, R. (ed.), John Wiley, New York.

Brookes, M.D., Hughes, D.J., and Howard, B.J. (1996) Spectroscopy and dynamics of rare gas-spherical top complexes. II. The infrared spectrum of the ν_3 band of Ne-SiH_4 ($j = 1 \longleftarrow 0$ and $j = 0 \longleftarrow 1$ transitions). *Journal of Chemical Physics*, **104**(14), 5391–5405.

Brookes, M.D., Hughes, D.J., and Howard, B.J. (1997) Spectroscopy and dynamics of rare gas-spherical top complexes. III. The infrared spectrum of the ν_3 band of Ne-SiH_4 ($j = 1 \longleftarrow 1$ and $j = 2 \longleftarrow 1$ transitions). *Journal of Chemical Physics*, **107**(8), 2738–2751.

Brookes, M.D. and McKellar, A.R.W. (1998) Infrared spectrum of the water-carbon monoxide complex in the CO stretching region. *Journal of Chemical Physics*, **109**(14), 5823–5829.

Bürger, H., Burczyk, K., Hollenstein, H., and Quack, M. (1985) High resolution FTIR spectra of $^{12}CF_3I$, $^{13}CF_3I$ and $^{12}CF_3^{79}Br$ near $1050\,cm^{-1}$ and $550\,cm^{-1}$. *Molecular Physics*, **55**(2), 255–275.

Bürger, H., Goergens, U., Ruland, H., Quack, M., and Schmitt, U. (1996) Supersonic jet spectroscopy and high resolution FTIR study of SPF_3 analysis of the ν_1, ν_2 and ν_3 bands. *Molecular Physics*, **87**(2), 469–483.

Bürger, H., Rahner, A., Amrein, A., Hollenstein, H., and Quack, M. (1989) Free-jet high-resolution FTIR spectroscopy of the complex structure of the ν_1 band of CF_3I near $9\,\mu m$. *Chemical Physics Letters*, **156**(6), 557–563.

Buus, J., Amann, M.-C., and Blumenthal, D. (2005) *Tunable Laser Diodes and Related Optical Sources*, John Wiley and Sons.

Cable, J.R., Tubergen, M.J., and Levy, D.H. (1987) Laser desorption molecular-beam spectroscopy-the electronic-spectra of tryptophan peptides in the gas-phase. *Journal of the American Chemical Society*, **109**(20), 6198–6199.

Callegari, C. and Ernst, W.E. (2011) Helium droplets as nanocryostats for molecular spectroscopy—from the vacuum ultraviolet to the microwave regime, in *Handbook of High-resolution Spectroscopy*, Quack, M. and Merkt, F. (eds), John Wiley & Sons, Ltd., Chichester, UK.

Caneau, C., Srivastava, A.K., Dentai, A.G., Zyskind, J.L., and Pollack, M.A. (1985) Room-temperature GaInAsSb/AlGaAsSb DH injection-lasers at $2.2\,\mu m$. *Electronics Letters*, **21**(18), 815–817.

Capasso, F., Gmachl, C., Paiella, R., Tredicucci, A., Hutchinson, A.L., Sivco, D.L., Baillargeon, J.N., Cho, A.Y., and Liu, H.C. (2000) New frontiers in quantum cascade lasers and applications. *IEEE Journal of Selected Topics in Quantum Electronics*, **6**(6), 931–947.

Castillo-Chara, J., McIntosh, A.L., Wang, Z., Lucchese, R.R., and Bevan, J.W. (2004) Near-infrared spectra and rovibrational dynamics on a four-dimensional ab initio potential energy surface of $(HBr)_2$. *Journal of Chemical Physics*, **120**(22), 10426–10441.

Cess, R.D., Zhang, M.H., Minnis, P., Corsetti, L., Dutton, E.G., Forgan, B.W., Garber, D.P., Gates, W.L., Hack, J.J., Harrison, E.F. *et al*. (1995) Absorption of solar-radiation by clouds: observations versus models. *Science*, **267**(5197), 496–499.

Chapovsky, P. and Hermans, L.J.F. (1999) Nuclear spin conversion in polyatomic molecules. *Annual Review of Physical Chemistry*, **50**, 315–345.

Cheo, P.K. (1994) Electrooptic waveguide modulators for frequency tuning of infrared lasers. *Journal of Quantitative Spectroscopy and Radiative Transfer*, **51**(4), 579–590.

Coudert, L.H., Çarçabal, P., Chevalier, M., Broquier, M., Hepp, M., and Herman, M. (2002) High-resolution analysis of the ν_6, ν_{17} and ν_{21} bands of dimethyl ether. *Journal of Molecular Spectroscopy*, **212**, 203–207.

D'Amico, G. and Snels, M. (2002) Diode laser slit-jet spectra and analysis of the ν_7 fundamental of 1-chloro-1,1-difluoroethane (HCFC-142b). *European Physical Journal D*, **D21**, 137–142.

D'Amico, G. and Snels, M. (2003) Diode laser slit-jet spectra and analysis of the ν_{14} fundamental of 1-chloro-1,1-difluoroethane (HCFC-142b). *Journal of Molecular Spectroscopy*, **217**, 72–78.

D'Amico, G., Snels, M., Hollenstein, H., and Quack, M. (2002) Analysis of the $\nu_3 + \nu_7$ combination band of CF_2Cl_2 from spectra obtained by high resolution diode laser and FTIR supersonic jet techniques. *Physical Chemistry Chemical Physics*, **4**(9), 1531–1536.

Davis, S., Anderson, D.T., Duxbury, G., and Nesbitt, D.J. (1997) Jet-cooled molecular radicals in slit supersonic discharges: sub-Doppler infrared studies of methyl radical. *Journal of Chemical Physics*, **107**, 5661–5675.

Davis, S., Fárník, M., Uy, D., and Nesbitt, D.J. (2001) Concentration modulation spectroscopy with a pulsed slit supersonic discharge expansion source. *Chemical Physics Letters*, **344**(1–2), 23–30.

Dehghany, M., Afshari, M., Moazzen-Ahmadi, N., and McKellar, A.R.W. (2008) The cyclic CO_2 trimer: observation of a parallel band and determination of an intermolecular out-of-plane torsional frequency. *Journal of Chemical Physics*, **128**(6), 064308-1–064308-5.

Demtröder, W. (2011) Doppler-free laser spectroscopy, in *Handbook of High-resolution Spectroscopy*, Quack, M. and Merkt, F. (eds), John Wiley & Sons, Ltd., Chichester, UK.

Di Lauro, C., D'Amico, G., and Snels, M. (2009) Torsional splittings in the diode laser slit-jet spectra of the ν_6 fundamental of 1-chloro-1,1-difluoroethane (HCFC-142b). *Journal of Molecular Spectroscopy*, **254**(2), 108–118.

Didriche, K., Macko, P., Herman, M., Thiévin, J., Benidar, A., and Georges, R. (2007) Investigation of the shape of the $R(0)$ absorption line in ν_3, N_2O recorded from an axisymmetric supersonic free jet expansion. *Journal of Quantitative Spectroscopy and Radiative Transfer*, **105**, 128–138.

Dietiker, P., Quack, M., Schneider, A., Seyfang, G., and Ünlü, F. (2010) Cavity enhanced saturation spectroscopy of NH_3 in the near infrared, in *Proceedings of the 17th SASP 2010*, Milewski, I., Kendl, A., and Scheier, P. (eds), Innsbruck University Press (IUP), Innsbruck, pp. 161–164.

Dopfer, O., Olkhov, R.V., and Maier, J.P. (1999a) Infrared dissociation spectra of the C-H stretch vibrations of $C_6H_6^+$-Ar, $C_6H_6^+$-N_2 and $C_6H_6^+$-$(CH_4)_{1-4}$. *Journal of Chemical Physics*, **111**, 10754–10757.

Dopfer, O., Roth, D., and Maier, J.P. (1999b) Infrared spectrum and ab initio calculations of the He-HNH^+ open shell ionic complex. *Chemical Physics Letters*, **310**, 201–208.

Dopfer, O., Roth, D., and Maier, J.P. (2002) Infrared spectra of $C_3H_3^+$-N_2 dimers: identification of proton-bound c-$C_3H_3^+$-N_2 and H_2CCCH^+-N_2 isomers. *Journal of the American Chemical Society*, **124**, 494–502.

Duan, C.X. and Luckhaus, D. (2004) High resolution IR-diode laser jet spectroscopy of malonaldehyde. *Chemical Physics Letters*, **391**(1–3), 129–133.

Duarte, F.J. (1985) Variable linewidth high-power TEA CO_2 laser. *Applied Optics*, **24**(1), 34–37.

Dübal, H.R., Quack, M., and Schmitt, U. (1984) High-resolution interferometric infrared spectroscopy of CO_2 and CH_4 vapor at low-temperature near 10 K: collisional cooling in supersonic jets and nuclear spin symmetry conservation. *Chimia*, **38**(12), 438–439.

Dyke, T.R., Howard, B.J., and Klemperer, W. (1972) Radiofrequency and microwave-spectrum of hydrogen-fluoride dimer-nonrigid molecule. *Journal of Chemical Physics*, **56**(5), 2442.

Dymanus, A. (1976) Beam maser spectroscopy in international review of science series 2, Vol. 3, pp. 127–204, Buckingham, A.D. and Ramsey, D.A. (eds), Butterworths, London.

Ebrahimzadeh, M. (2003) Mid-infrared ultrafast and continuous-wave optical parametric oscillators, in *Solid-State Mid-Infrared Laser Sources (Topics in Applied Physics)*, Sorokina, I.T. and Vodopyanov, K.L. (eds), Springer-Verlag, Berlin, pp. 179–218, Vol. 89.

Endo, Y. and Sumiyoshi, Y. (2011) Rotational spectroscopy of complexes containing free radicals, in *Handbook of High-resolution Spectroscopy*, Quack, M. and Merkt, F. (eds), John Wiley & Sons, Ltd., Chichester, UK.

Ernst, R., Bodenhausen, G., and Wokaun, A. (1987) *Principles of Nuclear Magnetic Resonance in One and Two Dimensions*, Clarendon Press, Oxford.

Faist, J., Capasso, F., Sivco, D.L., Sirtori, C., Hutchinson, A.L., and Cho, A.Y. (1994a) Quantum cascade laser. *Science*, **264**(5158), 553–556.

Faist, J., Capasso, F., Sivco, D.L., Sirtori, C., Hutchinson, A.L., and Cho, A.Y. (1994b) Quantum cascade laser-an intersub-band semiconductor-laser operating above liquid-nitrogen temperature. *Electronics Letters*, **30**(11), 865–866.

Fárník, M. and Nesbitt, D.J. (2004) Intramolecular energy transfer between oriented chromophores: high-resolution infrared spectroscopy of HCl trimer. *Journal of Chemical Physics*, **121**(24), 12386–12395.

Firanescu, G., Hermsdorf, D., Ueberschaer, R., and Signorell, R. (2006) Large molecular aggregates: from atmospheric aerosols to drug nanoparticles. *Physical Chemistry Chemical Physics*, **8**(36), 4149–4165.

Fischer, C. and Sigrist, M.W. (2003) Mid-IR difference frequency generation, in *Solid-State Mid-Infrared Laser Sources (Topics in Applied Physics)*, Sorokina, I.T. and Vodopyanov, K.L. (eds), Springer-Verlag, Berlin, pp. 97–140, vol. 89.

Flaud, J.-M. and Orphal, J. (2011) Spectroscopy of the earth's atmosphere, in *Handbook of High-resolution Spectroscopy*, Quack, M. and Merkt, F. (eds), John Wiley & Sons, Ltd., Chichester, UK.

Flaud, J-M., Lafferty, W.J., and Herman, M. (2001) First high resolution analysis of the absorption spectrum of propane in the 6.7 μm to 7.5 μm spectral region. *Journal of Chemical Physics*, **114**, 9361–9366.

Fraser, G.T., Pine, A.S., Lafferty, W.J., and Miller, R.E. (1987) Sub-Doppler infrared-spectrum of the carbon-dioxide trimer. *Journal of Chemical Physics*, **87**(3), 1502–1508.

Freed, C., Bradley, L., and O'Donnell, R. (1980) Absolute frequencies of lasing transitions in seven CO_2 isotopic species. *IEEE Journal of Quantum Electronics*, **16**, 1195–1206.

Frey, H.-M., Kummli, D., Lobsiger, S., and Leutwyler, S. (2011) High-resolution rotational Raman coherence spectroscopy with femtosecond pulses, in *Handbook of High-resolution Spectroscopy*, Quack, M. and Merkt, F. (eds), John Wiley & Sons, Ltd., Chichester, UK.

Frum, C.I., Engleman, R., Hedderich, H.G., Bernath, P.F., Lamb, L.D., and Huffman, D.R. (1991) The infrared-emission spectrum of gas-phase C_{60} (buckminsterfullerene). *Chemical Physics Letters*, **176**(6), 504–508.

Fukushima, M., Chan, M.C., Xu, Y.J., Taleb-Bendiab, A., and Amano, T. (1994) High-resolution infrared-absorption spectroscopy of jet-cooled molecular-ions. *Chemical Physics Letters*, **230**(6), 561–566.

Georges, R., Bonnamy, A., Benidar, A., Decroi, M., and Boissoles, J. (2002) FTIR free-jet set-up for the high resolution spectroscopic investigation of condensable species. *Molecular Physics*, **100**, 1551–1558.

Gerlach, W. (1925) Über die Richtungsquantelung im Magnetfeld II. Experimentelle Untersuchungen über das Verhalten normaler Atome unter magnetischer Kraftwirkung. *Annalen der Physik*, **381**(2–3), 163–197.

Gerlach, W. and Stern, O. (1924) The directional quantisation in the magnetic field. *Annalen der Physik*, **74**(16), 673–697.

Giesen, T.F., Vanorden, A., Hwang, H.J., Fellers, R.S., Provencal, R.A., and Saykally, R.J. (1994) Infrared-laser spectroscopy of the linear C_{13} carbon cluster. *Science*, **265**(5173), 756–759.

Gimmler, G. and Havenith, M. (2002) High-resolution IR spectroscopy of the N_2O-H_2O and N_2O-D_2O van der Waals complexes. *Journal of Molecular Spectroscopy*, **216**(2), 315–321.

Goldenberg, H.M., Kleppner, D., and Ramsey, N.F. (1960) Atomic hydrogen maser. *Physical Review Letters*, **5**(8), 361–362.

Gordon, J.P., Zeiger, H.J., and Towner, C.H. (1955) Majer-new type of microwave amplifier, frequency standard, and spectrometer. *Physical Review*, **99**, 1264–1274.

Gough, T.E., Miller, R.E., and Scoles, G. (1977) IR laser spectroscopy of molecular-beams. *Applied Physics Letters*, **30**(7), 338–340.

Gregory, J.K., Clary, D.C., Liu, K., Brown, M.G., and Saykally, R.J. (1997) The water dipole moment in water clusters. *Science*, **275**(5301), 814–817.

Gu, X.J., Levandier, D.J., Zhang, B., Scoles, G., and Zhuang, D. (1990) On the infrared spectroscopy of SiF_4 and SF_6 in Ar clusters: location of the solute. *Journal of Chemical Physics*, **93**(7), 4898–4906.

Gudeman, C.S. and Saykally, R.J. (1984) Velocity modulation of infrared laser spectroscopy of molecular ions. *Annual Review of Physical Chemistry*, **35**, 387–418.

Guennoun, Z. and Maier, J.P. (2011) Electronic spectroscopy of transient molecules, in *Handbook of High-resolution Spectroscopy*, Quack, M. and Merkt, F. (eds), John Wiley & Sons, Ltd., Chichester, UK.

Ha, T., He, Y., Pochert, J., Quack, M., Ranz, R., Seyfang, G., and Thanopoulos, I. (1995) Absolute integrated band strength and magnetic dipole transition moments in the $^2P_{3/2} \rightarrow 2P_{1/2}$ fine structure (with hyperfine structure) transition of the iodine atom: Experiment and theory. *Berichte der Bunsen-Gesellschaft für Physikalische Chemie*, **99**(3), 384–392.

Hagena, O.F. (1981) Nucleation and growth of clusters in expanding nozzle flows. *Surface Science*, **106**(1–3), 101–116.

Hartmann, M., Miller, R.E., Toennies, J.P., and Vilesov, A.F. (1996) High-resolution molecular spectroscopy of van der Waals clusters in liquid helium droplets. *Science*, **272**(5268), 1631–1634.

Havenith, M. (2002) The molecular beam, in *Infrared Spectroscopy of Molecular Clusters (Springer Tracts in Modern Physics)*, Springer-Verlag, Berlin, pp. 35–46, vol. 176.

Havenith, M. and Birer, Ö. (2011) High-resolution IR-laser jet spectroscopy of formic acid dimer, in *Handbook of High-resolution Spectroscopy*, Quack, M. and Merkt, F. (eds), John Wiley & Sons, Ltd., Chichester, UK.

Hayman, G.D., Hodge, J., Howard, B.J., Muenter, J.S., and Dyke, T.R. (1989) Infrared-absorption spectra of Ar-OCS and Kr-OCS van der Waals complexes in the carbonyl stretching region. *Journal of Molecular Spectroscopy*, **133**(2), 423–437.

He, Y., Hippler, M., and Quack, M. (1998) High-resolution cavity ring-down absorption spectroscopy of nitrous oxide and chloroform using a near-infrared cw diode laser. *Chemical Physics Letters*, **289**(5–6), 527–534.

He, Y., Hollenstein, H., Quack, M., Richard, E., Snels, M., and Bürger, H. (2002) High resolution analysis of the complex symmetric CF_3 stretching chromophore absorption in CF_3I. *The Journal of Chemical Physics*, **116**(3), 974–983.

He, Y., Pochert, J., Quack, M., Ranz, R., and Seyfang, G. (1995) Discussion contributions on unimolecular reactions dynamics. *Journal of the Chemical Society Faraday Discussions*, **102**, 354–358.

He, Y.B., Müller, H.B., Quack, M., and Suhm, M.A. (2007) High resolution FTIR and diode laser supersonic jet spectroscopy of the $N = 2$ HF-stretching polyad in $(HF)_2$ and (HFDF): hydrogen bond switching and predissociation dynamics. *Zeitschrift für Physikalische Chemie*, **221**, 1581–1645.

Heath, J.R., Cooksy, A.L., Gruebele, M.H.W., Schmuttenmaer, C.A., and Saykally, R.J. (1989) Diode-laser absorption-spectroscopy of supersonic carbon cluster beams-The ν_3 spectrum of C_5. *Science*, **244**(4904), 564–566.

Heath, J.R. and Saykally, R.J. (1990) The C_9 cluster-Structure and infrared frequencies. *Journal of Chemical Physics*, **93**(11), 8392–8394.

Heath, J.R. and Saykally, R.J. (1991a) Infrared-laser absorption-spectroscopy of the $\nu_4(\sigma_u)$ fundamental and associated $\nu_{11}(\pi_u)$ hot band of C_7-Evidence for alternating rigidity in linear carbon clusters. *Journal of Chemical Physics*, **94**(3), 1724–1729.

Heath, J.R. and Saykally, R.J. (1991b) The structure of the C_4 cluster radical. *Journal of Chemical Physics*, **94**(4), 3271–3273.

Heath, J.R., Sheeks, R.A., Cooksy, A.L., and Saykally, R.J. (1990) The C_7 cluster-structure and infrared frequencies. *Science*, **249**(4971), 895–897.

Herlemont, F., Lyszyk, M., Lemaire, J., Lambeau, C., and Fayt, A. (1979) Laser spectroscopy of ethylene with waveguide CO_2 and N_2O lasers. *Journal of Molecular Spectroscopy*, **74**(3), 400–408.

Herman, M. (2011) High-resolution infrared spectroscopy of acetylene: theoretical background and research trends, in *Handbook of High-resolution Spectroscopy*, Quack, M. and Merkt, F. (eds), John Wiley & Sons, Ltd., Chichester, UK.

Herman, M., Didriche, K., Hurtmans, D., Kizil, B., Macko, P., Rizopoulos, A., and Van Poucke, P. (2007) FANTASIO: a versatile experimental set-up to investigate jet-cooled molecules. *Molecular Physics*, **105**, 815–823.

Herman, M., Didriche, K., Rizopoulos, A., and Hurtmans, D. (2005) FT-jet spectroscopy: vibrational energy transfer in N_2O. *Chemical Physics Letters*, **414**, 282–286.

Herman, M., Georges, R., Hepp, M., and Hurtmans, D. (2000) High resolution Fourier transform spectroscopy of jet-cooled molecules. *International Reviews in Physical Chemistry*, **19**(2), 277–325.

Herrebout, W., Qian, H.B., Yamaguchi, H., and Howard, B.J. (1998) High-resolution infrared diode laser spectroscopy of Ne-N_2O, Kr-N_2O, and Xe-N_2O. *Journal of Molecular Spectroscopy*, **189**(2), 235–243.

Hilpert, G., Linnartz, H., Havenith, M., ter Meulen, J.J., and Meerts, W.L. (1994) Tunable infrared and far-infrared direct absorption spectroscopy of molecular ions in a supersonic jet expansion. *Chemical Physics Letters*, **219**(5–6), 384–388.

Hinkle, K.W., Keady, J.J., and Bernath, P.F. (1988) Detection of C_3 in the circumstellar shell of IRC+10216. *Science*, **241**(4871), 1319–1322.

Hippler, M. and Quack, M. (1999) Cw cavity ring-down infrared absorption spectroscopy in pulsed supersonic jets: nitrous oxide and methane. *Chemical Physics Letters*, **314**(3–4), 273–281.

Hippler, M. and Quack, M. (2002) High-resolution Fourier transform infrared and cw-diode laser cavity ringdown spectroscopy of the $\nu_2 + 2\nu_3$ band of methane near $7510\,cm^{-1}$ in slit jet expansions and at room temperature. *Journal of Chemical Physics*, **116**(14), 6045–6055.

Hippler, M. and Quack, M. (2005) Isotope Selective Infrared Spectroscopy and Intramolecular Dynamics, in *Isotope Effects in Chemistry and Biology, Part III, Isotope Effects in Chemical Dynamics, Chapter 10*, Kohen, A. and Limbach, H.-H. (eds), Marcel Dekker Inc., New York, pp. 305–359.

Hippler, M., Oeltjen, M., and Quack, M. (2007) High-resolution continuous-wave-diode laser cavity ring-down spectroscopy of the hydrogen fluoride dimer in a pulsed slit jet expansion: two components of the $N = 2$ triad near $1.3\,\mu m$. *Journal of Physical Chemistry A*, **111**, 12659–12668.

Hippler, M., Miloglyadov, E., Quack, M., and Seyfang, G. (2011) Mass and isotope-selective infrared spectroscopy, in *Handbook of High-resolution Spectroscopy*, Quack, M. and Merkt, F. (eds), John Wiley & Sons, Ltd., Chichester, UK.

Hofstetter, D. and Faist, J. (2003) High performance quantum cascade lasers and their applications, in *Solid-State Mid-Infrared Laser Sources (Topics in Applied Physics)*, Sorokina, I.T. and Vodopyanov, K.L. (eds), Springer-Verlag Berlin, pp. 61–96, vol. 89.

Hollenstein, H., Quack, M., and Richard, E. (1994) Slit jet diode laser and FTIR spectroscopy of CF_3I and improved analysis of the symmetric CF_3 stretching chromophore absorption. *Chemical Physics Letters*, **222**(1–2), 176–184.

Horká, V., Albert, S., Caviezel, M., Quack, M., Seyfang, G., and Sieben, A. (2008) Combined high resolution FTIR and supersonic jet-diode laser spectroscopic study of $PFCl_2$: rovibrational analysis of the PF-stretching mode ν_1, *The 20th International Conference on High Resolution Molecular Spectroscopy*, Prague, Czech Republic and manuscript in preparation.

Horká-Zelenková, V., Caviezel, M., Quack, M., and Seyfang, G. (2010) Test of nuclear spin symmetry conservation in partially deuterated methane isotopomers in expansion of a molecular supersonic jet. *Chimia*, **64**, 568 and manuscript in preparation.

Huang, Z.S. and Miller, R.E. (1988) The structure of the nitrous-oxide dimer from sub-Doppler resolution infrared-spectroscopy. *Journal of Chemical Physics*, **89**(9), 5408–5416.

Hugi, A., Terazzi, R., Bonetti, Y., Wittmann, A., Fischer, M., Beck, M., Faist, J., and Gini, E. (2009) External cavity quantum cascade laser tunable from 7.6 to 11.4 μm. *Applied Physics Letters*, **95**(6), 061103-1–061103-3.

Huneycutt, A.J., Casaes, R.N., McCall, B.J., Chung, C.Y., Lee, Y.P., and Saykally, R.J. (2004) Infrared cavity ringdown spectroscopy of jet-cooled polycylic aromatic hydrocarbons. *ChemPhysChem*, **5**(3), 321–326.

Hurtmans, D., Rizopoulos, A., Herman, M., Hassan, L.M.S., and Perrin, A. (2001) Vibration-rotation analysis of the jet-cooled ν_{12}, $\nu_7 + \nu_8$ and $\nu_6 + \nu_{10}$ absorption bands of $^{12}C_2H_4$. *Molecular Physics*, **99**, 455–461.

Hwang, H.J., van Orden, A., Tanaka, K., Kuo, E.W., Heath, J.R., and Saykally, R.J. (1993) Infrared-laser spectroscopy of jet-cooled carbon clusters-structure of triplet C_6. *Molecular Physics*, **79**(4), 769–776.

Ito, F. and Nakanaga, T. (2002) Jet-cooled infrared spectra of the formic acid dimer by cavity ring-down spectroscopy: observation of the O-H stretching region. *Chemical Physics*, **277**(2), 163–169.

Jäger, W. and Xu, Y. (2011) Fourier transform microwave spectroscopy of doped helium clusters, in *Handbook of High-resolution Spectroscopy*, Quack, M. and Merkt, F. (eds), John Wiley & Sons, Ltd., Chichester, UK.

Joullié, A., Christol, P., Baranov, A.N., and Vicet, A. (2003) Mid-infrared 2–5 μm heterojunction laser diodes, in *Solid-State Mid-Infrared Laser Sources (Topics in Applied Physics)*, Sorokina, I.T. and Vodopyanov, K.L. (eds), Springer-Verlag Berlin, pp. 1–59, vol. 89.

Kappes, M. and Leutwyler, S. (1988) Molecular beams of clusters, in *Atomic and Molecular Beam Methods*, Scoles, G. (ed.), Oxford University Press, Oxford, pp. 380–415, vol.1.

Kaur, D., Desouza, A.M., Wanna, J., Hammad, S.A., Mercorelli, L., and Perry, D.S. (1990) Multipass cell for molecular-beam absorption-spectroscopy. *Applied Optics*, **29**(1), 119–124.

Keutsch, F.N., Cruzan, J.D., and Saykally, R.J. (2003) The water trimer. *Chemical Reviews*, **103**(7), 2533–2577.

Kim, H., Dooley, K.S., Johnson, E.R., and North, S.W. (2005) Design and characterization of late-mixing flash pyrolytic reactor molecular-beam source. *Review of Scientific Instruments*, **76**(12), 124101.

Kim, K.C., Holland, R.F., and Filip, H. (1978) Infrared spectroscopy in supersonic molecular-beams-ν_3 band of SF_6 at 10.6 μm. *Applied Spectroscopy*, **32**(3), 287–289.

Klopper, W., Quack, M., and Suhm, M.A. (1996) A new ab initio based six-dimensional semi-empirical pair interaction potential for HF. *Chemical Physics Letters*, **261**(1–2), 35–44.

Klopper, W., Quack, M., and Suhm, M.A. (1998) HF dimer: empirically refined analytical potential energy and dipole hypersurfaces from ab initio calculations. *Journal of Chemical Physics*, **108**(24), 10096–10115.

Kolb, C.E., Jayne, J.T., Worsnop, D.R., Molina, M.J., Meads, R.F., and Viggiano, A.A. (1994) Gas-phase reaction of sulfur trioxide with water-vapor. *Journal of the American Chemical Society*, **116**(22), 10314–10315.

Kroto, H.W. (1987) The stability of the fullerenes C_{24}, C_{28}, C_{32}, C_{36}, C_{50}, C_{60} and C_{70}. *Nature*, **329**(6139), 529–531.

Kroto, H.W. (1997) Symmetry, space, stars, and C_{60} (Nobel lecture). *Angewandte Chemie (International ed. in English)*, **36**, 1578–1593.

Kroto, H.W., Heath, J.R., O'Brien, S.C., Curl, R.F., and Smalley, R.E. (1985) C_{60}-Buckminsterfullerene. *Nature*, **318**(6042), 162–163.

Lafferty, W.J., Flaud, J.-M., and Herman, M. (2006) Resolved torsional splitting in the ν_{18} and ν_{19} bands of propene. *Journal of Molecular Structure*, **780**, 65–69.

Lee, Y.C., Venkatesan, V., Lee, Y.P., Macko, P., Didriche, K., and Herman, M. (2007) Infrared spectra of C_2H_2 under jet-cooled and *para*-H_2 matrix conditions. *Chemical Physics Letters*, **435**, 247–251.

Lehmann, K.K., Scoles, G., and Pate, B.H. (1994) Intramolecular dynamics from eigenstate-resolved infrared-spectra. *Annual Review of Physical Chemistry*, **45**, 241–274.

Lehnig, R. and Jäger, W. (2006) Infrared spectroscopy of the antisymmetric stretching mode of $^{16}OC^{18}O$ in helium nanodroplets. *Chemical Physics Letters*, **424**(1–3), 146–150.

Levandier, D.J., McCombie, J., Pursel, R., and Scoles, G. (1987) Complex-forming reactions in neutral noble gas clusters. *Journal of Chemical Physics*, **86**(12), 7239–7241.

Levy, D.H. (1980) Laser spectroscopy of cold gas-phase molecules. *Annual Review of Physical Chemistry*, **31**, 197–225.

Li, Z., Barker, H.W., and Moreau, L. (1995) The variable effect of clouds on atmospheric absorption of solar-radiation. *Nature*, **376**(6540), 486–490.

Lin, H., Thiel, W., Yurchenko, S.N., Carvajal, M., and Jensen, P. (2002) Vibrational energies for NH_3 based on high level ab initio potential energy surfaces. *Journal of Chemical Physics*, **117**(24), 11265–11276.

Linnartz, H., Speck, T., and Maier, J.P. (1998) High-resolution infrared spectrum of the ν_3 band in Ar-HCO^+. *Chemical Physics Letters*, **288**, 504–508.

Linnartz, H., Verdes, D., and Speck, T. (2000) High resolution infrared direct absorption spectroscopy of ionic complexes. *Review of Scientific Instruments*, **71**(4), 1811–1815.

Liu, D-J. and Oka, T. (1985) Experimental determination of the ground-state inversion splitting in H_3O^+. *Physical Review Letters*, **54**(16), 1787–1789.

Liu, D.-J. and Oka, T. (1986) Observation of the rotational spectrum of OH^-. *Journal of Chemical Physics*, **84**(4), 2426–2427.

Liu, K., Brown, M.G., and Saykally, R.J. (1997) Terahertz laser vibration rotation tunneling spectroscopy and dipole moment of a cage form of the water hexamer. *Journal of Physical Chemistry A*, **101**(48), 8995–9010.

Liu, K., Cruzan, J.D., and Saykally, R.J. (1996) Water clusters. *Science*, **271**(5251), 929–933.

Liu, K., Elrod, M.J., Loeser, J.G., Cruzan, J.D., Pugliano, N., Brown, M.G., Rzepiela, J., and Saykally, R.J. (1994) Far-IR

vibration-rotation tunneling spectroscopy of the water trimer. *Faraday Discussions*, **97**, 35–41, Meeting on Structure and Dynamics of Van der Waals Complexes, Durham, England.

Liu, Z., Livingstone, R.J., and Davies, P.B. (1998) Pulse pyrolysis infrared laser jet spectroscopy of free radicals. *Chemical Physics Letters*, **291**, 480–486.

Luckhaus, D. and Quack, M. (1992) High-resolution FTIR spectra of NO_2 and N_2O_4 in supersonic jet expansions and their rovibrational analysis. *Chemical Physics Letters*, **199**(3–4), 293–301.

Luckhaus, D., Quack, M., Schmitt, U., and Suhm, M. (1995) On FTIR spectroscopy in asynchronously pulsed supersonic free jet expansions and on the interpretation of stretching spectra of HF clusters. *Berichte der Bunsen-Gesellschaft für Physikalische Chemie*, **99**(3), 457–468.

Lupo, D. and Quack, M. (1987) IR-laser photochemistry. *Chemical Reviews*, **87**(1), 181–216. 10.1021/cr00077a010.

Maerker, C., Schleyer, P., Liedl, K., Ha, T., Quack, M., and Suhm, M. (1997) A critical analysis of electronic density functionals for structural, energetic, dynamic, and magnetic properties of hydrogen fluoride clusters. *Journal of Computational Chemistry*, **18**(14), 1695–1719.

Manca, C., Quack, M., and Willeke, M. (2008) Vibrational predissociation in hydrogen bond dimers: the case of $(HF)_2$ and its isotopomers. *Chimia*, **62**(4), 235–239.

Marquardt, R. and Quack, M. (2001) Energy redistribution in reacting systems, in *Encyclopedia of Chemical Physics and Physical Chemistry, (Fundamentals)*, Moore, J. and Spencer, N. (eds), IOP Publications, Bristol, pp. 897–936, Chapter A.3.13, Vol. 1.

Marquardt, R. and Quack, M. (2011) Global analytical potential energy surfaces for high-resolution molecular spectroscopy and reaction dynamics, in *Handbook of High-resolution Spectroscopy*, Quack, M. and Merkt, F. (eds), John Wiley & Sons, Ltd., Chichester, UK.

Marquardt, R., Sagui, K., Klopper, W., and Quack, M. (2005) Global analytical potential energy surface for large amplitude nuclear motions in ammonia. *Journal of Physical Chemistry B*, **109**, 8439–8451.

Matsumura, K., Kanamori, H., Kawaguchi, K., and Hirota, E. (1988) Infrared diode-laser kinetic spectroscopy of the ν_3 band of C_3. *Journal of Chemical Physics*, **89**(6), 3491–3494.

Mazzotti, F.J., Achkasova, E., Chauhan, R., Tulej, M., Radi, P.P., and Maier, J.P. (2008) Electronic spectra of radicals in a supersonic slit-jet discharge by degenerate and two-color four-wave mixing. *Physical Chemistry Chemical Physics*, **10**, 136–141.

McCarthy, M.C., Gottlieb, C.A., Gupta, H., and Thaddeus, P. (2006) Laboratory and astronomical identification of the negative molecular ion C_6H^-. *Astrophysical Journal*, **652**(2, Part 2), L141–L144.

McIntosh, A.L., Wang, Z., Lucchese, R.R., and Bevan, J.W. (2000) 4.5 μm diode laser spectrum of $(HI)_2$. *Chemical Physics Letters*, **328**(1–2), 153–159.

McKellar, A.R.W. (2004) High resolution infrared spectra of helium clusters seeded with isotopic carbon monoxide, $He_N-{}^{13}C^{16}O$ and $He_N-{}^{12}C^{18}O$. *Journal of Chemical Physics*, **121**(14), 6868–6873.

McKellar, A.R.W. (2006) Infrared spectra of isotopic CO_2-He complexes. *Journal of Chemical Physics*, **125**(11), 114310-1–114310-5.

McKellar, A.R.W. (2008) Infrared spectra of CO_2-doped ^{4}He clusters, ^4He_N-CO_2, with $N = 1$-60. *Journal of Chemical Physics*, **128**(4), 044308-1–044308-9.

McKellar, A.R.W., Xu, Y.J., Jäger, W., and Bissonnette, C. (1999) Isotopic probing of very weak intermolecular forces: microwave and infrared spectra of CO-He isotopomers. *Journal of Chemical Physics*, **110**(22), 10766–10773.

McNaughton, D., McGilvery, D., and Robertson, E.G. (1994) High-resolution FTIR-jet spectroscopy of CCl_2F_2. *Journal of the Chemical Society Faraday Transactions*, **90**(8), 1055–1060.

Meerts, W.L. and Dymanus, A. (1975) Molecular-beam electric resonance study of hyperfine lambda-doubling spectrum of OH, OD, SH, and SD. *Canadian Journal of Physics*, **53**(19), 2123–2141.

Meerts, W.L., Bekooy, J.P., and Dymanus, A. (1979) Vibrational effects in the hydroxyl radical by molecular-beam electric resonance spectroscopy. *Molecular Physics*, **37**(2), 425–439.

Merkt, F. and Quack, M. (2011) Molecular quantum mechanics and molecular spectra, molecular symmetry, and interaction of matter with radiation, in *Handbook of High-resolution Spectroscopy*, Quack, M. and Merkt, F. (eds), John Wiley & Sons, Ltd., Chichester, UK.

Miller, D.R. (1988) Free jets sources, in *Atomic and Molecular Beam Methods*, Scoles, G. (ed.) Oxford University Press, Oxford, pp. 14–53, vol.1.

Miller, R.E. (1992) Infrared spectroscopy, in *Atomic and Molecular Beam Methods*, Scoles, G. (ed.), Oxford University Press, Oxford, pp. 192–212, vol.2.

Miller, R.E. and Pedersen, L. (1997) The structure of nitrous oxide tetramer from near infrared laser spectroscopy. *Chemical Physics Letters*, **275**(3–4), 307–313.

Miller, R.E. and Pedersen, L. (1998) The infrared spectrum and structure of the nitrous oxide trimer. *Journal of Chemical Physics*, **108**(2), 436–443.

Nizkorodov, S.A., Meuwly, M., Maier, J.P., Dopfer, O., and Bieske, E.J. (1998) Infrared predissociation spectra of Ne_n-HN_2^+ clusters ($n = 1 - 5$). *Journal of Chemical Physics*, **108**, 8964–8975.

Novick, S.E. (2008) *Bibliography of Rotational Spectra of Weakly Bound Complexes*, http://www.wesleyan.edu/chem/faculty/novick/vdw.html.

Novick, S.E., Davies, P., Harris, S.J., and Klemperer, W. (1973) Determination of structure of ArHCl. *Journal of Chemical Physics*, **59**(5), 2273–2279.

Ohshima, Y., Matsumoto, Y., Takami, M., and Kuchitsu, K. (1988) Free-jet infrared-absorption spectroscopy of the $(N_2O)_2$ van der Waals complex in the 8 μm region. *Chemical Physics Letters*, **152**(4–5), 294–298.

Oka, T. (1980) Observation of the infrared spectrum of H_3^+. *Physical Review Letters*, **45**(7), 531–534.

Oka, T. (2011) Orders of magnitude and symmetry in molecular spectroscopy, in *Handbook of High-resolution Spectroscopy*, Quack, M. and Merkt, F. (eds), John Wiley & Sons, Ltd., Chichester, UK.

Olafsson, A. and Henningsen, J. (1995) Intraline tunable CO_2 waveguide lasers and applications in high resolution spectroscopy. *Infrared Physics & Technology*, **36**(1), 309–319. Proceedings of the Sixth International Conference on Infrared Physics.

Ortlieb, M. and Havenith, M. (2007) Proton transfer in $(HCOOH)_2$: an IR high-resolution spectroscopic study of the antisymmetric C-O stretch. *Journal of Physical Chemistry A*, **111**(31), 7355–7363.

Owrutsky, J.C., Gudeman, C.S., Martner, C.C., Tack, L.M., Rosenbaum, N.H., and Saykally, R.J. (1986) Determination of the equilibrium structure of protonated nitrogen by high resolution infrared laser spectroscopy. *Journal of Chemical Physics*, **84**(2), 605–617.

Pak, I., Roth, D.A., Hepp, M., Winnewisser, G., Scouteris, D., Howard, B.J., and Yamada, K.M.T. (1998) High resolution spectroscopy of Ar-CH_4 and Kr-CH_4 in the 7 μm region ($j = 1 \leftarrow 0$ transition). *Zeitschrift für Naturforschung Section A-A Journal of Physical Sciences*, **53**(8), 725–732.

Papoušek, D. and Aliev, M.R. (1982) *Molecular Vibrational-Rotational Spectra*, Academia, Prague.

Patel, C.K.N. (1965) Cw high power N_2-CO_2 laser. *Applied Physics Letters*, **7**(1), 15–17.

Paul, J.B., Collier, C.P., Saykally, R.J., Scherer, J.J., and O'Keefe, A. (1997) Direct measurement of water cluster concentrations by infrared cavity ringdown laser absorption spectroscopy. *Journal of Physical Chemistry A*, **101**(29), 5211–5214.

Pratt, D.W. (2011) Electronic spectroscopy in the gas phase, in *Handbook of High-resolution Spectroscopy*, Quack, M. and Merkt, F. (eds), John Wiley & Sons, Ltd., Chichester, UK.

Petry, R., Klee, S., Lock, M., Winnewisser, B.P., and Winnewisser, M. (2002) Spherical mirror multipass system for FTIR jet spectroscopy: application to the rovibrationally resolved spectrum of OC_5O. *Journal of Molecular Structure*, **612**, 369–381.

von Puttkamer, K. and Quack, M. (1987) High-resolution interferometric FTIR spectroscopy of $(HF)_2$: analysis of a low frequency fundamental near 400 cm^{-1}. *Molecular Physics*, **62**(5), 1047–1064.

von Puttkamer, K., Quack, M., and Suhm, M.A. (1988) Observation and assignment of tunnelling rotational transitions in the far infrared-spectrum of $(HF)_2$. *Molecular Physics*, **65**(5), 1025–1045.

von Puttkamer, K., Quack, M., and Suhm, M.A. (1989) Infrared spectrum and dynamics of the hydrogen bonded dimer $(HF)_2$. *Infrared Physics*, **29**(2–4), 535–539.

Qian, H.B., Herrebout, W.A., and Howard, B.J. (1997) Infrared diode laser jet spectroscopy of the van der Waals complex $(N_2O)_2$. *Molecular Physics*, **91**(4), 689–696.

Quack, M. (1977) Detailed symmetry selection rules for reactive collisions. *Molecular Physics*, **34**(2), 477–504.

Quack, M. (1983) Detailed symmetry selection rules for chemical reactions, in *Studies in Physical and Theoretical Chemistry*, Maruani, J. and Serre, J., (eds), Elsevier Scientific Publishing Company, Amsterdam, *Symmetries and Properties of Non-Rigid Molecules: A Comprehensive Survey*, pp. 355–378, vol. 23. Proceedings of an International Symposium, Paris, France, 1–7 July 1982.

Quack, M. (1985) On the densities and numbers of rovibronic states of a given symmetry species: rigid and nonrigid molecules, transition states, and scattering channels. *Journal of Chemical Physics*, **82**(7), 3277–3283.

Quack, M. (1990) Spectra and dynamics of coupled vibrations in polyatomic molecules. *Annual Review of Physical Chemistry*, **41**, 839–874.

Quack, M. (2001) Molecules in motion. *Chimia*, **55**(10), 753–758.

Quack, M. (2002) How important is parity violation for molecular and biomolecular chirality? *Angewandte Chemie (International ed. in English)*, **41**(24), 4618–4630.

Quack, M. (2003) Molecular spectra, reaction dynamics, symmetries and life. *Chimia*, **57**(4), 147–160.

Quack, M. (2011) Fundamental symmetries and symmetry violations from high-resolution spectroscopy, in *Handbook of High-resolution Spectroscopy*, Quack, M. and Merkt, F. (eds), John Wiley & Sons, Ltd., Chichester, UK.

Quack, M. and Kutzelnigg, W. (1995) Molecular spectroscopy and molecular dynamics: theory and experiment. *Ber. Bunsen-Gesellschaft für Physikalische Chemie*, **99**(3), 231–245.

Quack, M., Schmitt, U., and Suhm, M. (1993a) Evidence for the $(HF)_5$ complex in the HF stretching FTIR absorption spectra of pulsed and continuous supersonic jet expansions of hydrogen fluoride. *Chemical Physics Letters*, **208**(5–6), 446–452.

Quack, M., Stohner, J., and Suhm, M. (1993b) Vibrational dynamics of $(HF)_n$ aggregates from an ab initio based analytical $(1 + 2 + 3)$-body potential. *Journal of Molecular Structure*, **294**, 33–36.

Quack, M., Schmitt, U., and Suhm, M. (1997) FTIR spectroscopy of hydrogen fluoride clusters in synchronously pulsed supersonic jets. Isotopic isolation, substitution and 3-d condensation. *Chemical Physics Letters*, **269**(1–2), 29–38.

Quack, M., Stohner, J., and Suhm, M. (2001) Analytical three-body interaction potentials and hydrogen bond dynamics of hydrogen fluoride aggregates, $(HF)_n$, $n \geq 3$. *Journal of Molecular Structure*, **599**(1–3), 381–425.

Quack, M., Stohner, J., and Willeke, M. (2008) High-resolution spectroscopic studies and theory of parity violation in chiral molecules. *Annual Review in Physical Chemistry*, **59**, 741–769.

Quack, M. and Suhm, M.A. (1990a) Observation and assignment of the hydrogen bond exchange disrotatory in-plane bending vibration ν_5 in $(HF)_2$. *Chemical Physics Letters*, **171**(5–6), 517–524.

Quack, M. and Suhm, M.A. (1990b) Potential energy surface and energy levels of $(HF)_2$ and its D isotopomers. *Molecular Physics*, **69**(4), 791–801.

Quack, M. and Suhm, M.A. (1991) Potential energy surfaces, quasiadiabatic channels, rovibrational spectra, and intramolecular dynamics of $(HF)_2$ and its isotopomers from quantum Monte-Carlo calculations. *Journal of Chemical Physics*, **95**(1), 28–59.

Quack, M. and Suhm, M.A. (1997) Potential energy hypersurfaces for hydrogen bonded clusters $(HF)_n$, in *Conceptual Perspectives in Quantum Chemistry*, Calais, J.-L. and Kryachko, E.S. (eds), Kluwer Academic Publishers, Dordrecht, *Conceptual Trends in Quantum Chemistry*, pp. 415–463, Vol. III.

Quack, M. and Suhm, M.A. (1998) Spectroscopy and quantum dynamics of hydrogen fluoride clusters, in *Advances in Molecular Vibrations and Collision Dynamics*, Bowman, J. and Bavcic, Z. (eds), *Molecular Clusters*, JAI Press, pp. 205–248, Vol. III.

Rabi, I.I. (1937) Space quantization in a gyrating magnetic field. *Physical Review*, **51**(8), 652–654.

Randall, R.W., Ibbotson, J.B., and Howard, B.J. (1994a) A model for the energy-levels of rare gas-spherical top van der Waals complexes. *Journal of Chemical Physics*, **100**(10), 7042–7050.

Randall, R.W., Ibbotson, J.B., and Howard, B.J. (1994b) Spectroscopy and dynamics of rare gas-spherical top complexes. The infrared spectrum of the ν_3 band of argon-silane. *Journal of Chemical Physics*, **100**(10), 7051–7060.

Repond, P. and Sigrist, M.W. (1996) Continuously tunable high-pressure CO_2 laser for spectroscopic studies on trace gases. *IEEE Journal of Quantum Electronics*, **32**(9), 1549–1559.

Rey, M., Boudon, V., Loëte, M., Asselin, P., Soulard, P., and Manceron, L. (2001) The spectrum of an octahedral molecule in a degenerate electronic state: the ν_6 fundamental band of jet-cooled $V(CO)_6$. *Journal of Chemical Physics*, **114**, 10773–10779.

Rizzo, T.R., Stearns, J.A., and Boyarkin, O.V. (2009) Spectroscopic studies of cold, gas-phase biomolecular ions. *International Reviews in Physical Chemistry*, **28**(3), 481–515.

Roth, D., Dopfer, O., and Maier, J.P. (2000) Infrared spectrum and ab initio calculations of the HNH^+-Ne open-shell ionic dimer. *Physical Chemistry Chemical Physics*, **2**, 5013–5019.

Scheele, I., Conjusteau, A., Callegari, C., Schmied, R., Lehmann, K.K., and Scoles, G. (2005) Near-infrared spectroscopy of ethylene and ethylene dimer in superfluid helium droplets. *Journal of Chemical Physics*, **122**, 104307.

Schlemmer, S., Cook, D., Harrison, J., Wurfel, B., Chapman, W., and Saykally, R. (1994) The unidentified interstellar infrared bands: PAHs as carriers? *Science*, **265**, 1686.

Schuder, M.D., Nelson, D.D., and Nesbitt, D.J. (1993) Slit-jet near-infrared diode-laser spectroscopy of $(DCl)_2$: ν_1, ν_2 DCl stretching fundamentals, tunneling dynamics, and the influence of large-amplitude geared intermolecular rotation. *Journal of Chemical Physics*, **99**(7), 5045–5060.

Scoles, G. (ed.) (1988) *Atomic and Molecular Beam Methods*, Oxford University Press, Oxford, Vol. 1.

Scoles, G. (ed.) (1992) *Atomic and Molecular Beam Methods*, Oxford University Press, Oxford, Vol. 2.

Scotoni, M., Boschetti, A., Oberhofer, N., and Bassi, D. (1991) The $3 \longleftarrow 0$ CH stretch overtone of benzene-An optothermal study. *Journal of Chemical Physics*, **94**(2), 971–977.

Scott, C.D., Arepalli, S., Nikolaev, P., and Smalley, R.E. (2001) Growth mechanisms for single-wall carbon nanotubes in a laser-ablation process. *Applied Physics A: Materials Science and Processing*, **72**, 573–580.

Sears, T.J. (1987) Infrared absorption spectroscopy of molecular ions using tunable lasers. *Journal of Chemical Society, Faraday Transactions 2*, **83**, 111–126.

Sigrist, M.W. (2011) High-resolution infrared laser spectroscopy and gas sensing applications, in *Handbook of High-resolution Spectroscopy*, Quack, M. and Merkt, F. (eds), John Wiley & Sons, Ltd., Chichester, UK.

Sinha, M.P., Schultz, A., and Zare, R.N. (1973) Internal state distribution of alkali dimers in supersonic nozzle beams. *Journal of Chemical Physics*, **58**(2), 549–556.

Smalley, R.E., Ramakris, B.L., Levy, D.H., and Wharton, L. (1974) Laser spectroscopy of supersonic molecular-beams-Application to NO_2 spectrum. *Journal of Chemical Physics*, **61**(10), 4363–4364.

Smalley, R.E., Wharton, L., and Levy, D.H. (1977) Molecular optical spectroscopy with supersonic beams and jets. *Accounts of Chemical Research*, **10**(4), 139–145.

Snavely, D.L., Colson, S., and Wiberg, K.B. (1981) Rotational cooling in a supersonic expansion of ammonia. *Journal of Chemical Physics*, **74**(12), 6975–6976.

Snavely, D.L., Walters, V.A., Colson, S.D., and Wiberg, K.B. (1984) FTIR spectrum of benzene in a supersonic expansion. *Chemical Physics Letters*, **103**(5), 423–429.

Snavely, D.L., Wiberg, K.B., and Colson, S.D. (1983) The infrared-absorption spectrum of a supersonic expansion of methyl-chloride. *Chemical Physics Letters*, **96**(3), 319–323.

Snels, M., Beil, A., Hollenstein, H., Quack, M., Schmitt, U., and D'Amato, F. (1995) Rotational analysis of the ν_1 band of trichlorofluoromethane from high resolution Fourier transform and diode laser spectra of supersonic jets and isotopically enriched samples. *Journal of Chemical Physics*, **103**(20), 8846–8853.

Snels, M. and D'Amico, G. (2003) Diode laser jet spectra and analysis of the ν_{14} fundamental of 1,1,1,2-tetrafluoroethane (HFC-134a). *Journal of Molecular Spectroscopy*, **221**(2), 156–162.

Snels, M., D'Amico, G., Piccarreta, L., Hollenstein, H., and Quack, M. (2001) Diode–laser jet spectra and analysis of the ν_1 and ν_4 fundamentals of CCl_3F. *Journal of molecular spectroscopy*, **205**(1), 102–109. 10.1006/jmsp.2000.8241.

Snels, M. and Fantoni, R. (1986) IR dissociation of dimers of high symmetry molecules: SF_6, SiF_4 and SiH_4. *Chemical Physics*, **109**(1), 67–83.

Snels, M., Fusina, L., Hollenstein, H., and Quack, M. (2000) The ν_1 and ν_3 bands of ND_3. *Molecular Physics*, **98**(13), 837–854.

Snels, M., Hollenstein, H., and Quack, M. (2003) The NH and ND stretching fundamentals of $^{14}ND_2H$. *Journal of Chemical Physics*, **119**(15), 7893–7902.

Snels, M., Hollenstein, H., and Quack, M. (2006a) Mode selective tunneling dynamics observed by high resolution spectroscopy of the bending fundamentals of $^{14}NH_2D$ and $^{14}ND_2H$. *Journal of Chemical Physics*, **125**(19), 194319.

Snels, M., Hollenstein, H., and Quack, M. (2006b) The NH and ND stretching fundamentals of $^{14}NH_2D$. *Journal of Molecular Spectroscopy*, **237**(2), 143–148.

Snels, M. and Meerts, W.L. (1988) High-resolution spectroscopy of CF_2Cl_2 in a molecular jet. *Applied Physics B-Photophysics and Laser Chemistry*, **45**(1), 27–31.

Snels, M. and Quack, M. (1991) High resolution Fourier-transform infrared spectroscopy of $CHCl_2F$ in supersonic jets: analysis of ν_3, ν_7, and ν_8. *Journal of Chemical Physics*, **95**(9), 6355–6361.

Steimle, T.C., Fletcher, D.A., Jung, K.Y., and Scurlock, C.T. (1991) Refractory radicals generated by pick-up molecular beam techniques. *Chemical Physics Letters*, **184**(5–6), 379–382.

Suhm, M.A., Farrell, J.T., Ashworth, S.H., and Nesbitt, D.J. (1993) High-resolution infrared spectroscopy of DF trimer: A cyclic ground state structure and DF stretch induced intramolecular vibrational coupling. *Journal of Chemical Physics*, **98**(7), 5985–5989.

Sumiyoshi, Y., Imajo, T., Tanaka, K., and Tanaka, T. (1994) Infrared diode laser spectroscopic detection of the propargyl radical produced in a supersonic jet expansion by UV laser photolysis. *Chemical Physics Letters*, **231**(4–6), 569–573.

Tam, W.S., Leonov, I., and Xu, Y. (2006) Pulsed slit jet cavity ring-down spectroscopy with a mid infrared lead salt diode laser. *Review of Scientific Instruments*, **77**(6), 063117.

Tanaka, K., Tachikawa, Y., Sakaguchi, K., Hikida, T., and Tanaka, T. (1999) Time-resolved infrared diode laser spectroscopy of the ν_3 band of the jet-cooled $Fe(CO)_2$ radical produced by ultraviolet photolysis of $Fe(CO)_5$. *Journal of Chemical Physics*, **111**(9), 3970–3977.

Tanaka, K., Tachikawa, Y., and Tanaka, T. (1997) Time-resolved infrared diode laser spectroscopy of jet-cooled FeCO and $Fe(CO)_2$ radicals produced by the UV photolysis of $Fe(CO)_5$. *Chemical Physics Letters*, **281**(4–6), 285–291.

Tang, J. and McKellar, A.R.W. (2004) Infrared spectra of seeded hydrogen clusters: $(para H_2)_N$-OCS, $(ortho H_2)_N$-OCS, and $(HD)_N$-OCS, $N = 2 - 7$. *Journal of Chemical Physics*, **121**(7), 3087–3095.

Tembreull, R. and Lubman, D.M. (1987) Resonant two-photon ionization in biomolecules using laser desorption in supersonic beam-mass spectrometry. *Applied Spectroscopy*, **41**, 431–436.

Thiévin, J., Cadudal, Y., Georges, R., and Vigasin, A.A. (2006) Direct FTIR high resolution probe of small and medium size $Ar_n(CO_2)_m$ van der Waals complexes formed in a slit supersonic expansion. *Journal of Molecular Spectroscopy*, **240**, 141–152.

Thompson, C.D., Robertson, E.G., Evans, C.J., and McNaughton, D. (2003) High resolution FTIR spectroscopy of the 1,1,1,2-tetrafluoroethane: ν_6. *Journal of Molecular Spectroscopy*, **218**, 48–52.

Thompson, C.D., Robertson, E.G., and McNaughton, D. (2004) Completing the picture in the rovibrational analysis of chlorodifluoromethane ($CHClF_2$): ν_3 and ν_8. *Molecular Physics*, **102**, 1687–1695.

Tittel, F.K., Richter, D., and Fried, A. (2003) Mid-infrared laser applications in spectroscopy, in *Solid-State Mid-Infrared Laser Sources (Topics in Applied Physics)*, Sorokina, I.T. and Vodopyanov, K.L. (eds), Springer-Verlag Berlin, pp. 445–510, Vol. 89.

Toennies, J.P. and Vilesov, A.F. (2004) Superfluid helium droplets: a uniquely cold nanomatrix for molecules and molecular complexes. *Angewandte Chemie-International Edition*, **43**(20), 2622–2648.

Trischka, J.W. (1962) Molecular beams, in *Methods of Experimental Physics*, Williams, D. (ed.), Academic Press, New York, pp. 589–636, Vol. 3.

Urban, R.D., Jörissen, L.G., Matsumoto, Y., and Takami, M. (1995) Free jet infrared-spectroscopy of SiF_4-rare gas complexes. *Journal of Chemical Physics*, **103**(10), 3960–3965.

Urban, R.D. and Takami, M. (1995a) Free jet infrared-spectroscopy of $(^{28}SiF_4)_2$ in the 10 μm region. *Journal of Chemical Physics*, **102**(8), 3017–3023.

Urban, R.D. and Takami, M. (1995b) Free jet IR diode spectroscopy of $(^{32}SF_6)_2$ in the 10 μm region. *Journal of Chemical Physics*, **103**(21), 9132–9137.

Utkin, Y.G., Goshe, M., Adamovich, I.V., and Rich, J.W. (2006) Compact overtone band carbon monoxide laser. *Optics Communications*, **263**(1), 105–110.

Vaida, V., Daniel, J.S., Kjaergaard, H.G., Goss, L.M., and Tuck, A.F. (2001) Atmospheric absorption of near infrared and visible solar radiation by the hydrogen bonded water dimer. *Quarterly Journal of the Royal Meteorological Society*, **127**(575, Sp. Iss. A), 1627–1643.

Verdes, D., Linnartz, H., Maier, J.P., Botschwina, P., Oswald, R., Rosmus, P., and Knowles, P.J. (1999) Spectroscopic and theoretical characterization of linear centrosymmetric $N_2 \ldots H + \ldots N_2$. *Journal of Chemical Physics*, **111**, 8400.

Viant, M.R., Fellers, R.S., McLaughlin, R.P., and Saykally, R.J. (1995) Infrared-laser spectroscopy of uracil in a pulsed slit jet. *Journal of Chemical Physics*, **103**(21), 9502–9505.

Wagner, K-G. (1984) A brief review of Knudsen-cells for applications in experimental research. *Vacuum*, **34**(8–9), 743–746.

Walsh, M.A., England, T.H., Dyke, T.R., and Howard, B.J. (1987) Pulsed molecular-beam infrared absorption spectroscopy of CO_2 dimer. *Chemical Physics Letters*, **142**(3–4), 265–270.

Wang, Z., McIntosh, A.L., Lucchese, R., and Bevan, J.W. (2004) Near infrared diode laser cw slit jet investigations of $O^{13}C$: HCl, $^{14}N_2$: HBr and OC : HBr. *Journal of Molecular Structure*, **695**(Sp. Iss. SI), 171–180.

Wangler, M., Roth, D.A., Winnewisser, G., Pak, I., and McKellar, A.R.W. (2001) Diode laser spectroscopy of the weakly bound complex Ne-CH_4. *Canadian Journal of Physics*, **79**(2–3), 423–434.

Watson, J.K.G. (1977) Planarity relation for sextic centrifugal-distortion constants. *Journal of Molecular Spectroscopy*, **65**(1), 123–133.

Weber, A. (2011) High-resolution Raman spectroscopy of gases, in *Handbook of High-resolution Spectroscopy*, Quack, M. and Merkt, F. (eds), John Wiley & Sons, Ltd., Chichester, UK.

Weida, M.J. and Nesbitt, D.J. (1996) Geometric isomerism in clusters: high resolution infrared spectroscopy of a noncyclic CO_2 trimer. *Journal of Chemical Physics*, **105**(23), 10210–10223.

Weida, M.J. and Nesbitt, D.J. (1997) High resolution mid-infrared spectroscopy of Ar-H_2O: The ν_2 bend region of H_2O. *Journal of Chemical Physics*, **106**(8), 3078–3089.

Weida, M.J., Sperhac, J.M., and Nesbitt, D.J. (1995) High-resolution infrared diode laser spectroscopy of $(CO_2)_3$: vibrationally averaged structures, resonant dipole vibrational shifts, and tests of CO_2-CO_2 pair potentials. *Journal of Chemical Physics*, **103**(18), 7685–7699.

Werle, P., Maurer, K., Kormann, R., Mucke, R., D'Amato, F., Lancia, T., and Popov, A. (2002) Spectroscopic gas analyzers based on indium-phosphide, antimonide and lead-salt

diode-lasers. *Spectrochimica Acta Part A-Molecular and Biomolecular Spectroscopy*, **58**(11), 2361–2372.

White, J.U. (1942) Long optical paths of large aperture. *Journal of the Optical Society of America*, **32**, 285–288.

Willey, D.R., Bittner, D.N., and De Lucia, F.C. (1989) Collisional cooling of the NO-He system The pressure broadening cross sections between $4 \cdot 3$ and $1 \cdot 8$ K. *Molecular Physics*, **67**, 455–463.

Willitsch, S. (2011) Experimental methods in cation spectroscopy, in *Handbook of High-resolution Spectroscopy*, Quack, M. and Merkt, F. (eds), John Wiley & Sons, Ltd., Chichester, UK.

Witteman, W.J. (1967) High-output powers and long lifetimes of sealed-off CO_2 lasers. *Applied Physics Letters*, **11**(11), 337–338.

Xu, Y., Liu, X., Su, Z., Kulkarni, R.M., Tam, W.S., Kang, C., Leonov, I., and D'Agostino, L. (2009) Application of quantum cascade lasers for infrared spectroscopy of jet-cooled molecules and complexes. *Quantum Sensing and Nanophotonic Devices VI*, **7222**(1), 722208.

Xu, Y.J., Jäger, W., Tang, J., and McKellar, A.R.W. (2003) Spectroscopic studies of quantum solvation in $^4He_{(N)}-N_2O$ clusters. *Physical Review Letters*, **91**(16), 163401-1–163401-4.

Yin, Z. and Tang, X. (2007) A review of energy bandgap engineering in III-V semiconductor alloys for mid-infrared laser applications. *Solid-State Electronics*, **51**(1), 6–15.

RELATED ARTICLES

Albert *et al*. 2011: **Fundamentals of Rotation–Vibration Spectra**
Albert *et al*. 2011: **High-resolution Fourier Transform Infrared Spectroscopy**
Bauder 2011: **Fundamentals of Rotational Spectroscopy**
Boudon *et al*. 2011: **Spherical Top Theory and Molecular Spectra**
Demtröder 2011: **Doppler-free Laser Spectroscopy**
Endo and Sumiyoshi 2011: **Rotational Spectroscopy of Complexes Containing Free Radicals**
Flaud and Orphal 2011: **Spectroscopy of the Earth's Atmosphere**
Frey *et al*. 2011: **High-resolution Rotational Raman Coherence Spectroscopy with Femtosecond Pulses**
Guennoun and Maier 2011: **Electronic Spectroscopy of Transient Molecules**
Havenith and Birer 2011: **High-resolution IR-laser Jet Spectroscopy of Formic Acid Dimer**
Herman 2011: **High-resolution Infrared Spectroscopy of Acetylene: Theoretical Background and Research Trends**
Hippler *et al*. 2011: **Mass and Isotope-selective Infrared Spectroscopy**
Jäger and Xu 2011: **Fourier Transform Microwave Spectroscopy of Doped Helium Clusters**
Marquardt and Quack 2011: **Global Analytical Potential Energy Surfaces for High-resolution Molecular Spectroscopy and Reaction Dynamics**
Merkt and Quack 2011: **Molecular Quantum Mechanics and Molecular Spectra, Molecular Symmetry, and Interaction of Matter with Radiation**
Oka 2011: **Orders of Magnitude and Symmetry in Molecular Spectroscopy**
Pratt 2011: **Electronic Spectroscopy in the Gas Phase**
Quack 2011: **Fundamental Symmetries and Symmetry Violations from High-resolution Spectroscopy**
Sigrist 2011: **High-resolution Infrared Laser Spectroscopy and Gas Sensing Applications**
Weber 2011: **High-resolution Raman Spectroscopy of Gases**
Willitsch 2011: **Experimental Methods in Cation Spectroscopy**